PRESSURES IN BINS

Andrew Gordon Schreiner Hofmeyr

A dissertation submitted to the Faculty of Engineering, University of the Witwatersrand, Johannesburg, in fulfilment of the requirements for the degree of Master of Science in Engineering.

Johannesburg, 1986

DECLARATION

I declare that this dissertation is my own, unaided work. It is being submitted for the Degree of Master of Science in Engineering in the University of the Witwatersrand, Johannesburg. It has not been submitted before for any degree or examination in any other University.

A.G.S. Hofmeyr
(Signature of candidate)

16th day of October 1986

ABSTRACT

Pressures in bins are still relatively unknown, particularly at emptying. To measure pressures a two-dimensional model of a shallow bin was constructed in which normal and shear stresses can be measured. Two shapes of bin were tested, one with straight inclined sides and one with vertical and and inclined sides. Five sets of readings were taken with a data logger for each shape. The results were very repeatable on filling and emptying. Tests were conducted to detect the switch pressure. No switch was found, instead a smooth transition from filling to emptying pressures was found.

Several theories both for filling and emptying were used to calculate pressures that were compared with the experimental results. These included the use of straight line framework models, Booth's pile theory, Walker's theory and the radial stress field. Some reasonably good fits were obtained. Recommendations are made for further experiments and for pressure calculations using computers.

ACKNOWLEDGEMENTS

I wish to thank Mr F B Thompson, formerly of Dorman Long for my initial interest in the problem. Thanks also to Professor A R Kemp and Professor G E Blight for their advice and assistance.

CONTENTS **PAGE**

CONTENTS

CONTENTS

CONTENTS

LIST OF FIGURES

FIGURE:

LIST OF FIGURES

LIST OF FIGURES

FIGURE:

LIST OF FIGURES

FIGURE :

LIST OF FIGURES

FIGURE :

LIST OF FIGURES

LIST OF TABLES

LIST OF TABLES

LIST OF SYMBOLS

A	slope of graph kg/μv
	area under curve
B	slope of graph μv/kg
	width of bin
C	BD/tanθ – Walker
D	Walker's factor relating vertical stress at wall to average vertical stress
ABCDEF	constants in Booth's pile theory
	constants in $y = A+B \times Cx^2 + Dx^3 + Ex^4$
Ei	emptying theory i
Fi	filling theory i
H	horizontal force
L	side length
N	normal force
P_1	force on vertical wall
P_2	force on sloping wall
R	hydraulic radius
	resultant force on side wall
Ri	residual
S	sum of squares of errors
T	shear force on wall
$\bar{V}$	average vertical stress – Walker
V_w	vertical stress at wall
V_o	surcharge – Walker
W	weight of sand mass considered
a	constant in $y = ax^n$
a,b	constants in $p = a + bx^2$
b	width of base of pile
f	function of θ in radial stress field
g	distance to centroid
h	height from apex
	height to surface
	horizontal pressure – Booth
k	ratio of horizontal to vertical pressure
k_A	active earth pressure coefficient
k_o	coefficient of earth pressure at rest

LIST OF SYMBOLS

n	constant in $y = ax^n$
	vertical pressure - Booth
p	normal wall pressure
q	normal pressure at top of slope
r	radius
	ratio
s	shear stress - Booth
w	weight at node
x, y	co-ordinates
α	angle between wall and vertical
β	inclination of σ_1 to normal to the radius
γ	density
δ	effective internal sand friction angle
ε	surface slope, angle of repose
θ	angle from vertical to radius from outlet
θ_w, θ'	θ at wall
ρ	$1 + \sin^2\phi$
	internal friction angle
σ	stress
σ', σ_w	stress normal to wall
σ_r	stresses in polar co-ordinates
σ_1, σ_2	*major, minor principal stress*
σ_x	vertical compressive stress
σ_y	horizontal compressive stress
σ'	normal stress on wall
τ	shear stress
$\tau_{r\theta}$	shear stress in polar co-ordinates
τ_w	shear stress at wall
ϕ	internal friction angle - Booth
ϕ_w, ϕ'	wall friction angle
ψ	inclination of σ_1 to radial direction
ψ'	ψ at wall
ω	inclination of σ_1 to vertical
μ	$45 - \delta/2$

LIST OF SYMBOLS

Note : Following Jenike[16] δ has been used for the effective angle of internal friction, except in Appendix F, Booth's pile theory.

CHAPTER 1

INTRODUCTION

1.1 Preamble

Bins for storing particulate material whether grain, sugar, crushed stone, sand, coal or other substances too numerous to mention, are a vital part of industry. Many failures have occurred in the past because the behaviour of the material and the pressures exerted by it on the bin have not been exactly known, especially during emptying. Therefore a lot of research is being applied to this problem.

Containers for storing particulate material are variously termed bins, bunkers, hoppers or silos. The term silo originally meant a pit of airtight structure for storing crops in and today is used for containers in the shape of long vertical cylinders. Bin is a general term but is used here to refer to shallow containers.

This work deals with the pressures exerted by contained materials on the walls of two-dimensional bins. By two-dimensional is meant that conditions in any plane cross-section through the bin are the same and strain in the third-dimension is zero. Most theories that apply to the two-dimensional case can be applied to the axi-symmetric case, where conditions do not vary on rotation about an axis.

In this report tests have been carried out on a model with a maximum depth of material (sand) of 800mm. It is assumed that if the particles are small enough there will be no appreciable scale effect so that these results would also apply to a full size bin. This is similar to saying that the same theory will apply to a model and full size retaining wall. This point is discussed further in the final chapter.

In this chapter the problems of pressure and flow are introduced, followed by an introduction to the rest of the dissertation and a brief chronological survey of the literature.

1.2 Behaviour of material in bins

The pressures on the walls of a bin should be known as accurately as possible when the structure is designed. This has led to many theories and experiments. In the past a shallow bin has been treated like a retaining wall supporting backfill in the active state [1]. Later it was found that a change in distribution of pressure takes place as discharge commences. This is because the column of material over the opening is no longer supported vertically. The major principal stress changes from the vertical to the horizontal direction on the centreline, Fig. 1.1. This effect spreads very rapidly through the mass in the bin as discharge starts.

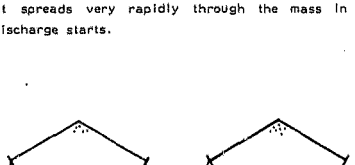

(a) Filling (b) Discharge

Figure 1.1 Change of stress state from filling to discharge

Evidence for change in the stress state between filling and emptying can be seen in the behaviour of a suspension or catenary bunker, Fig. 1.2. A catenary bunker has

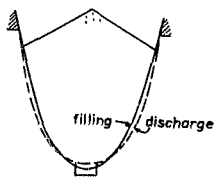

Figure 1.2 Behaviour of a catenary bunker

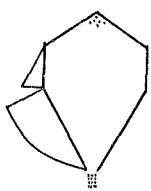

Figure 1.3 Bin with vertical and inclined sides

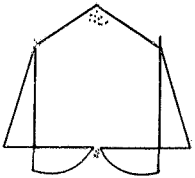

Figure 1.4 Bin with flat bottom

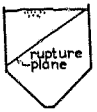

Figure 1.5 One definition of a shallow bin

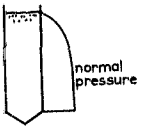

Figure 1.6 Deep bin or silo

flexible sides which take up the shape of the funicular polygon.

As discharge starts the bottom lifts and the sides move outward, showing a redistribution in pressure.

The distribution of pressure will also depend on the shape of the bunker. Fig. 1.3 shows a bin with part of each side vertical and Fig. 1.4, a flat bottomed bunker.

The pressures in a deep bin or silo, Fig. 1.6 will differ from those in a shallow bin.

A shallow bin will have a depth of up to two times its width, while a deep bin will have a depth three or four times its width. A shallow bin is more affected by conditions at the surface and the outlet than a deep bin. A shallow bin is sometimes defined as one in which the "rupture plane" intersects the surface [1],[2], Fig. 1.5.

Fundamentally there is no difference between the behaviour of the material in a shallow bin and in a deep bin.

An interesting case of a natural bin is a diamond pipe mined by block caving, Fig. 1.7. If material is drawn off from tunnel B the pressure on adjacent tunnels increases to such an extent that it can cause them to fail structurally. With a model it is possible to vary the pressure on the bottom at will by changing the drawoff point. In a bin the material on the surface directly above the drawoff point moves down before the material on the sides. In the block caving this fact is troublesome, drawing off unwanted overburden.

A bin may be considered for analysis as either two dimensional or axisymmetric. In a two dimensional bin there is no variation in conditions normal to a cross-section of the bin. The material in the bin is in a state of plane strain. An axisymmetric bin is formed by rotating a plane

curve around an axis in the plane. The stresses in the material in the bin do not vary with rotation around the axis. A square cross-section is similar in effect to a circular cross-section.

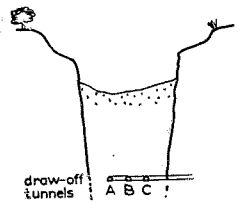

Figure 1.7 Diamond Pipe

As discharge starts downward movement of the material in the bin takes place. The resulting pressures are sometimes called "dynamic". This is correct in terms of the definition of dynamics [3] which can be stated as "the effect of force on motion". However, it can be misleading as the term dynamics has the implication of forces due to acceleration. In most cases of discharge the movement will be so slow that the acceleration forces are negligible. There will, however, be acceleration forces if arching forms a void followed by sudden collapse. There may also be pressures due to trapped air or gas in this instance. Therefore it is perhaps better to talk of flow pressures [4] or discharge pressures.

There are similarities between the behaviour of sand in a container and water with important differences. Water as a liquid can have no internal friction at rest whereas sand can. The surface of water at rest is thus horizontal, while the surface of sand at rest may be as steep as its angle of repose. When water runs out of an opening at the bottom of a bin it may be directed upwards but sand only flows downwards and no matter how deep the sand in the bin is, flow ceases when it reaches the angle of repose, Fig.1.8.

The rate of discharge of water through an opening depends on the size of the opening and the head, while the rate of discharge of sand is independent of head and depends only on the conditions near the outlet [2]. In both water and sand a small element of the continuum must be in equilibrium under the stresses acting on it and continuity must be satisfied. Sand consists of individual grains which may be regarded as almost rigid bodies pressing against each other in point contact. It is convenient to treat the cumulative effect of these interacting contacts as the behaviour of a continuum with a constitutive law, the simplest of which is that of Möhr-Coulomb friction. On a plane of limiting slip

$$\tan\delta = \tau_n/\sigma_n \qquad 1.1$$

where δ is the effective angle of internal friction and is usually greater than the angle of repose ε. Water is an incompressible fluid, whereas usually in a bin sand must dilate to shear and flow.

In a bin flow may either occur throughout the mass, termed mass flow, or in a zone of limited width above the opening, termed piping, ratholing of plug flow. Mass flow is desirable for a complete turnover of material in the bin, but often not possible because a very steep hopper section is necessary. To limit flow pressures plug flow is sometimes ensured by an insert in the bin [5].

This dissertation concentrates on a shallow bin of two-dimensional shape with rigid sides which are either vertical or sloping. The material used in the tests was a uniform size sand. The theories used to predict filling and discharge pressures have been restricted to the simplest available. Chapter 2 gives details of tests on the sand used and the construction and function of the model.

Chapter 3 gives the results of tests on bins of two shapes. Chapter 4 gives theories for shape 1 and chapter 5 gives theories for shape 2. In chapter 6 theoretical and experimental results are compared. The final chapter, 7, discusses the results and gives conclusions and suggestions for further investigation.

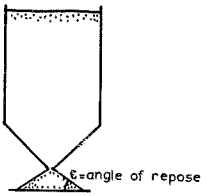

Figure 1.8 Flow ceases at angle of repose

1.3 Survey of past work

Dealing with shallow bins Ketchum [1] states that "the problems of the calculation of the pressures on bin walls is the same as the problem of the calculation of pressures on retaining walls". Deep bins are calculated by Janssen's [6] or Airy's [7] formula which give similar results. Ketchum devotes a chapter to experiments on deep bins. He concludes that the pressures from moving grain are very slightly greater than the pressure of grain at rest (10 per cent maximum). The points at which lateral pressures were measured were few. Often pressures were measured only at one point and that point, when its location was given, was near the bottom where there is a drop in pressure at discharge anyway. When a large increase in lateral pressure with discharge was measured it was put down to an eccentric opening. Ketchum states that in one test by Bovey sudden stoppage produced no appreciable effect. This supports the theory that acceleration forces are negligible.

Booth [8] developed an ingenious theory for the pressures within a two dimensional pile of granular material. He verified his theory with careful measurements on the base of a pile. He contends that the Rankine and wedge theories of

pressure are difficult to apply in some cases of bin pressures. In his method the bin is superimposed on the pile as shown by the dotted line in Fig. 1.9. The friction on the sides will provide the major difference from conditions in a

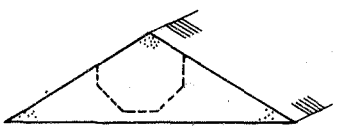

Figure 1.9 Booth's pile theory

pile, but Booth claims that for a shallow bin this is of minor importance. As horizontal pressures on the centreline of the pile are the *Rankine active pressures*, *Booth's analysis* provides an approximation to the filling case. As he points out, his analysis results in equilibrium being satisfied in all respects. In Booth's analysis, pressure increases in direct proportion to the distance from the apex of the pile. This may be thought of as a type of "radial stress field" to be mentioned later. An analysis appearing in the book by *Nadai* [9] *produces similar* results to Booth's and also results for the case of a trough shown in Fig.1.10. An analysis of a pile based on a replacement framework[10] produces results generally in agreement with Booth's theory.

Bridges [11] gives the Rankine method for shallow bins and Janssen's and Airy's method for deep bins. An interesting comment in the discussion by Squire [11] points out that the method may result in the coefficient of friction on the walls being exceeded, in which case an adjustment is required which could product considerable increase in lateral pressure. Rogers [12] applies Coulomb's theory (wedge theory) to

shallow bins with or without wall friction and Janssen's theory to deep bins. He also applies Janssen's theory to a steeply inclined hopper with interesting results, Fig. 1.11 The normal and horizontal pressures reduce towards the bottom. This is achieved by using a different hydraulic radius at each level. His analysis is thus linked to Walker's analysis [14],[15]

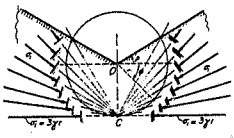

Figure 1.10 Nadai's analysis of a trough

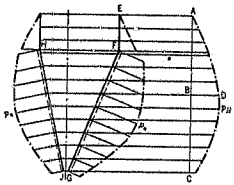

Figure 1.11 Roger's application of Janssen's theory

Zakrewski [13] gives empirical factors for increase in lateral pressures during flow, based on Russian research in 1939. He explains the increase as the action of a wedge shaped core moving downwards, Fig. 1.12.

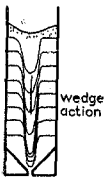

Figure 1.12 Zakrewski's explanation of flow pressures

Jenike's report, Gravity Flow of Bulk Solids[16] is an important advance in the field of bin behaviour. There is very little experimental work reported, but an organized attempt is made to apply the methods of plasticity to the flow condition. Equations for stresses are developed after Sokolovski[17], in addition the stress field is linked to the velocity field. Jenike's[16] major achievement is the definition of the radial stress field, similar to those mentioned above[8], [9], but centred at the outlet. The importance of the radial stress field is that it governs at the outlet of a converging channel during discharge, regardless of what happens at the surface. Jenike concentrates more on conditions for flow than on wall pressures. Graphs produced by computer for pressures in radial stress fields are given. The analysis allows for internal friction, friction on the channel wall and wall slope.

Johanson and Jenike[18] extend the work of reference (16). The method of calculating the radial stress field is explained in detail and the method of characteristics is set out for the numerical calculation of stress and velocity fields. Diagrams are given Fig. 1.13, showing stress in a converging channel but without any scale. These results

are not compared with tests. The tests reported were observations of flow patterns through glass-walled two dimensional bunkers and of sectioned axisymmetric cones. A useful feature of references (16) and (18) is that the theory is developed both for plane strain and axial symmetry.

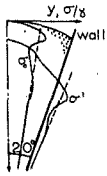

Figure 1.13 Discharge wall stresses according to Johanson

Turitzin[5] *summarizes the results of French and Russian* tests on silos. Emptying pressures were up to 2,4 times pressures from Janssen's theory. Filling pressures agreed reasonably with Janssen's theory. Pressures were found to vary a lot with time during emptying.

Nadai [8] adopts a plasticity approach to the analysis of "loose and generally plastic substances" and gives results produced by Hartmann in an unpublished doctoral thesis. Two very interesting diagrams due to Hartmann are shown in Fig. 1.14 indicating the slip lines in granular material between rough converging walls that move in or out. This shows the equivalence of filling to outward movement of the walls and of discharge to the inward movement of the walls.

The German code for loads in silo bins [10] differentiates between filling and emptying pressures. The ratio of lateral to vertical pressure is to be taken as 0,5 for *filling and* 1,0 for emptying. The latter does not imply

fluid pressure, for unlike a fluid wall friction determines the limiting horizontal pressure at infinite depth. The difference between emptying and filling horizontal pressures results from the defined wall friction angles. This results in a ratio of 1,28 for granular materials with an internal friction angle of 34° and 1,0 for powdery filling material. these values are less than those reported by Turitzin [5] .

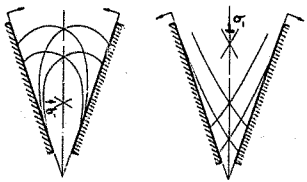

Inward wall movement Outward wall movement

Figure 1.14 Hartmann's analysis of rough converging channels

Kvapil [20] observes the flow of material from a a bin and defines the main active zone as approximately an ellipse.

Lightfoot [21] measures pressures in a power station coal bunker during filling only. The results are in fair agreement with the Rankine pressures.

Walker [14] derives a theory for filling of a conical hopper or plane hopper with sloping sides by ignoring shear on vertical planes. He determines the horizontal pressure so that for a triangular element at the wall the correct wall friction angle is satisfied. For the discharge case the vertical equilibrium of a horizontal slice is considered.

fluid pressure, for unlike a fluid wall friction determines the limiting horizontal pressure at infinite depth. The difference between emptying and filling horizontal pressures results from the defined wall friction angles. This results in a ratio of 1,28 for granular materials with an internal friction angle of 34° and 1,0 for powdery filling material. these values are less than those reported by Turitzin [5] .

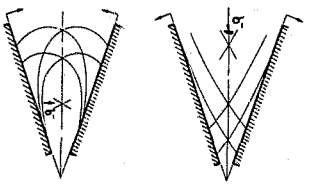

Inward wall movement Outward wall movement

Figure 1.14 Hartmann's analysis of rough converging channels

Kvapil [20] observes the flow of material from a a bin and defines the main active zone as approximately an ellipse.

Lightfoot [21] measures pressures in a power station coal bunker during filling only. The results are in fair agreement with the Rankine pressures.

Walker [14] derives a theory for filling of a conical hopper or plane hopper with sloping sides by ignoring shear on vertical planes. He determines the horizontal pressure so that for a triangular element at the wall the correct wall friction angle is satisfied. For the discharge case the vertical equilibrium of a horizontal slice is considered.

The analysis is similar to Janssen's except that there is a converging channel. The variation in vertical stress over the element is allowed for by a factor D where the vertical stress at wall = D x average vertical stress , D is approximated as 1. The wall pressure thus obtained satisfies the condition that it must be zero at the top and bottom. Material in a section with vertical sides above the hopper is treated as a surcharge. He shows test results that agree well with his theory for a steep sided cone. The steeper the cone the more nearly constant the factor D will be. He also considers the conditions under which arches would form to prevent flow. A series of tests on pyramidal and conical hoppers[15] were used to compare with Walker's theory. Hopper half angles to vertical of 3°, 15° and 30° were used. The material was fine coal with an internal friction angle of 41° and a wall friction angle of 16° on stainless steel. Rough walls were also tested. A series of diaphragm electrical transducers were used to measure normal pressure. A water filled football bladder was used to measure internal pressures. During discharge rapid oscillations about a mean level were recorded for the 15° hoppers. Drastic pressure changes were recorded as discharge started. A gauge near the hopper mouth would show a drop in pressure and one higher up an increase. No switch pressure or moving point load was detected. Internal pressure measurements near the outlet showed a rapid decrease with discharge.. For the 30° hopper fluctuations away from the outlet were almost absent, suggesting stationary material at the wall. Initial pressures showed a linear pressure increase with depth then a reduction near the bottom, Fig. 1.15. At discharge the peak moved up and the pressure near the outlet dropped. Agreement between theory and experiment was better for the 15° than for the 30° hopper.

It was found that the flow pressure was independent of the rate of flow, even if the flow was stopped, thus

confirming the small part played by acceleration forces.

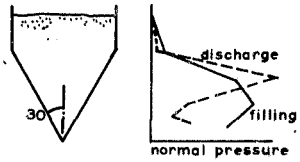

Figure 1.15 Walker and Blanchard's tests

Jenike and Johanson[22] in a paper on bin loads calculate the initial pressure in a hopper using elasticity theory. This theory shows a reduction near the bottom as measured by Walker and Blanchard. For discharge a radial stress field with linear reduction to zero at the top is proposed, Fig. 1.16. Without experimental verification a "switch" pressure is proposed, which is a line load necessary to maintain equilibrium at the level below which discharge pressures have started and above which filling pressures exist, Fig. 1.17. It is also stated that inertia forces are negligible.

Platonov and Ivanov[23] develop more rigorously than Janssen a theory for a deep cylindrical bin which relates more to the discharge case. The expression for lateral pressure is similar to Janssen's but the values are almost 50% greater.

Mroz and Drescher[24] apply an ingenious kinematic approach to a bin, with a cylindrical part and a converging hopper. The method is analogous to the mechanism method *for plastic collapse of a frame. They derive formulas* for both parts. The pressure on the upper part has the shape of the Janssen pressure and on the lower part of the radial stress field.

Pieper [25] conducted tests to check DIN 1055 [19]. He showed that for the Janssen formula there can be no scale effect. He concludes that DIN 1055 is adequate though not correct in all aspects.

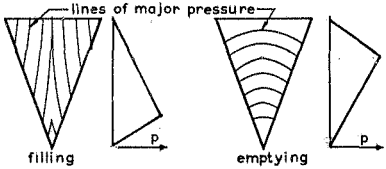

Figure 1.16 Jenike and Johanson's filling and emptying pressures

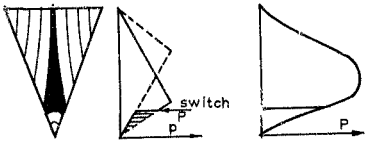

Figure 1.17 The switch pressure

Deutsch and Schmidt [26] found extreme values of discharge pressures up to four times the Janssen values, considerably more than others [23],[25].

Jenike, Johanson and Carson [4] in three papers on bin loads to follow up previous papers [22] make use of energy concepts to produce a locus of pressure peaks based on strain energy. If the cylindrical part diverges slightly

from top to bottom (1 or 2 degrees) then the pressures are close to the Janssen values during discharge, but if there are ledges or slight convergence the pressure peaks are considerably above Janssen but less than the strain energy line.

Walters[27],[28] and Walters and Clague[29] extend the work of Walker[14]. They calculate the value of D which relates the wall stress to the average vertical stress by assuming that the shear stress varies linearly from zero to the value at the wall. D values for filling are either less than or equal to 1. At discharge for practical wall friction angles, values of D can be as high as 2. For normal combinations of δ and ϕ', D will be about 1,4. In the parallel walled part this leads to higher stresses than Janssen for small depths and Janssen's stresses for large depths. For a converging hopper with no surcharge Walters obtains the normal wall stress shown in Fig. 1.18 for a case with half angle of 4° (ie a very steep hopper). Note that the areas under the filling and emptying curves are not equal. It is shown in Appendix E that for D values other than 1, there can be no vertical equilibrium.

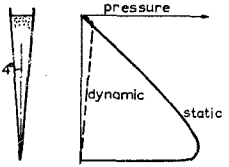

Figure 1.18 Walters' normal wall stress for $\delta = 50°$, $\phi'_w = 25°$ and $\alpha = 4°$

Blair-Fish and Bransby[30],[31],[32] report on flow patterns and wall stresses measured simultaneously in a bunker. These are probably the best and most complete measurements taken up to this time. Some of the results are shown in Fig. 1.19 :

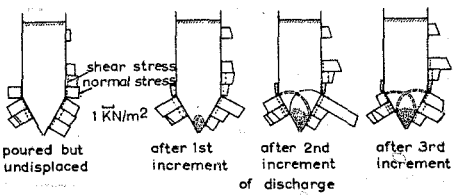

Figure 1.19 *Results shown by Blair-Fish and Bransby*

There is a marked change from filling to discharge. During discharge zones of intense shearing form, move down and then re-form and pressure peaks form and die away with them. Bransby, Blair-Fish and James[33] determined displacement fields and directions of major compressive strain during flow from the movement of lead markers, Fig. 1.20 :

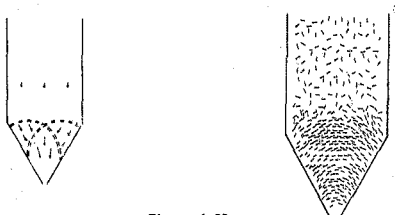

Figure 1.20

Displacement fields (from reference (33))

Directions of major compressive strain

Bransby and Blair-Fish [34] examine the region where vertical wall and hopper meet. Predictions for ratios between wall stress above and below are higher than measured. Bransby and Blair-Fish [35] develop expressions for displacements and strains in a hopper that agree with observations. These could be useful in calculating strain states. Drescher, Couzens and Bransby [36] define velocity fields to agree with test results for a plane hopper.

Following on the work of Walters [27], Arnold and McLean [37] have produced a closed form solution for the radial stress field that compares well with the numerical results obtained by Jenike [18].

Horne and Neddermann [38],[39] find the pressures in a parallel sided bin and in a hopper by the method of characteristics for both filling and emptying cases. In both cases the results are not smooth but oscillate along the wall. In the parallel sided bin the results oscillate about the Janssen solution and in the hopper the wall pressure oscillates about the radial stress field towards the outlet.

Häussler and Eibl [40] have applied the finite element method to a deep bin. They analyse the filling state and the transition to a discharge state. Possibly the best available constitutive law [41] has been used and large displacements have been allowed for. Both 45° and 15° half angle hoppers were analysed. Filling conditions compare reasonably well with test results. Emptying pressures are shown but not compared with test results. It is interesting to note that there is a steady transition from filling to emptying with time without any switch pressures moving along the bin, although the peak pressures at the transition are loosely referred to as switch pressures.

Blight [45][46] has measured pressures on the walls of full size silos. He plots pressures against calculated overburden. The pressures are not given as the variation up the wall at a given instant, presumably because a limited number of cells were used near the bottom. Instead pressures are plotted against calculated overburden pressure equal to depth times density. Thus changes between *filling* and emptying in an individual test are not shown. Instead an envelope of *filling or emptying pressure* is obtained. In some tests, readings were taken to fit in with operational condition of partial emptying followed by refilling. He obtained a large scatter and found little difference between filling and emptying. He proposed a simple containing envelope

$$\sigma_w \approx Ko\ \gamma z \qquad 1.1$$

for all pressures where Ko is the coefficient of earth pressure at rest.

In this section there has been a discussion of selected references from the many available, as an attempt to define a pattern of bin behaviour emerging from the results of the theories and experiments mentioned.

There seems to be a change in pressure regime between filling and emptying. This is due to reduction in vertical *support* when outflow starts. A change in direction of major principal stress from vertical to horizontal on the centreline is likely to occur. This is clearly seen in the change in shape of a catenary bunker with the sides moving out and the bottom moving up. Most bins have a parallel sided section followed by a converging section. In the parallel sided section if deep enough, in theory a limiting normal pressure is reached [5].

$$\sigma_w = \frac{\gamma R}{\tan \phi_w} \qquad 1.2$$

This is the maximum pressure in the Jansen theory. In theory the difference in emptying values is that this pressure is approached nearer the surface [27], Fig. 1.21, provided that the wall friction angle remains constant.

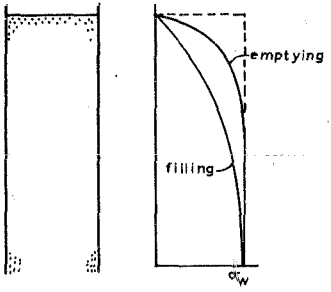

FIGURE 1.21 Pressures in a silo

Most investigators [5][25][26] found greater pressures during discharge. Simple evidence like opening up of cracks upon emptying shows an increase in pressure.

In the converging part emptying pressures show a decrease towards the outlet [15][30][45][46]. Jenike [16] and Walker [14] produced theories to accommodate this. Pressure variations with time during emptying were found to occur. These were not found to be due to acceleration effects. The likely

explanation is given by the results of Bransby and Blair-Fish [34], Fig. 1.19, where x-ray analysis showed pressures to vary with the formation of asymmetric shearing zones. Some of the pressures were measured on full size bins or silos but most were measured on models and there is some doubt whether the behaviour of a granular material is governed by the same type of stress regime in a model as in a larger bin.

In applying more sophisticated methods of analysis the limit stress on blocks [24], the method of characteristics [38] and the finite element method [40] have been used. The latter method [40] has produced results that agree with experimental results and look like the results from reference [34].

A moving peak pressure or switch pressure postulated by Jenike and Johanson [22] has not been detected [45][46].

CHAPTER 2

EXPERIMENTAL WORK - MATERIAL AND CALIBRATIONS

2.1 Sand and its properties

The material used in the bin was a well-rounded quartzitic sand from Philippi in the Cape Flats. It was almost single size and was virtually free from dust when poured. The properties of the sand are summarised in table 2.1 :

TABLE 2.1 : Properties of Sand

Density loose		1,593 g/cc
dense		1,757 g/cc
Internal friction angle	δ =	33,8°
Wall friction angle (steel)		
from triaxial	ϕ_w =	20,1°
from shear box	ϕ_w =	18,8°
Wall friction angle (glass)		
from shear box	ϕ_w =	9,1°
Angle of repose	α =	31,0°

2.2 Triaxial test for internal friction angle

Tests were carried out on dry sand. Each specimen formed a cylinder 38mm diameter x approximately 64mm long. Tests were carried out with confining pressures (σ_3) of 25, 50, 75 and 100kPa in drained test. The results are given in Appendix A. The value of 33,8° for internal friction angle was obtained from direct calculation rather than from the Möhr's circles in Appendix A.

A close fitting rubber membrane was placed over the pedestal and the two parts of the mould were placed around it and clamped together with two O rings. The projecting top of the membrane was then turned over the mould and sand was poured in from a container that had been weighed. The sand was lightly tamped down with the blade of a medium sized screw driver after a porous disc had been placed on top of the pedestal inside the membrane. A perspex top with steel loading ball was then held on top while

the membrane was turned up around it and an O ring was carefully rolled up onto the top off the split mould. The lower O ring was then rolled down onto the pedestal and the split halves were carefully removed. The lower O ring was then rolled up to clam the bottom of the membrane to the pedestal. Any wrinkles were carefully straightened out. The cell was then placed carefully over the sample so as not to disturb it, and was then screwed down. The confining pressure was then applied, suitably adjusting the pressure gauge according to it's calibration (Appendix A). The proving ring was then put in position and the table was raised to take up the play. The deflection gauge and proving ring gauge were then set to zero and the drive was engaged at a speed of 0,012 inches/minute (0,031mm/minute). After a deflection of 0,1mm the speed was changed to 0,06 inches/minute (1,52mm/minute). Readings were taken to a deflection of 5mm or more. Some details appear in Figure 2.1.

2.3 Tests for friction angles of sand on steel and sand on glass

Two types of test were used to measure the sand-steel friction angle. In the first type a triaxial test was carried out. The procedure described in section 2.2 was followed after a steel plate of elliptical shape had been introduced at an angle of 45° into the specimen. At an angle of 45° the greatest shear stress occurs. Graphs of $\sigma_1 - \sigma_3$ against deflection (Appendix A) show that after a sharp change in direction all of them increased at about the same slope. This point of change was taken as the correct value of $\sigma_1 - \sigma_3$ for determining the wall friction angle. It is likely that the large deformations of the membrane in the vicinity of the plate account for the subsequent upward slope. The Möhr's circle plot gave a value for wall friction angle of 20,6°. However, the calculated value of 20,1° was preferred.

A shear box test was the second type of test used to find the sand-steel friction angle. A 100mm x 100mm shear box

was used. Packs were used to support a 3mm steel plate flush with the top of the lower half of the shear box. The surface of the plate was sanded with medium emery paper and was free from rust and mill scale. The results are shown in Appendix A. Seven tests were conducted with vertical pressures ranging from 5,3kPa to 19,90kPa. A speed of 40mm horizontal movement per hour was used. Readings of horizontal load were taken every 0,25mm up to 3mm maximum displacement. A friction angle of 15,3° was obtained with the sanding direction (from the emery paper) parallel to the shear direction (table A.5). The steel plate was then sanded with coarser paper and the direction of sanding was made perpendicular to the shear direction. A friction angle of 18,8° was obtained (table A.6). This is the value shown in table 2.1. In the triaxial test the steel plate had been sanded with medium emery paper in both directions.

A 3mm thick piece of clear window glass was used in the 100mm x 100mm shear box to determine the sand-glass friction angle, table A.7. A friction angle of 9,1° was obtained. The lower the friction angle the closer the condition in the bin approaches a true two-dimensional stress state. This angle is approximately half that for sand on steel.

2.4 Determination of sand density

A container with very rigid walls, 102mm diameter x 112,5mm high internally was used. For the loose determination of density sand was poured in and struck off level. For the dense determination the container was placed on a cube mould vibrator, vibrated, and then topped up and struck off level.

2.5 Bin apparatus

An overall view of the apparatus is shown in Figs. 2.2 and 2.3. A rigid frame of welded construction made from 50,8 x 50,8 hollow square tube supports, two sheets

of 6mm glass approximately 860mm x 1010mm in size in parallel planes 400mm apart. Each glass pane is supported around its edge and by a flat bar 38mm x 6,2mm on edge on the vertical centreline. The glass plates form the ends of the bunker. A bunker side consists of three plates of 0,416mm thick steel plate, Fig. 2.3. Each plate measures 226mm down the slope x 398mm wide and is arranged to overlap the lower plate by 3mm without touching it giving an effective covering length of 225mm down the slope. The plate is stiffened by being screwed to six machined steel ribs, 4,76mm wide x 10mm deep, by countersunk head screws at 35mm centres. The ribs are at 40mm centres down the slope which leaves a 14mm plate cantilever at top and bottom. The ribs in turn are screwed to machined steel flats of size 18mm x 4,76mm running down the slope. Each plate and its supporting frame is equipped with four ball races which rest on members made from 50,8mm x 25,4mm cold rolled channel. The bearings ensure virtually frictionless movement down the slope. Location on the slope is provided by a short cantilever of section 5 x 5mm on either side which engages a square hole with a knife edge in the supporting channel. Plates are held down by springs and split pins through the cantilevers. A supporting channel pivots at the bottom and can be inclined at 60°, 45° or 30° to the vertical. Another section of channel can be bolted onto the inclined support to provide both vertical and sloping sides.

Normal pressure is measured on each of the five 40mm one-way spanning panels per plate. Strains are measured, Fig. 2.4 with 120 ohm electrical resistance foil gauges connected in a full bridge circuit. It is assumed that there is no interaction between plate panels although this is not strictly true. (See the section on calibration). Shear stresses, averaged for each plate are measured by strain gauges on the cantilevers, Fig. 2.5. The total load in the bin is measured by four C shaped load cells, Fig. 2.6, placed under the feet of the bin and instrumented with strain gauges connected into a single full bridge circuit.

A slot of width 30mm has a screw operated slide with a row of holes, Fig. 2.2, to provide discharge at the bottom of the bin. A loading box equipped with a bottom discharge slot is raised by crane and held slightly above the bunker to fill it. To empty the bunker the loading box is lowered onto a trolley which is pushed under the bunker. Each plate is sealed against the glass with a thin bead of plasticine. Dust proof sealing for filling or emptying prevents a health hazard.

Squares of sides 100mm drawn on a glass end panel and a vertical central millimetre rule are used to determine the position of the sand surface. With six plates there are a total of 37 strain gauge circuits which are connected to a data logger, Fig. 2.7. The data logger consists of a Fluke 2240B data logger which is sensitive to microvolts and independent voltage sources with zero adjustment for each channel.

2.6 Calibration for shear

Each panel was removed from the bin and calibrated in the apparatus shown in Fig. 2.8. The panel was supported on a rigid frame welded from angle iron. The cantilever shear arms passed through rectangular holes with machined knife edges, as in the bin supports. A plate 90mm x 85mm was screwed to the surface of the panel to provide the attachment point for a light cable which was connected over a pulley to a scale pan which provided the horizontal load. The load was applied in steps of 2kg up to 10kg, and readings were recorded in microvolts on the data logger. The slopes were calculated by least squares, and are shown in table 2.2 together with correlation coefficients. Graphs were also plotted to ensure that there were no points far off the lines.

TABLE 2.2 : Calibration of Shear Circuits

Plate	Graphical Slope kg/μV	A Least Squares Slope kg/μV	Correlation Coefficient	B Slope* Pa/μV
1	0,02551	0,02588	0,999300	2,76
2	0,02272	0,02276	0,997787	2,48
3	0,02400	0,02412	0,999932	2,63
4	0,02230	0,02213	0,998092	2,41
5	0,02347	0,02326	0,999200	2,54
6	0,02415	0,02406	0,999[illegible]7	2,51

* $B = \frac{A \times 9,81}{0,400 \times 0,225} = 109,0\ A.$ 1 Pa = 1 N/m²

2.7 Calibration for normal pressure

A panel has five plate spans down the bin slope and each is separately instrumented. Because it was suspected that a load on one span would cause readings on adjacent spans, a test was carried out to see how big this effect would be, as it was intended to ignore it. Pressure was applied to each span in turn through a rubber bag filled with water, Fig. 2.8. Readings were taken from the circuit on the second span. In each case the water pressure was increased in stages up to a head of one metre. The slopes and correlation coefficients were determined by least squares. The results are shown in table 2.3.

TABLE 2.3 : The Effect of Loading Other Spans on the Reading from Span 2

Span Loaded	Slope μV/mm	Correlation Coefficient
1	29,5	0,00879
2	359,2	0,999995
3	18,6	0,99220
4	15,0	0,99560
5	0	

It can be seen that the readings when adjacent panels are loaded are small but not insignificant. Therefore another method of calibration was tried. The plate was placed in the lowest position in the bin and the bin was sealed with plastic sheeting and plasticine and filled with water in stages up to a depth of 0,5 metres.

The result for span 2 was a slope of 467,2 μV/mm with a correlation coefficient of 0,99982. This value is greater than the value of 359,2 in table 2.3 for two possible reasons. First the effect of loading all the spans would increase the reading and second the rubber bag may not have applied pressure to the whole area intended.

Consequently it was decided that calibration for normal pressure would be carried out in the bin and that the interacting effects of load on other spans would be neglected for simplicity. Each panel was placed in turn at the lowest position in the bin. The bin was then sealed and water pressure was applied at eight levels from a depth of 200mm to a depth of 550mm above the discharge slot. The results are given in table 2.4, where the slopes were calculated by least squares.

Table 2.4 Calibration for Normal Pressure using Water on Plates at Lowest Bin Position

Plate	Span	Slope Pa/μV	Correlation Coefficient	Plate	Span	Slope Pa/μV	Correlation Coefficient
1	1	23,38	0,999518	4	1	23,11	0,999787
	2	23,65	0,999927		2	25,22	0,999851
	3	18,91	0,999901		3	21,84	0,999836
	4	19,98	0,999933		4	22,97	0,999914
	5	21,81	0,999932		5	21,10	0,999876
2	1	23,78	0,999811	5	1	33,38	0,999919
	2	23,17	0,999885		2	27,95	0,999888
	3	24,02	0,999926		3	35,63	0,999930
	4	25,41	0,999739		4	25,45	0,999913
	5	28,55	0,99375		5	28,62	0,999791
3	1	27,36	0,999822	6	1	22,49	0,998926
	2	18,84	0,999938		2	27,55	0,999930
	3	25,77	0,999962		3	24,16	0,999904
	4	26,87	0,99969		4	26,11	0,999776
	5	27,36	0,999677		5	27,67	0,999726

The plates were then placed in the bin in the order 1,2 and 3 from top to bottom on the left hand side and 4,5 and 6 on the right hand side. The slope of each side was 30° to the vertical. The bin was sealed and readings were taken at five depths of water. The object of the test was to check the method of calibration.

The readings and pressures are tabulated in Appendix B and are plotted in Fig. 2.. The calculated pressures are shown by the straight solid lines. It can be seen that some of the values, particularly on the left hand side are quite far from the line.

In view of this rather unsatisfactory result it was decided to use test 25 itself as the calibration. The difference between this and the previous calibration was that the plates would be in their positions in which they would be when loaded with sand. It is true that the spans on the highest plates would have fewer points on their calibrations but this is not too important because the pressure will be lower near the top under sand anyway. Thus each circuit in top plates 1 and 4 has only two points on its calibration curve. Table 2.5 gives the calibration from test 25 that was finally used. Fig. 2.10 shows the comparison between calculated water pressures and the results from test 25. The fit is far more satisfactory than before.

2.8 Calibration of load

The strain gauges on the four C shaped bending elements placed under each leg were connected to form a single bridge circuit, as mentioned earlier. For calibrations the four elements were loaded in parallel in a testing machine. The voltage supplied to the bridge was adjusted to make 1 microvolt correspond as closely as possible to a newton. The results are shown in table 2.6.

Table 2.5 Calibration for normal pressure using test 25 (water pressure)

Plate	Span	Slope Pa/μV	Correlation Coefficient	Plate	Span	Slope Pa/μV	Correlation Coefficient
1	1	26,19	-	4	1	19,62	-
	2	23,82	-		2	22,74	-
	3	17,34	-		3	23,30	-
	4	28,67	-		4	24,85	-
	5	20,71	-		5	19,62	-
2	1	26,48	0,998650	5	1	31,48	0,999978
	2	24,19	0,999354		2	30,29	0,999924
	3	22,48	0,999810		3	38,48	0,999491
	4	22,20	0,999823		4	24,69	0,999863
	5	21,06	0,999971		5	30,57	0,999972
3	1	24,52	0,999980	6	1	22,54	0,999792
	2	18,22	0,999982		2	26,90	0,999760
	3	25,42	0,999989		3	23,58	0,999895
	4	23,16	0,999981		4	27,58	0,999895
	5	23,21	0,999997		5	26,20	0,999931

Note Bridge voltage = 2,0 in all cases

Table 2.6 Calibration of load cells with bridge voltage = 2,735

Load N	Reading μV
0	0
500	502
1000	994
1500	1487
2000	1971
2500	2518
3000	2997
3500	3496
4000	3972
0	3

Slope = 1,0031 N/μV

Correlation coefficient = 0,999946

2.9 Summary

Table 2.1 summarises the measured properties of the sand. The largest wall friction angle obtained was 20,1° from the triaxial test with a steel plate at 45°. This was the value used in the calculations because the values obtained from the actual tests, table 3.3 for bin 1 and table 3.6 for bin 2 were greater (21,0° and 23,4° respectively). The greater values for the bin (assuming that they were not a result of error in measurement) could be due to the indentations at close centres (39 x 40mm) where the countersunk screws attach the sheet to the ribs. The glass friction angle of 9,1° shows that the end walls have some effect on the bin but much less than if they were made of steel.

The bin with glass end walls is intended to represent a two-dimensional stress state. Normal and shear stresses can be measured. The walls can be inclined at various angles. Sand is poured in from above and is let out in controlled amounts at a 30mm wide outlet running the full width of the bin. Satisfactory calibration for normal pressures was carried out by lining the bin with plastic and filling it with water. Calibration for shear stress was achieved with a shear force applied to each plate while supported on a calibration frame. The total weight in the bin is measured by four load cells. Sand is caught under the bin with an auxilliary bin which is lifted above the model to discharge into it uniformly over the full width. Readings of wall stresses are recorded on a data logger while the glass is marked with a grid so that the sand surface can be plotted.

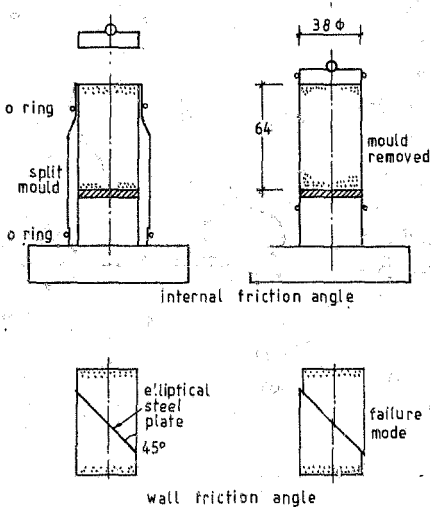

Figure 2.1 Triaxial tests on sand

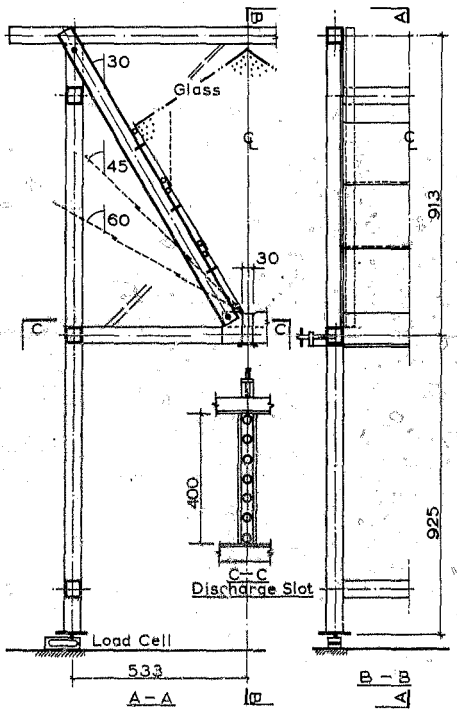

FIGURE 2.2 Overall view of the apparatus

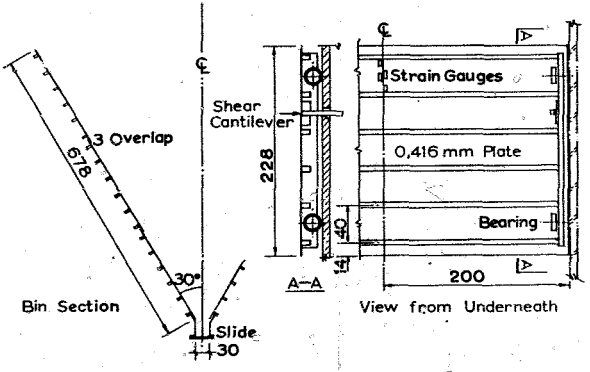

FIGURE 2.3 Details of slide plate

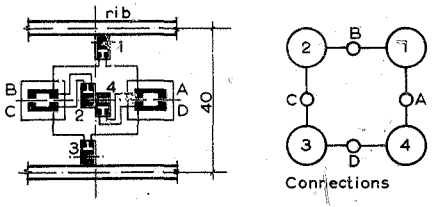

FIGURE 2.4 Strain gauge arrangement for normal stress measurement

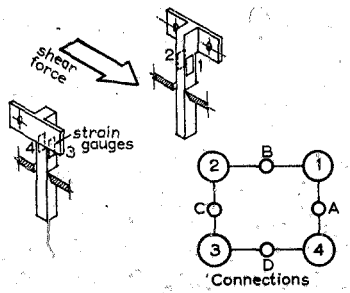

FIGURE 2.5 Strain gauge arrangement for shear measurement

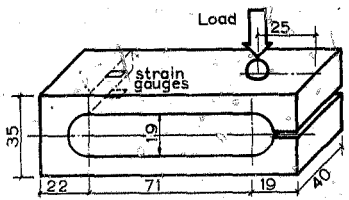

FIGURE 2.6 Cell for measuring bin load

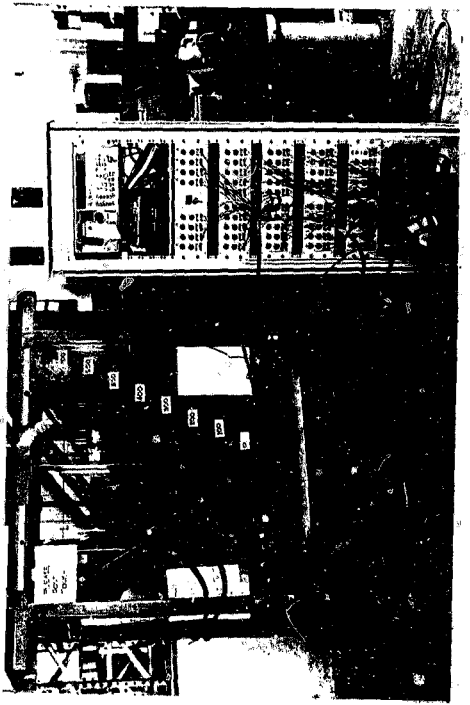

Figure 2.7 Data logger and test apparatus

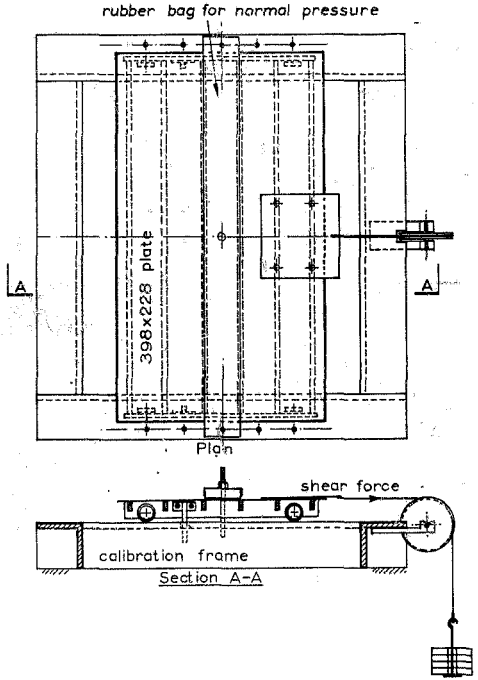

FIGURE 2.8 Calibration for shear and calibration for normal pressure with rubber bag

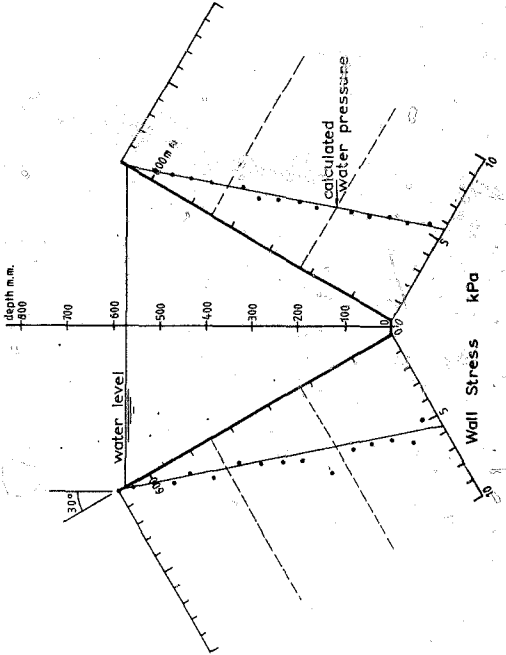

FIGURE 2.9 Test 25 . Water pressure to check calibration

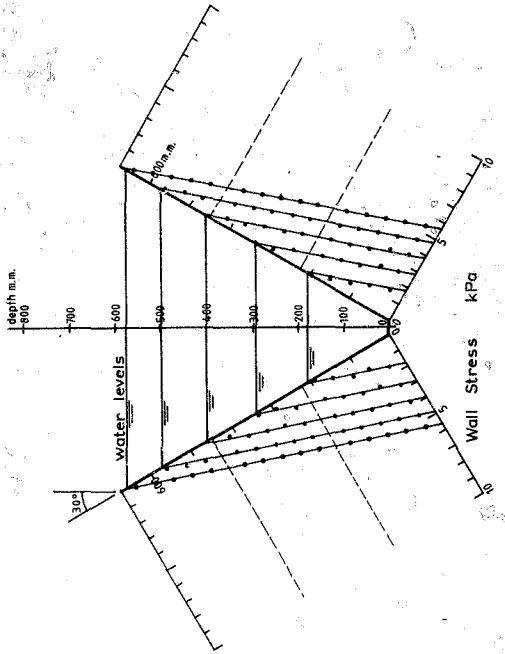

FIGURE 2.10 Test 25 with calibration from test 25

CHAPTER 3

TESTS

3.1 Test procedure

Two different bin shapes were tested, Fig.3.1. Shape 1 had straight sides sloping at 30° to the vertical. Shape 2 had a vertical side, AB, formed from one plate and a sloping bottom, BC, formed from two plates at 30° to the vertical. In each test several sets of 37 readings were taken on the data logger. Before each set, sand was either added to the bin or let out from it. Thus test 20, set 5, refers to the fifth set of readings taken in test 20.

The raw data was processed by a computer program which subtracted the initial reading from the reading for that set. This value in microvolts was then multiplied by the appropriate calibration constant to produce either a normal stress or a shear stress. There were five normal stresses measured on each plate and one average shear stress. For each set, depths of sand were recorded at horizontal intervals of 100mm. These were used to calculate the volume, and with the measured weight the average density for the set. The weight was also calculated from the measured wall stresses. This was always less than the weight determined by the load cells under the legs of the bin. The difference must be due to the friction on the glass end walls and the upward pressure at the 30mm wide outlet. The stresses were therefore increased by the ratio of measured to summed weight so that direct comparisons could be made with theory. The friction on the glass was also evident during discharge as the surface dropped slightly more between th glass ends than at them.

3.2 Tests on bin of shape 1

Six tests were conducted. These were tests 20, 21, 22, 23, 24 and 26. The experimental readings are given in Appendix C1 and the derived factors and stresses in Appendix C2. Table 3.1 summarises the ratios of measured to summed weight for tests 20 to 25. The average ratio is 1,24. Density values are summarised in table 3.2.

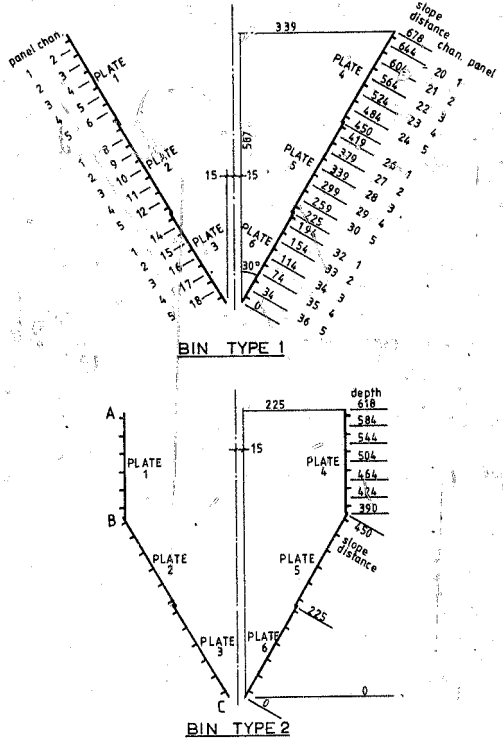

Figure 3.1 Bin shapes, dimensions, and data logger channels

Table 3.1 **Ratios of Measured Weight to summed weight for tests 20 to 24**

Test / Set	20	21	22	23	24
2F	1,32	1,52	1,0	1,4	1,37
3F	1,17	1,19	1,11	1,24	1,12
4F	1,26	1,23	1,17	1,24	1,22
5E	1,28	1,12	1,16	1,29	1,20
6E	1,23	1,18	1,16	1,31	1,22
7E	1,28	1,23	1,23	1,33	1,26
8E	1,23	1,28	1,25	1,31	1,30
9E	1,24	1,24	1,20	1,24	1,32
10E	1,16	1,24	1,19	1,19	1,23
11E	1,09	1,20	1,11	1,31	1,18
12E		1,26			

F = filling E = emptying Average = 1,24

Standard deviation = 0,08

Table 3.2 Summary of Densities for Tests 20 to 24 (kg/m³)

Test / Set	20	21	22	23	24
2F	1566	1672	1472	1723	1606
3F	1580	1591	1534	1655	1559
4F	1608	1533	1571	1649	1594
5E	1611	1549	1571	1652	1593
6E	1531	1594	1584	1664	1604
7E	1609	1592	1584	1557	1606
8E	1615	1630	1584	1661	1605
9E	1620	1611	1583	1638	1617
10E	1616	1628	1606	1632	1599
11E	1617	1612	1577	1532	1582
12E		1736			1595

F = Filling E = Emptying; Average 1602 kg/m³

Standard deviation 43 kg/m³

There is quite a random variation in density. For example, from set 4 to set 5 density should decrease as the mass loosens up to discharge, but the values change in the reverse direction. This could be mainly due to difficulty in estimating the average surface height at each point, especially during emptying when due to friction the surface is higher next to the glass than it is in between. The average value of 1602 kg/m³ lies between the extreme values from sample tests given in table 2.1.

Friction angles are tabulated for each of the six plates for each test. Some of the values are very different from the rest. In three cases there is no load on the plates and should be ignored. For set 2 the sand covers the lower plate, for set 3 the second plate, and set 4 fills the bin. Average friction angles for all loaded plates are shown in table 3.3.

Table 3.3 Average Wall Friction Angles for tests 20 to 24 (Degrees)

Test / Set	20	21	22	23	24
2F	18,0	18,8	16,4	18,6	17,2
3F	20,6	21,2	19,1	21,8	19,2
4F	20,0	20,7	18,6	21,9	19,1
5E	20,6	18,8	18,9	21,7	19,3
6E	19,9	18,8	18,8	21,8	19,4
7E	21,2	19,4	19,4	22,1	19,6
8E	22,8*	20,3	19,4	21,9	20,0
9E	24,3	22,0*	21,9*	23,2	21,1
10E	24,6	22,4	22,2	22,5	22,1*
11E	26,4	26,7	22,5	24,3	22,4
12E		24,2			27,4

F = Filling E = Emptying

* Visible sliding on walls noticed

Average before visible slip = 19,8°

Average after visible slip = 23,6°

Overall Average = 21,0

There is quite a wide scatter with a marked difference between the average before visible slip (19,8°) and after (23,6°). The overall average is 21°. This compares with the laboratory value of 20,1° from table 3,1.

Several graphs have been plotted showing the wall stresses and surface levels. Figs. 3.2 to 3.11 show the normal wall pressures for filling and emptying for tests 20 to 24. Filling and emptying pressures have been shown separately. In a typical case, Fig. 3.2, during filling normal stresses increase from zero at the surface to a maximum near the bottom, then there is a slight decrease at the lowest point. The pressure curve is not linear but bulges outward. The surface has a flatter slope in the first set than in the third where it is at the angle of repose. The flatter slope is due to the impact of the falling grains which fall further for set 1 than for set 3. At the start of discharge, Fig. 3.3., set 5, the pressure drops almosts to zero at the bottom and increases halfway up. Then as the surface drops the pressure gradually decreases. The surface flattens out and becomes lower in the centre showing faster movement there than at two walls. The pressure graph for each set is not smooth and slopes change considerably locally.

Sometimes local peaks form, for example, test 22, Fig 3.6. Two corresponding peaks formed on either side just where the upper plate overlaps the lower. This suggests that the slight steps tend to act as arch abutments. The local peaks remained imprinted on the emptying diagram, Fig. 3.7. In tests 23 and 24, Figs. 3.8 to 3.11, peaks formed at the lower laps only.

The maximum filling and discharge pressures for each test are compared in [illegible] to 3.16. Average shear stresses are also shown. In [illegible] there is a marked difference between filling and emptying. Notice the shear stresses increase towards the bottom in filling and then decrease on the bottom plate and increase on the middle plate for emptying. The very slight drop in surface level show that the graphs should have approximately the same areas.

The normal filling pressures and the surface levels for tests 20 to 25 are compared in Fig. 3.17. It can be seen that apart from the peaks there is close agreement. The normal emptying pressures for tests 20 to 24 are compared in Fig 3.18. Again there is close agreement except for the peaks.

3.3 Attempt to detect switch pressure in bin of shape 1

An attempt was made in test 26 to detect the switch pressure postulated by Jenike [22]. Fig. 3.19 shows the usual normal pressures during filling. Fig. 3.20 shows the last filling set and sets 5, 6 and 7 during emptying. Fig 3.21 shows sets 7 to 10 during emptying. Before each emptying set only 1 kg of sand was discharged. There is a sudden change from filling to emptying pressures from set 4 to set 5 (Fig. 3.20). Thereafter to set 10 there is a gradual change further towards the emptying distribution between sets. There is no evidence of a large point load moving down the bin as postulated in the switch theory, Fig. 1.17.

3.4 Tests on bin of shape 2

Five tests, 27 to 31, as nearly identical as possible were conducted on shape 2. For set 1 the bin was empty, and for set 2 it was completely full. Intermediate filling cases were left out as they would be the same as for shape 1. The experimental readings (raw data) are given in Appendix D1 and the derived factors and stresses are given in Appendix D2.

The ratios of measured to summed weight are summarised in table 3.4. The average is 1,18 and is less than the average of 1,25 for shape 1, table 3.1. Density values are summarised in table 3.5. At 1596 kg/m^3 the average is less than that for bin 1 at 1602 kg/m^3. In view of the size of the standard deviation which is 43 kg/m^3 for shape 1 and 24 kg/m^3 for shape 2, the difference is not significant.

The measured wall friction angles are given in table 3.6. It was found that the friction angle was greater when movement was noticed in bin 1, table 3.3. The friction angle for bin 2 averages 26,1° on the vertical walls and 22,1 on the sloping walls, with an overall average of 23,4° compared to the overall average of 21° for bin 1. The higher value for bin 2 is caused by its shape with vertical walls which mobilise friction more effectively.

Table 3.4 Ratios of Measured Weight to Summed Weight for tests 27 to 31

Test S	27	28	29	30	31
2F	1,21	1,17	1,23	1,18	
3E	-	1,18	1,13	1,21	1,15
4E	-	1,19	1,14	1,20	1,16
5E	-	1,18	1,14	1,20	1,16
6E	1,19	1,19	1,14	1,21	1,20
7E	1,17	1,19	1,16	1,22	
8E	1,15				
9E	1,12				

F = Filling E = Emptying Average = 1,18
Standard deviation = 0,03.

Table 3.5 Summary of Densities for tests 27 to 31 (kG/m³)

Test / Set	27	28	29	30	31
2F	1607	1599	1573	1585	1578
3E	1599	1589	1585	1579	1566
4E	1615	1606	1584	1604	1579
5E	1612	1614	1581	1605	1592
6E	1623	1607	1596	1606	1601
7E	1622	1629	1593	1610	
8E	1621				
9E	1673				

F = Filling E = Emptying Average = 1596 kg/m³

Standard deviation = 24 kg/m³

Table 3.6 Average Wall Friction Angles for tests 27 to 31 (Degrees)

Test / Set	27	28	29	30	31
2F	23,2	22,4	21,8	22,9	23,9
3E	23,2	22,9	22,2	24,1	23,9
4E	23,2	23,1	22,5	23,3	24,0
5E	23,5	22,4	22,4	23,1	23,5
6E	23,6	22,8	22,0	23,2	24,6
7E	25,8	22,9	22,5	23,0	
8E	29,7				
9E	23,9				

Average on vertical sides = 26,1°

Average on sloping parts = 22,1

Overall average = 23,4°

Figs. 3.23 to 3.32 show experimental pressures and surface levels for the five tests 27 to 31 on bin shape 2. For test 27, Fig. 3.23, a full bin set 2, has a surface sloping at the angle of repose and an almost linear increase of pressure down from the surface on the vertical walls. On the sloping walls the pressure increases almost linearly, decreasing in a slight curve from the line at the top and bottom of the slope. At the start of emptying, set 3, there is no detectable drop in the surface but marked changes in pressure. On the vertical walls the shape is unchanged but pressures increase. On the sloping walls there is a complete change in shape. The pressure drops to near zero at the outlet and then increases up the slope to cross the filling line and then decreases a bit at the top of the slope. As discharge proceeds, the surface drops, sets 3 to 6 and there is a gradual increase in pressure on the vertical walls without much change in shape, to about 50% more than the filling case, set 2. The pressures on the slopes change slightly with further discharge. Some oscillation is evident. Fig. 3.24 shows the change in pressures as the surface level drops eventually to the wall junction. The surface flattens out and eventually slopes towards the centre showing faster movement there. It was noticed through the glass that a central column of 250mm width moved downwards with little noticeable movement outside it. As the surface drops the pressures on the vertical wall decrease. On the lower parts of the walls the pressures remain virtually unaltered but pressures reduce at the top as the surface drops, until they are zero when the surface is at the junction of sloping and vertical wall. Through all the tests, Figs. 3.23 to 3.32, no pressure peaks were formed as for shape 1.

Maximum filling and emptying pressures are compared for tests 27 to 31 in Figs. 3.33 to 3.37. Shear stresses are also shown. A marked difference, Fig. 3.33, can be seen between filling and emptying. There is a big increase in pressure on the vertical walls. There is also an increase in shear stress. There is a big change in pressure distribution on the sloping walls. The pressure increases at the top of the slope and drops almost

to zero at the bottom. The shear stress changes from a maximum at the bottom of the slope to a maximum at the top.

Maximum filling pressures are compared in Fig. 3.38. There is very close agreement. A slight assymmetry is evident between sides which shows a small inadequacy in the measuring system. Pressures increase almost linearly on the vertical walls down from the surface. Pressures on the bottom are almost linear, dropping off slightly at the top and bottom of the slope. Maximum emptying pressures are compared in Fig. 3.39. There is excellent agreement on the vertical walls and evidence of some oscillation on the sloping walls although agreement is good. Again slight assymmetry is evident.

On the vertical walls pressures increase almost linearly and are about 50% greater than for filling, Fig. 3.38. Pressures are small at the bottom of the slope and increase almost linearly at first to reach a maximum at about 70% of the slope length and then decrease a bit at the top of the slope.

3.5 Attempt to detect switch pressure in bin of shape 2

Test 31 was used for this purpose. Fig. 3.30 shows the filling condition, set 2, and the start of emptying, sets 3 to 6. Very small amounts of sand were discharged between each set, about 1 kg at a time. There is a measureable difference in pressures between sets 3 to 6, with some oscillation lower down. Fig. 3.31 continues to monitor very small changes for additional discharge. Fig. 3.32 shows large drops in surface level and eventual decrease in pressure. No switch pressure in the form of a moving point load was detected as postulated by Jenike [22], Fig. 1.17.

3.6 Summary

In this chapter the experimental results are given. In the tests for each bin shape reasonable agreement was obtained between five tests for filling and emptying. There was a marked difference between filling and emptying pressures and no switch pressure could be detected. Even an outflow of only 1kg of sand would cause a large change from filling to emptying pressures over the whole wall without any switch pressure. Densities and wall friction angles were in reasonable agreement with values measured on samples.

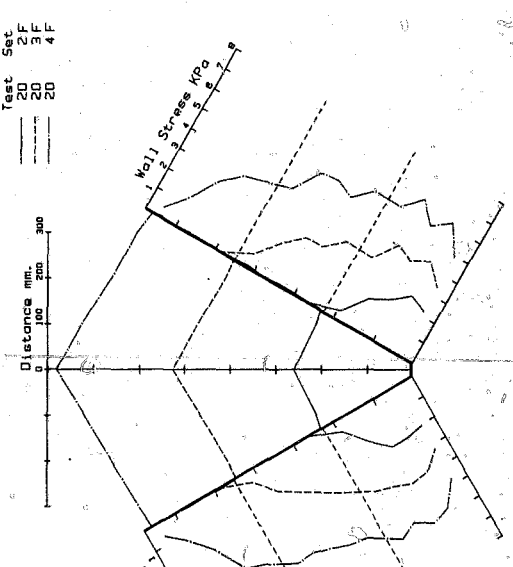

Figure 3.2 Test 20 : Filling

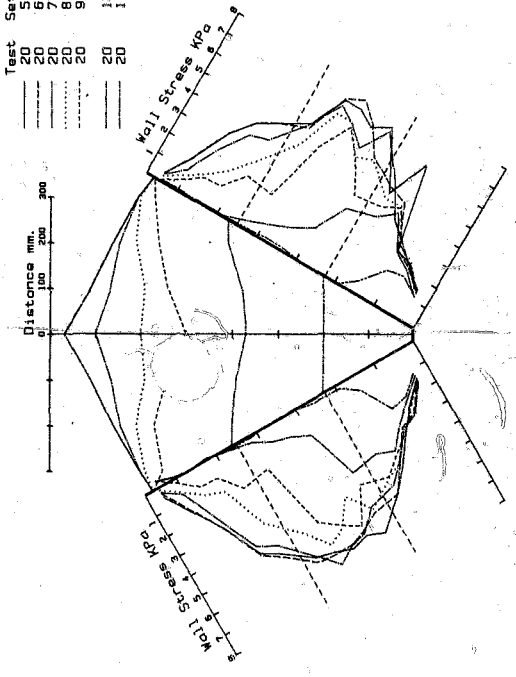

Figure 3.3 Test 20 : Emptying

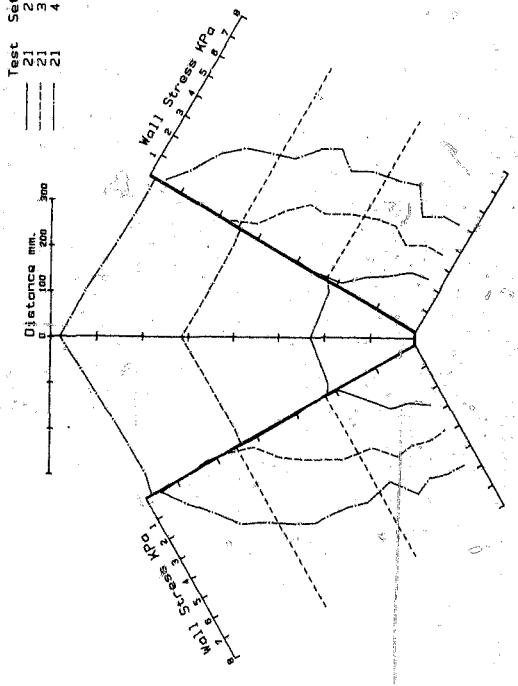

Figure 3.4 Test 21 : Filling

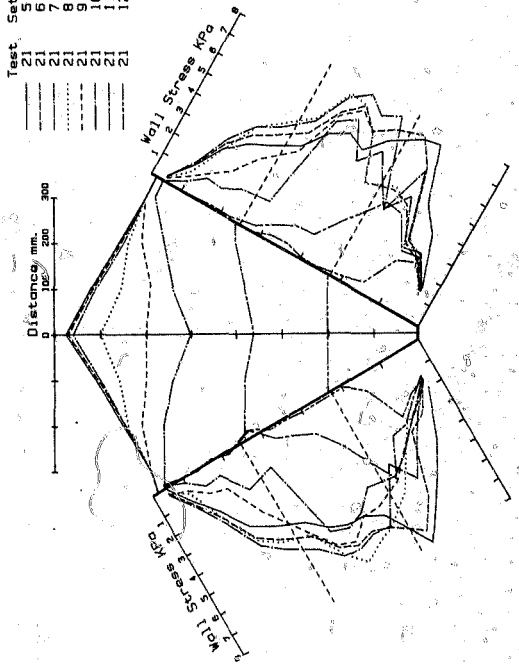

Figure 3.5 Test 21 : Emptying

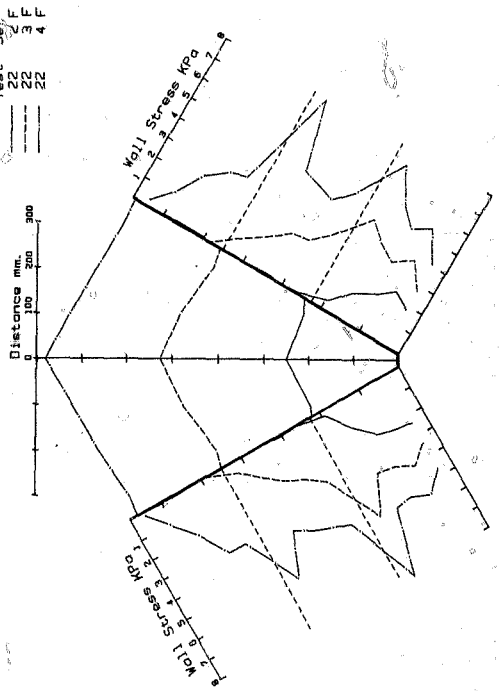

Figure 3.6 Test 22 : Filling

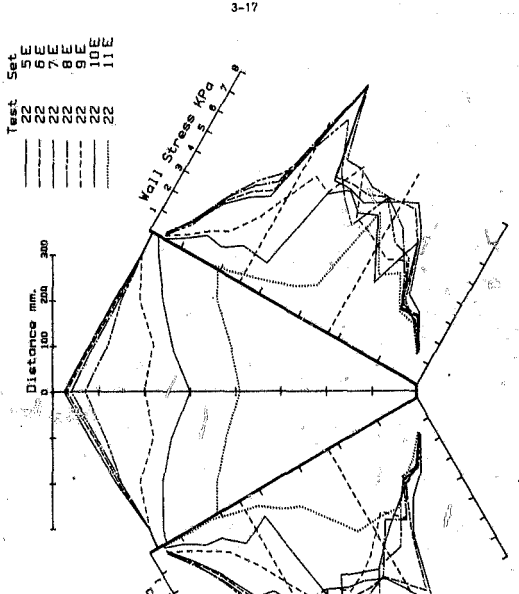

Figure 3.7 Test 22 : Emptying

Figure 3.8 Test 23 : Filling

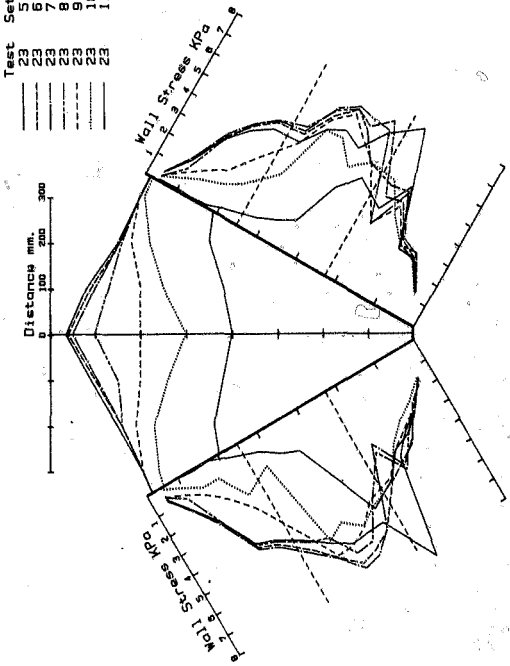

Figure 3.9 Test 23 : Emptying

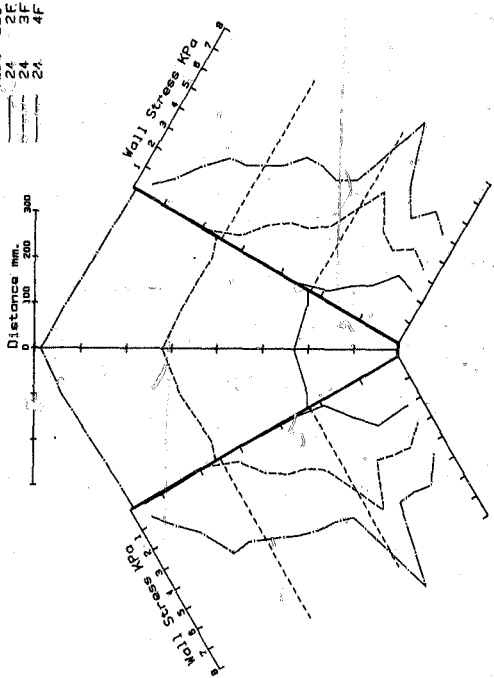

Figure 3.10 Test 24 : Filling

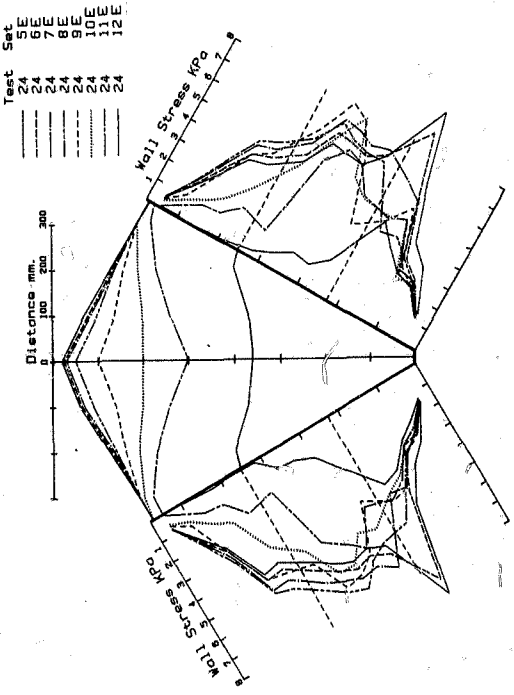

Figure 3.11 Test 24 : Emplying

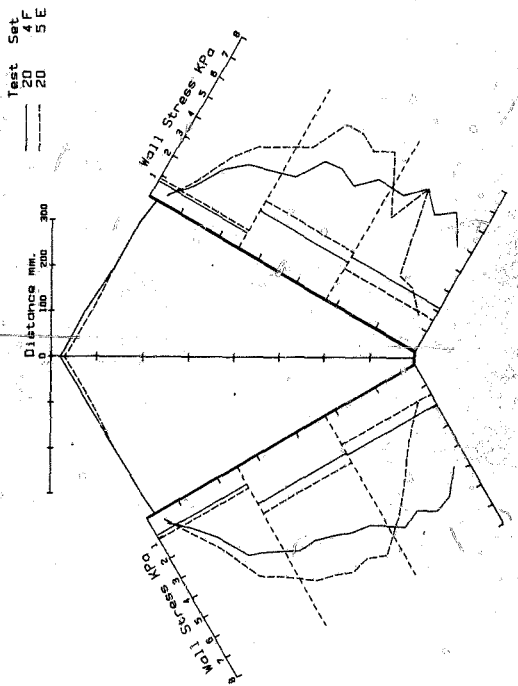

Figure 3.12 Test 20 : Filling and emptying

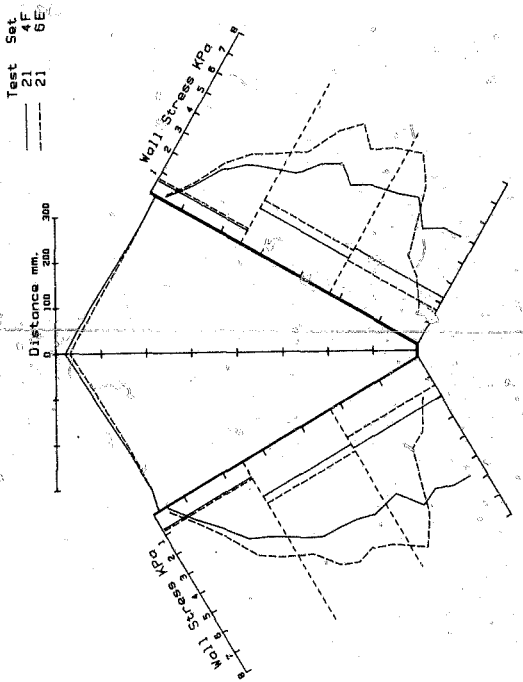

Figure 3.13 Test 21 :Filling and emptying

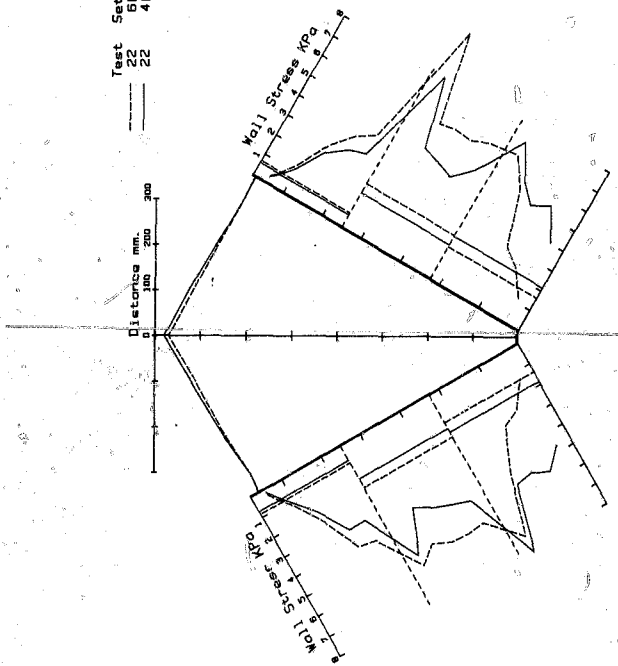

Figure 3.14 Test 22:Filling and Emptying

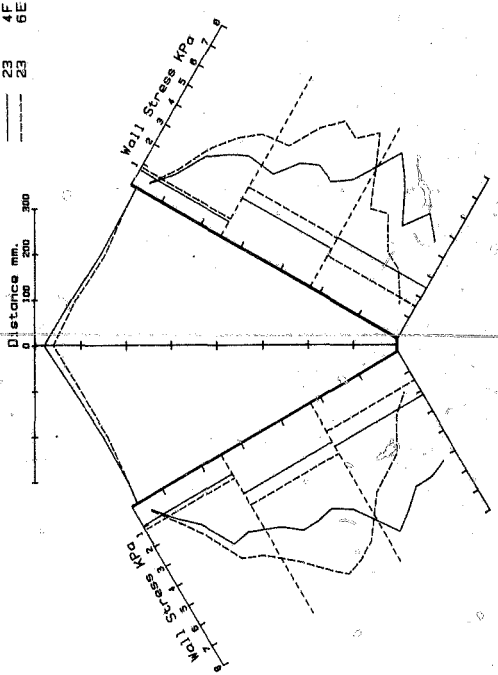

Figure 3.15 Test 23 : Filling and emptying

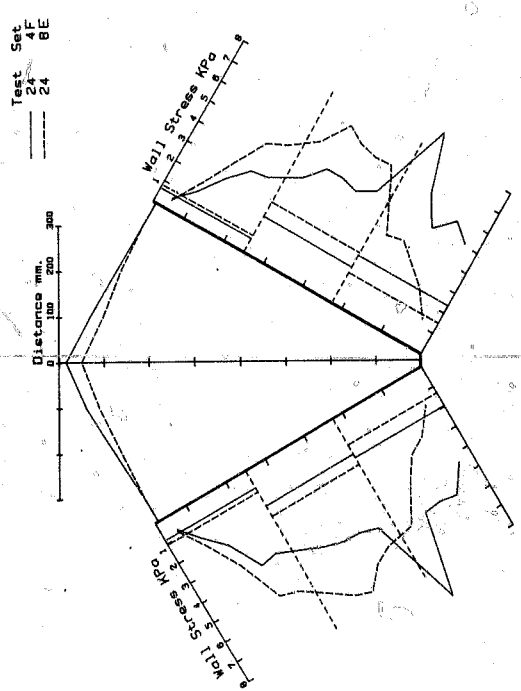

Figure 3.16 Test 24 : Filling and emptying

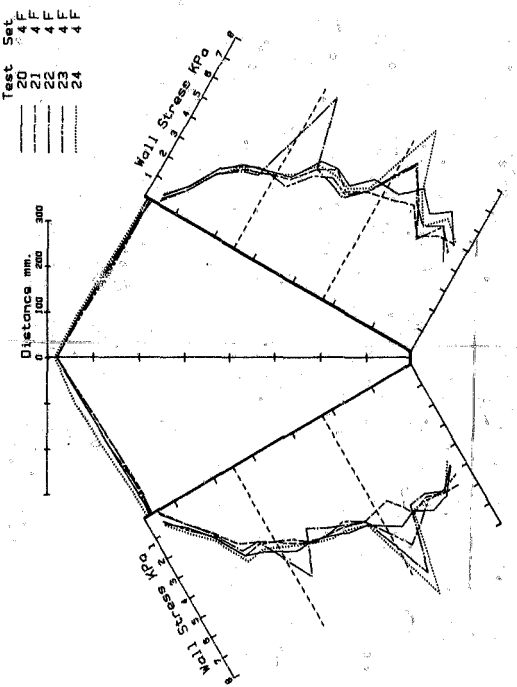

Figure 3.17 Comparison of tests 20 to 24 : Filling

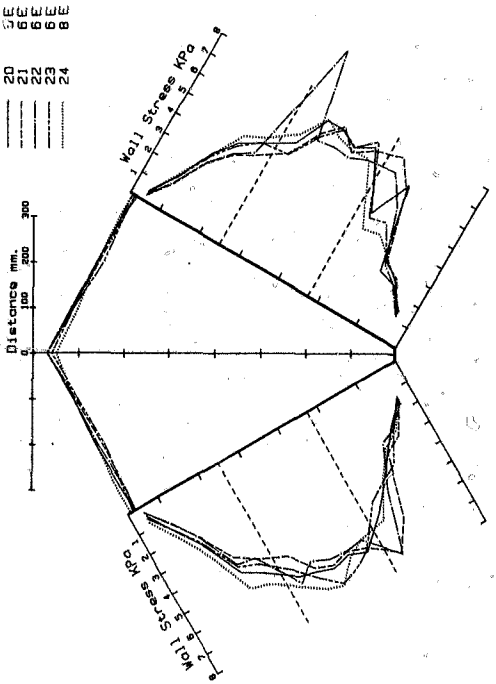

Figure 3.18 Comparison of tests 20 to 24: Emptying

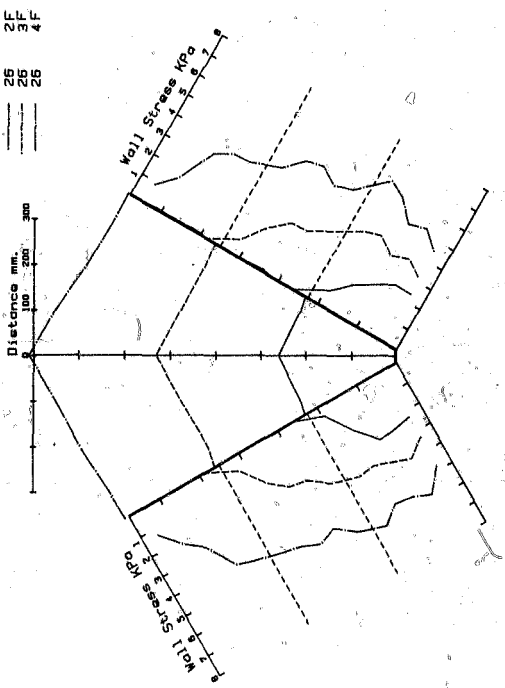

Figure 3.19 Test 26 : Filling

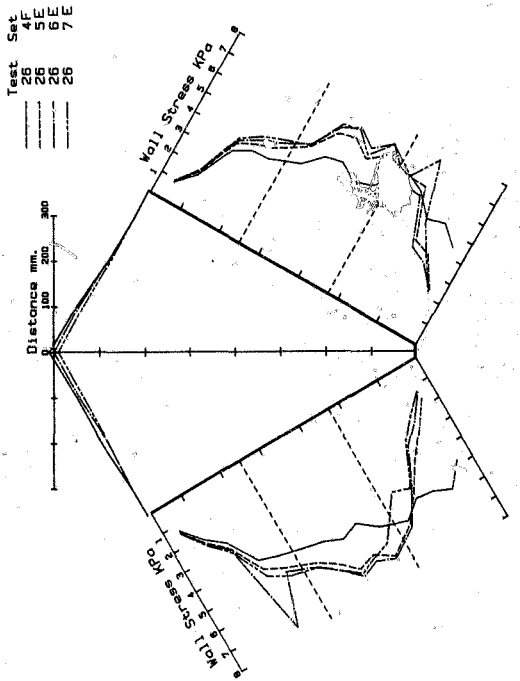

Figure 3.20 Test 26 : Switch pressure detection (1)

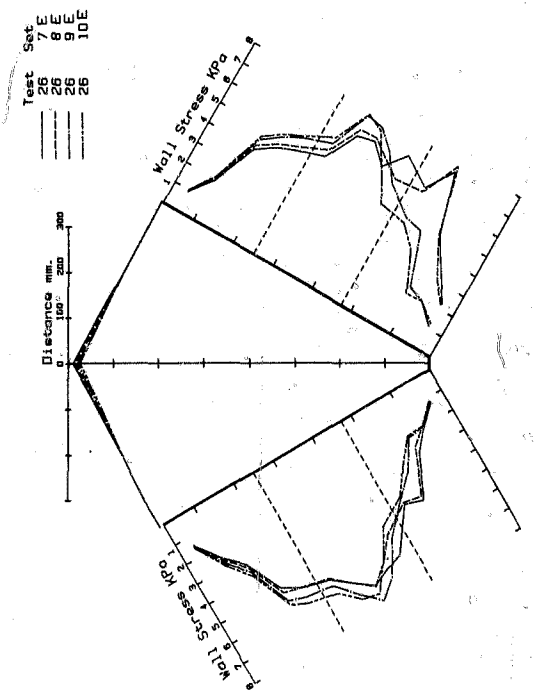

Figure 3.21 Test 26 : Switch pressure detection (2)

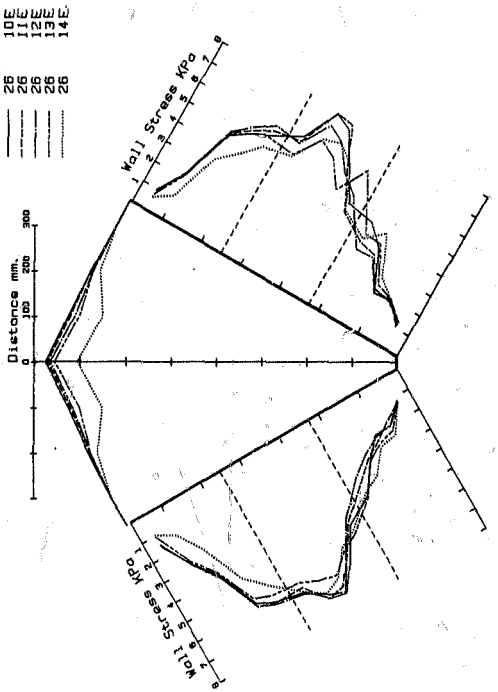

Figure 3.22 Test 26 : Switch pressure detection (3)

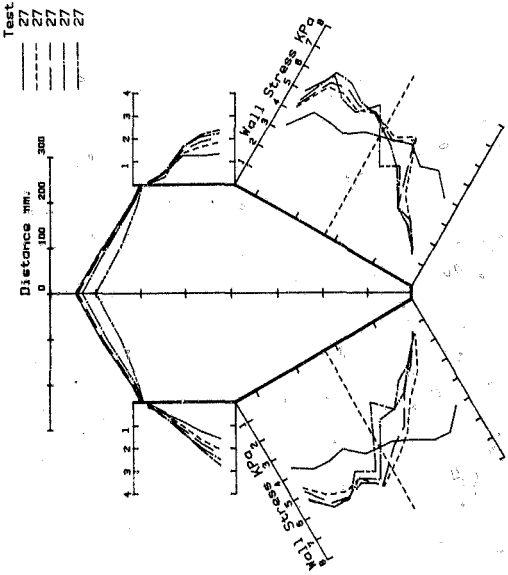

Figure 3.23 Test 27 (1)

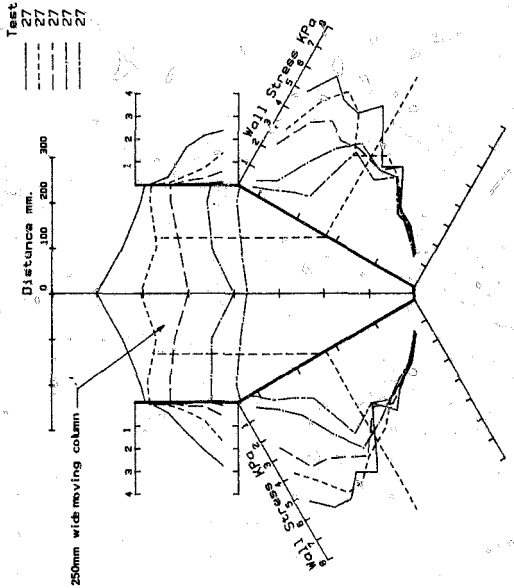

Figure 3.24 Test 27 (2)

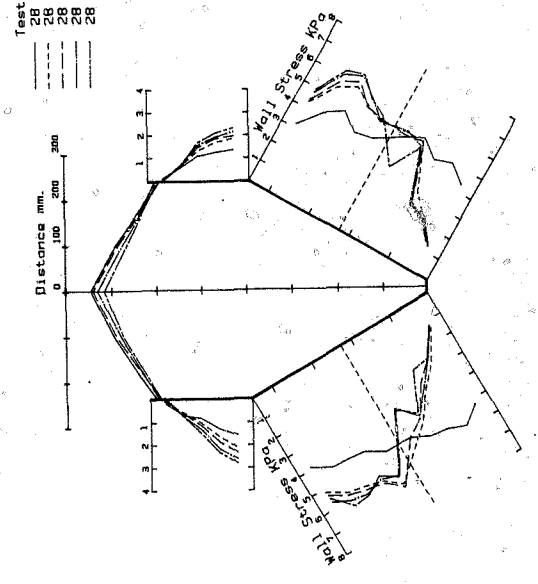

Figure 3.25 Test 28 (1)

Figure 3.26 Test 28 (2)

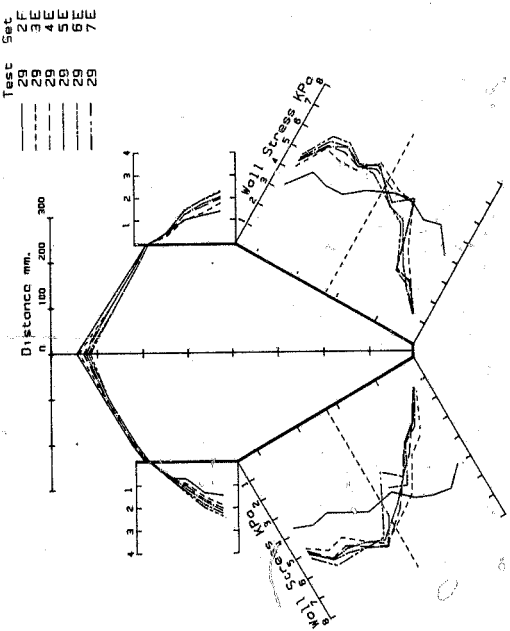

Figure 3.27 Test 29 (1)

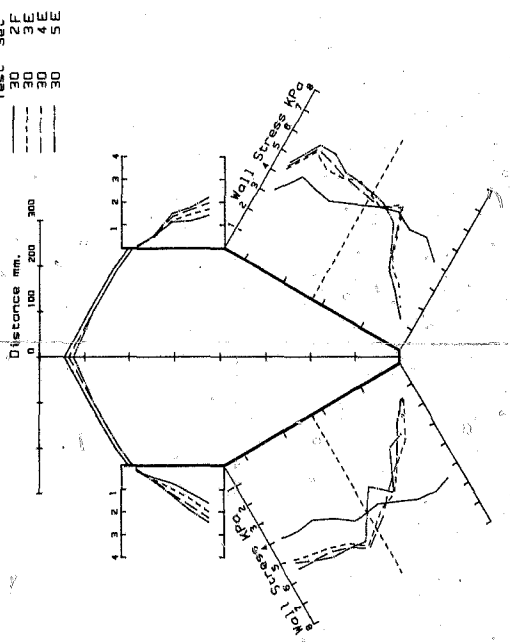

Figure 3.28 Test 29 (2)

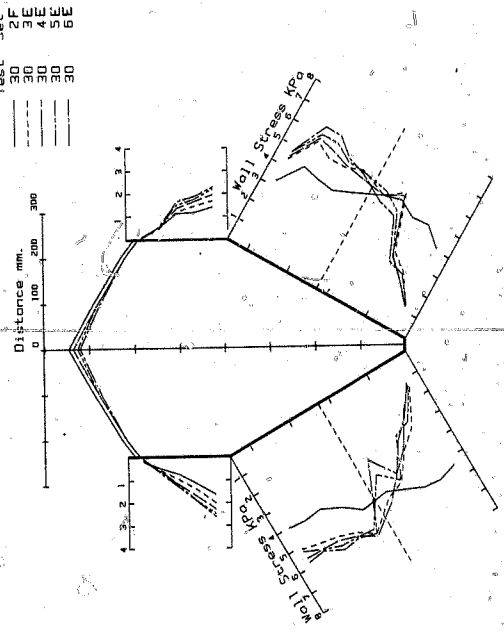

Figure 3.29 Test 30 (1)

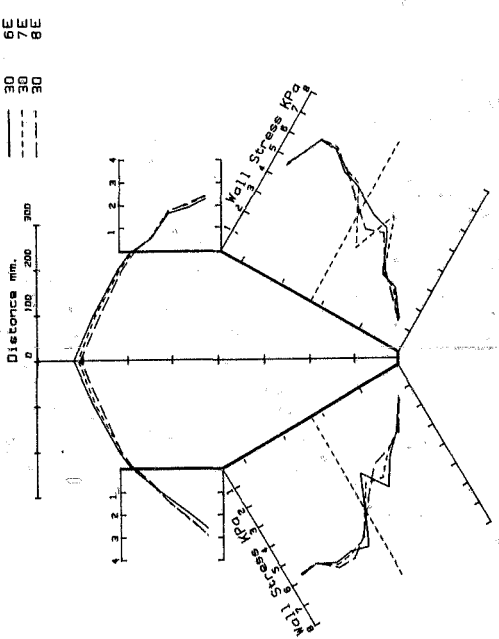

Figure 3.29 A Test 30 (2)

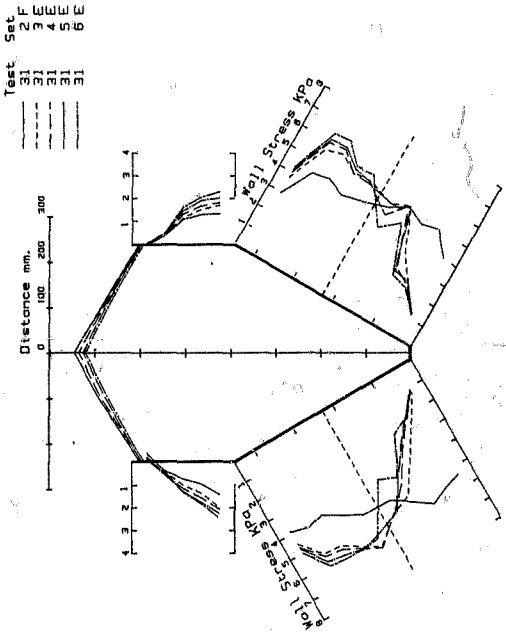

Figure 3.30 Test 31 (1)

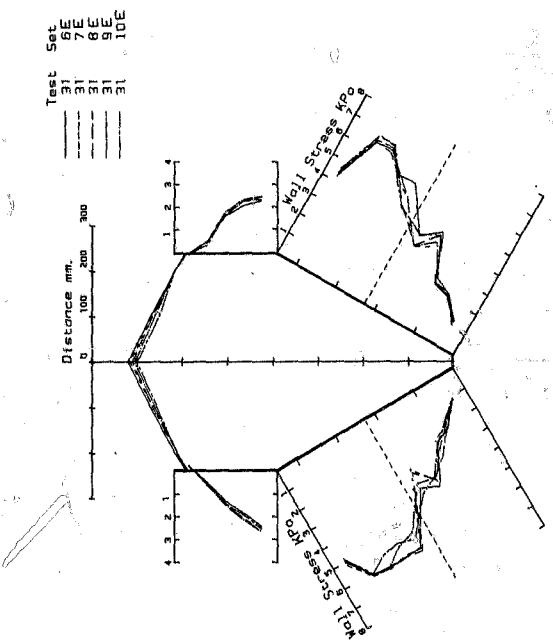

Figure 3.31 Test 31 (2)

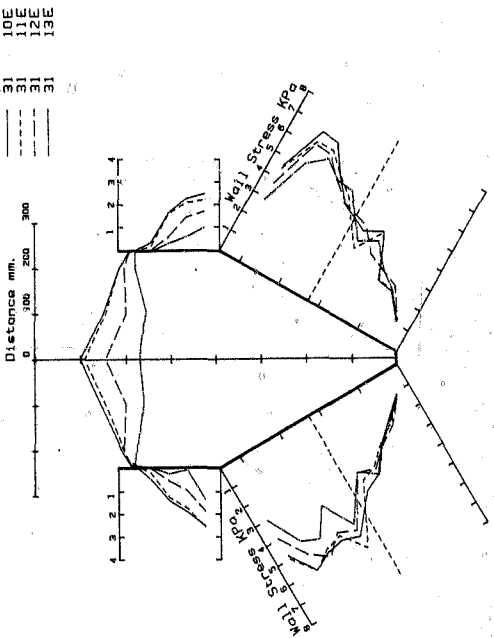

Figure 3.32 Test 31 (3)

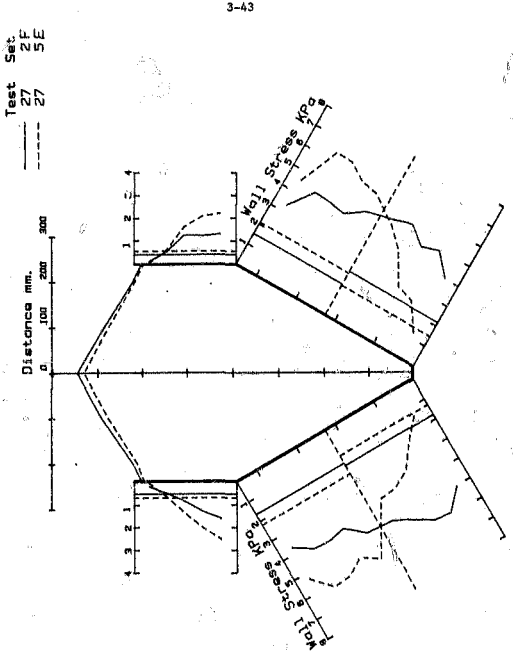

Figure 3.33 Test 27 : Filling and emptying

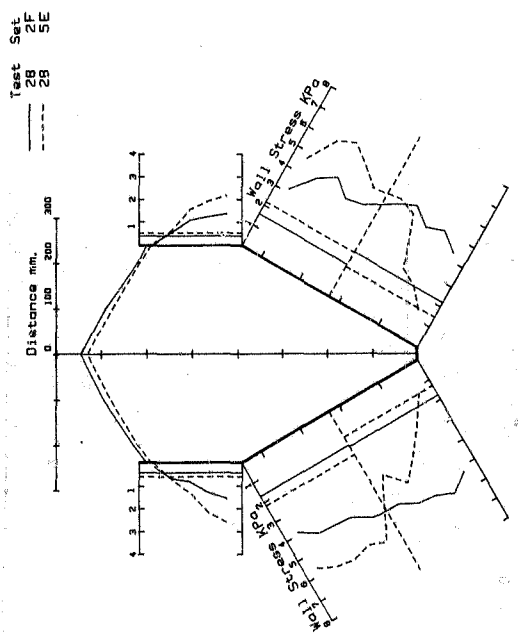

Figure 3.34 Test 28 : Filling and emptying

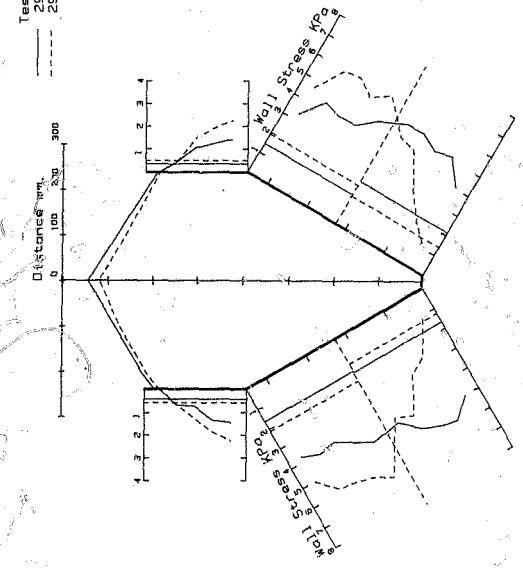

Figure 3.35 *Test 29 : Filling and emptying*

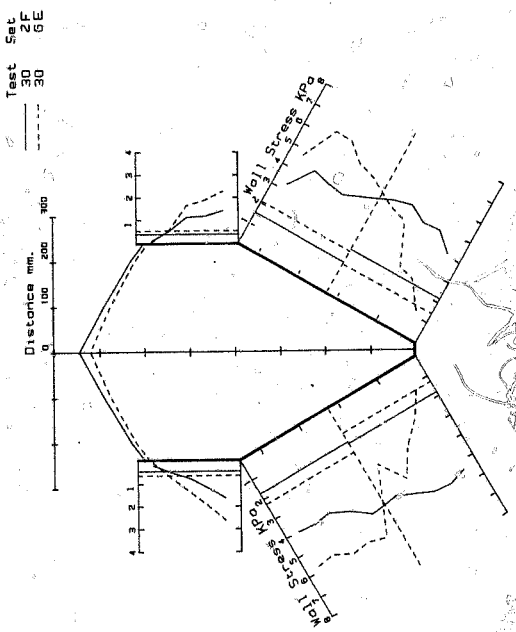

Figure 3.36 Test 30 : Filling and emptying

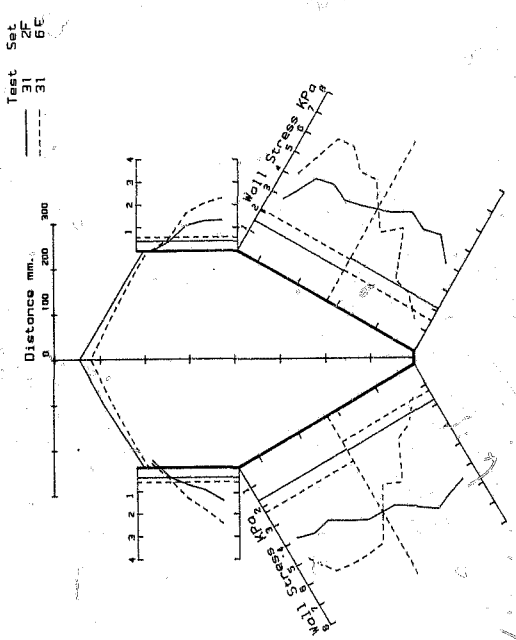

Figure 3.37 Test 31 : Filling and emptying

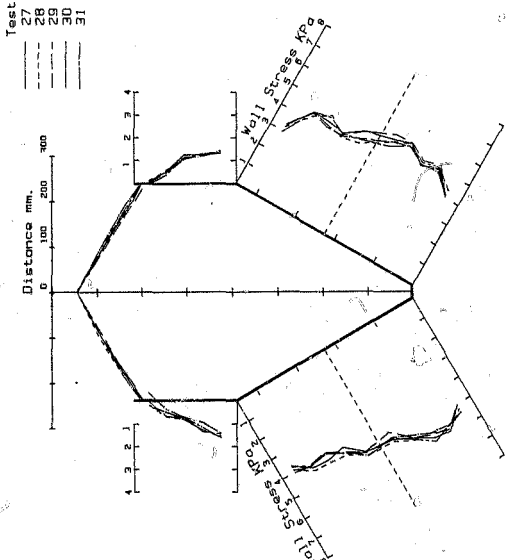

Figure 3.38 Tests 27 to 31 : Comparison of filling pressures

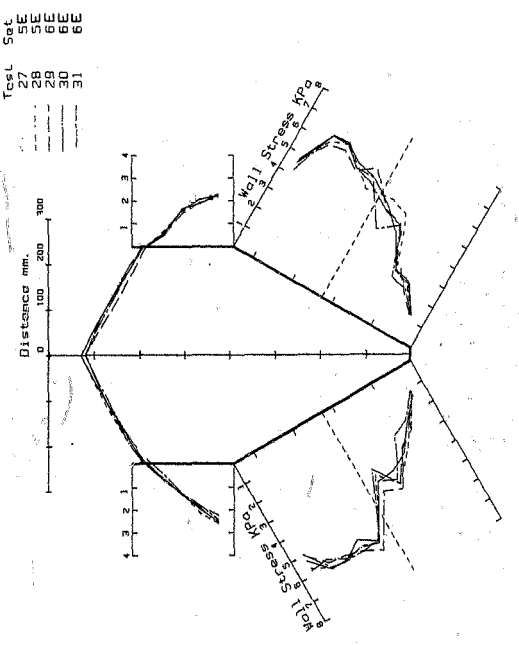

Figure 3.39 Tests 27 to 31 : Comparison of emptying pressures

CHAPTER 4

THEORETICAL PRESSURE DISTRIBUTIONS - BIN 1

4.1 Methods for analysing pressures

A distinction is made between methods applied to the filling case and methods applied to the emptying case. All the methods have this in common : they are simple and easily applied. For reference each analysis is given a number with a prefix F for filling and E for emptying. Numbers for bins 1 and 2 may not necessarily be the same.

4.2 Geometry for filling

For bin 1, five tests, 2o to 24, were combined for comparison with the various theories. Fig. 4.1 shows the configuration and table 4.1 shows the derivation of the average values.

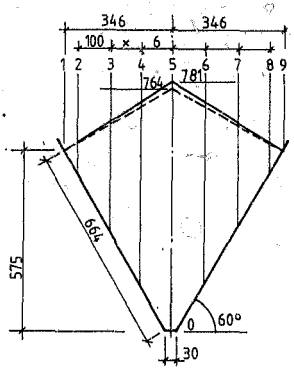

Figure 4.1 : Dimensions for analysis

Table 4.1 Values for Bin 1 to be used in Analysis of Filling

Average density = (1608+1533+1571+1649+1594)/5 = 1591 kg/m³
Note: It was decided to use the overall average value from table 3.1 of γ = 1602 kg/m³ = 15716 N/m³

Surface heights mm

Test	Set	Position 1	2	3	4	5	6	7	8	9
20	4	520	600	660	720	780	725	660	605	570
21	4	575	590	650	715	780	725	660	600	575
22	4	570	590	660	720	780	725	665	605	580
[illegible]	[illegible]	575	595	650	715	780	720	655	600	575
[illegible]	[illegible]	580	610	675	740	785	730	670	610	[illegible]
Average		564	596	659	722	781	725	662	604	57[illegible]
Average both sides						781	723	660	600	570

Surface slope = $\alpha = \tan^{-1}\left(\frac{781 - 600}{300}\right)$

= 31,1° (compare with 31,0° table 2.1)

Contained weight = 15716 × (0,807 × 0,344 − 0,015 × 0,026)

= 4357 N per metre width

4.3 Filling pressures - bin 1

4.3.1 *Active state pressure*

The vertical pressure σ_x at any depth is given by

$$\sigma_x = \gamma h \qquad 4.1$$

and the horizontal pressure by

$$\sigma_y = \gamma k h \qquad 4.2$$

where k = active pressure coefficient

$$k = \frac{1 - \sin\gamma}{1 + \sin\gamma} \qquad 4.3$$

$$k = \frac{1 - \sin 33{,}6°}{1 + \sin 33{,}6°} = 0{,}2846$$

For equilibrium perpendicular to the slope, Fig. 4.2

$$\sigma_w = \sigma_x \sin^2 30 + \sigma_y \cos^2 30$$

$$= \sigma_x (0{,}25 + 0{,}2846 \times 0{,}75) = 0{,}4635\sigma_x \qquad 4.4$$

For equilibrium parallel to the slope

$$\tau_w = (\sigma_x - \sigma_y)\sin 30 \cos 30$$

$$= \sigma_x(1 - 0{,}2846) \times 0{,}5 \times 0{,}866 = 0{,}3098\sigma_x \qquad 4.5$$

At *bottom* h = 781 mm

$\therefore$ $\sigma_x = 15716 \times .781 = 12274$ N/m²

$\sigma_y = 0{,}2846 \times 12274 = 3528$ N/m²

$\sigma_w = 0{,}4635 \times 12274 = 5688$ N/m²

$\tau_w = 0{,}3098 \times 12274 = 3802$ N/m²

Angle $\phi_w = \text{atn}\ \frac{\tau_w}{\sigma_w} = \text{atn}\ (3802/5688) = 33{,}8°$

This exceeds the wall friction angle = 20,13°.

The stress is shown plotted in Fig. 4.2. Note - it is assumed that the shear stress on the vertical and horizontal planes, τ_{xy} is zero.

4.3.2. F2 Equilibrium of forces - linear distribution of σ_w

The resultant horizontal force H at the centreline acting on half the contents, Fig. 4.3, is assumed to act at one third the height. This force together with the weight of

half the contents must balance the resultant force R on the side which is inclined at the angle of wall friction to the normal. The pressure distribution on the wall is assumed to be linear. From the value of R and its position the extreme values can be found. This does not produce a zero pressure at the surface.

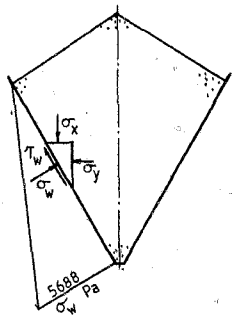

Figure 4.2: Active state pressure

$W = 4382 = 2191$ N from table 4.1.

For vertical equilibrium $R\sin 50{,}13^\circ = W = 2191$ N

$\therefore \quad R = 2855$ N

Normal component $N = R\cos 20{,}13^\circ = 2681$ N

$$p_1 = \frac{6}{0{,}658^2} \times 2681 \times (2/3 \times 0{,}658 - 0{,}2596)$$

$$= 6653 \text{ N/m}^2 \qquad 4.6$$

$$p_2 = \frac{6}{0{,}658^2} \times 2681 \times (0{,}2596 - 0{,}658/3)$$

$$= 1496 \text{ N/m}^2 \qquad 4.7$$

4.3.3 F3 Equilibrium of forces - parabolic distribution of σ_w

This method is an improvement over F2 as it allows a zero wall stress at the free surface. The arrangement of forces is still as in Fig. 4.3. The parabola used is shown in Fig. 4.4.

Let the equation be $p = ax + bx^2$

$$\int_0^L p dx = \int_0^L (ax + bx^2)\, dx = \frac{L^2}{2}.a + \frac{L^3}{3}.b = N \qquad (I)$$

$$\int_0^L px dx = \int_0^L (ax^2 + bx^3)\, dx = \frac{L^3}{3}.a + \frac{L^4}{4}.b = N.g \qquad (II)$$

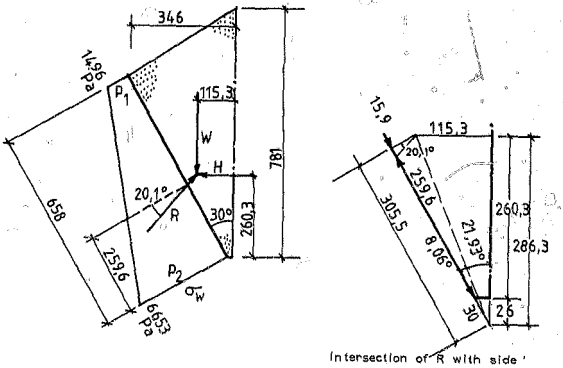

Figure 4.3 F2 : Equilibrium of forces with Linear distribution of σ_w

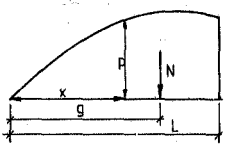

Figure 4.4 : F3 Equilibrium of forces with parabolic distribution of σ_w

(i) and (ii) are solved for a and b :

$$a = 72(L/4 - g/3)\frac{N}{L^3} \qquad 4.9$$

$$b = 72(g/2 - L/3)\frac{N}{L^4} \qquad 4.10$$

From 4.3.2 N = 2681 N

from Fig. 4.3 L = 0,658m,

g = 0,658 - 0,260 = 0,398 m

$\therefore$ a = 72(0,658/4 - 0,398/3) 2681/$0,658^3$ = 21 569

b = 72(0,398/2 - 0,658/3) 2681/$0,658^4$ = -20 938

Values of pressure with slope distance from the free surface are given in table 4.2 .

Table 4.2 F3 Pressures

x_m	0	0,058	.0,158	0,258	0,358	0,458	0,558	0,658
p N/m²	0	1181	2885	4171	5038	5487	5516	5127

4.3.4 F4 Walker theory for filling [14]

This method is similar to F1 in that shear on vertical planes is assumed to be zero. The sloping surface is averaged out as surcharge and the horizontal pressure is determined so that the correct friction angle is obtained at the wall, Fig. 4.5:

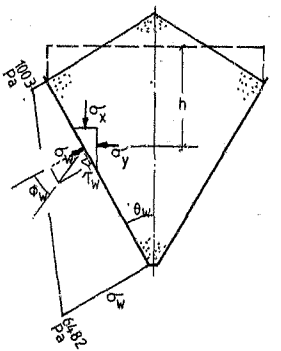

Figure 4.5:F4 Walker's Theory for filling

Vertical pressure $\sigma_w = \gamma h$

for vertical equilibrium

$$\sigma_w \sin\theta_w + \sigma_w \tan\phi_w \cos\theta_w = \sigma_x \cdot \cos\theta_w$$

$$\therefore \quad \sigma_w = \frac{\sigma_x}{1 + \tan\phi_w \cot\theta_w} = 0.6117\ \sigma_x \qquad 4.11$$

γ = 15716 N/m, ϕ_w = 20,13° θ = 30°

$\therefore$ σ_w = 15716 h x 0,6117 = 9613 h N/m²

At top h = 0,1043 m, σ_w = 9613 x 0,1043 = 1003 Pa.

at bottom h = 0,6743 m, σ_w = 9613 x 0,6743 = 6482 Pa.

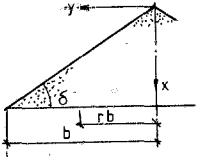

Figure 4.6 : F5 Co-ordinates for Booth's Pile Theory

4.3.5 F5 Booth's pile theory[8]

The stresses within a pile of granular material, Fig. 4.6 are represented as polynomial functions in r, the ratio of the horizontal distance from the centreline of the pile to the point concerned, to the horizontal distance from the centreline to the surface. If the bin is now imagined within

the pile, Fig. 4.7, the stresses may be calculated along the wall from the stresses σ_x, σ_y and τ_{xy}. Fig. 4.7 also shows the values of B and rB for points on the wall. In general the relationship $\tau_w / \sigma_w = \tan\phi_w$ will not be satisfied. There is no distinction made between the angle of repose and the internal friction angle. Therefore the surface has been adjusted slightly to an angle of repose of 34° which is close to the internal friction angle of 33,8°. The normal pressure on the wall is shown as the dotted line in Fig. 4.7.

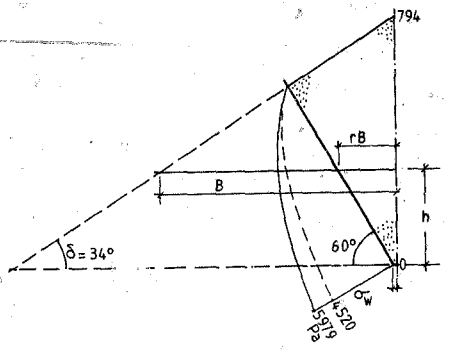

Figure 4.7 : Bin within a pile of sand

Values of constants for friction angle $\delta = 34°$.

$\gamma = 15716\ N/m^3$

$k = 0{,}28272$ $\qquad E = 0{,}52362$

$A = 0{,}04971$ $\qquad F = 0{,}36662$

$B = 0{,}06242$

$C = 0{,}63575$

Vertical compressive stress

$$\sigma_x = \gamma b\,(Ar^4 + Br^3 + Cr^2 + E) \qquad 4.12$$

Horizontal compressive stress

$$\sigma_y = \frac{\gamma b r^2}{\tan^2\delta}\left(\frac{2}{5}Ar^4 + \frac{3}{10}Br^3 + \frac{1}{6}Cr^2\right) + \gamma bkE \qquad 4.13$$

Shear stress

$$\tau_{xy} = \frac{\gamma br}{\tan\delta}\left(\frac{3}{5}Ar^4 + \frac{1}{2}Br^3 + \frac{1}{3}Cr^2 - E\right) + \gamma br \qquad 4.14$$

The wall stresses, Fig. 4.8 are given by the standard conversion

$$\sigma_w = \sigma_x \sin^2\alpha + \sigma_y \cos^2\alpha + 2\tau_{xy}\sin\alpha\cos\alpha \qquad 4.15$$

$$\tau_w = \tau_{xy}(\cos^2\alpha - \sin^2\alpha) + (\sigma_x - \sigma_y)\sin\alpha\cos\alpha \qquad 4.16$$

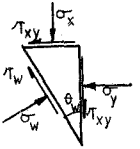

Figure 4.8 : Determination of wall stresses

Table 4.3 gives the stresses at vertical intervals of 100mm. The second last column shows the resulting angle of wall friction which considerably exceeds the required value of 21,0°.

4.3.6 F6 Booth's adjusted pile theory

The results from Booth's pile theory may be adjusted to produce the right friction angle at the wall. This is equivalent to introducing an additional horizontal stress, Fig. 4.9:

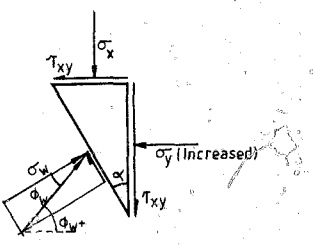

Figure 4.9: Wall stresses adjusted pile theory

For vertical equilibrium

$$\frac{\sigma_w}{\cos_w} \cdot \sin(\phi_w + \alpha) = \sigma_w \sin\alpha + \tau_{xy}\cos\alpha$$

$$\therefore \quad \sigma_w = \frac{\cos\phi_w}{\sin(\phi_w+\alpha)} (\sigma_x \sin\alpha + \tau_{xy}\cos\alpha) \qquad 4.17$$

If $\phi_w = 20,1°$ and $\alpha = 30°$ are substituted then

$$\sigma_w = 0,612\ \sigma_x + 1,059\ \tau_{xy} \qquad 4.18$$

Table 4.3 Booth's pile theory

Point	Height h mm	B mm	r	σ_x Pa	σ_y Pa	τ_{xy} Pa	σ_w Pa	τ_w Pa	ϕ_w deg.	Adjusted σ_w
1	0	1177	0,0134	9683	2738	53	4520	3034	33,9	5982
2	100	1029	0,0709	8417	2394	254	4120	2735	33,6	5420
3	200	881	0,1476	7061	2048	441	3686	2392	33,0	4788
4	300	732	0,2568	5556	1692	594	3180	1974	31,8	4029
5	400	554	0,4212	3631	1232	604	2380	1356	29,7	2862
6	500	436	0,6972	1696	718	356	1364	655	25,3	1415

4.3.7 F7 Framework theory [10]

If the material in the bin has its internal friction fully mobilised it is said to be in a critical state[17]. It is possible to show that there are two sets of planes on which limiting friction occurs. These planes are inclined at 90- δ to each other, Fig. 4.10. The direction of the major principal stress σ_1 bisects the angle so that σ_1 is inclined to either set of slip lines at an angle of

$$\mu = 45 - \delta/2 \qquad 4.19$$

Fig. 4.10 shows that the resultant stress on a slip line of one type is parallel to the other type of slip line . For analysis this enables the replacement of the material (sand) by a framework model in which the weight of the material in the diamond shaped element is concentrated at a node placed at the element centroid. Members then frame into the node parallel to the slip lines, Fig. 4.11. Stresses are found at a wall or along a given line by dividing the forces by the member spacing along the wall or line. It has been shown [10] that exact results are obtained for the classic active and passive pressure states in a uniform mass with horizontal surface. The principal limitation of the method is in determining the correct orientation and extent of the slip line field. During filling the major principal stress will probably be vertical on the centreline. Fig. 4.12 shows a framework with straight members arranged so that σ_1 is always vertical. The dotted lines indicate extra horizontal members required to preserve the correct wall friction angle for vertical equilibrium at a support

$$R\sin 50{,}1° = F\cos 28{,}1° + W$$

$$\therefore \quad R = 1{,}149F + 1{,}303W \qquad 4.20$$

The reactions and normal stresses from the surface down are shown in table 4.4. The spacing down the slope is 40mm.

Therefore the normal stress is given by

$$\sigma w = \frac{R\cos 20{,}1}{0{,}04} = 25{,}33F + 26{,}98W \text{ Pa.} \qquad 4.21$$

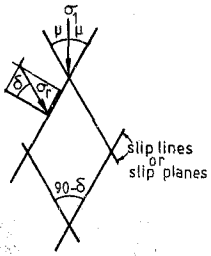

Figure 4.10 : Stresses associated with slip lines

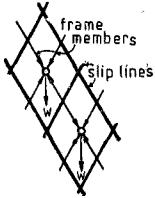

Figure 4.11 : Construction of substitute framework

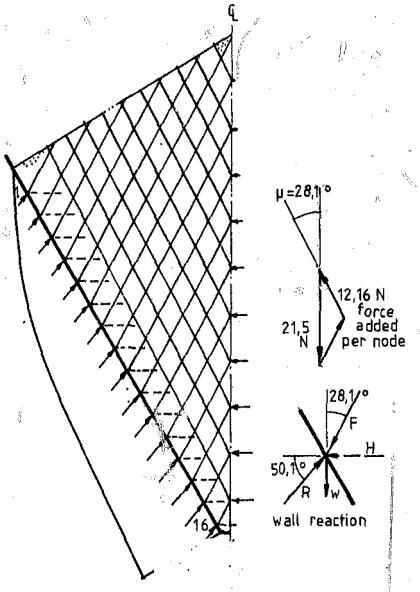

Figure 4.12 : F7 Framework for filling

Table 4.4 F7 Framework

POINT	REACTION R N	NORMAL STRESS σ_w Pa.
1	55	759
2	74	1737
3	101	2371
4	129	3028
5	147	3451
6	175	4108
7	180	4225
8	184	4318
9	193	4530
10	200	4695
11	207	4859
12	211	4953
13	217	5094
14	225	5281
15	230	5399
16	258	6056

4.4 Geometry for emptying

Table 4.5 gives the calculation of the average surface heights. The resulting profile is plotted as the dotted line in Fig. 4.1 and it is slightly below that for filling.

Table 4.5 Values for bin 1 to be used in analysis of emptying condition

Surface heights mm

Test	Set	Position								
		1	2	3	4	5	6	7	8	9
20	5	570	600	660	710	770	710	660	605	570
21	6	575	590	645	705	770	715	655	600	575
22	6	570	590	655	710	770	715	660	605	580
23	6	575	595	640	700	760	710	645	600	575
24	8	580	610	660	710	750	700	660	610	580
Average		574	597	652	707	764	710	656	604	576
Average both sides						764	708	654	600	575

Density $15\ 716\ N/m^3$

Surface slope $= \tan\left(\frac{764 - 575}{340}\right) \approx 29{,}1°$

Contained weight $= 15716 \times (0{,}792 \times 0{,}346 - 0{,}015 \times 0{,}026)$

$= 4301$ N per metre width of bin

4.5 Emptying pressures - bin 1

4.5.1 Walker theory for emptying[14]

Walker analyses the forces on a horizontal slice in a bin, Fig. 4.13. As he uses the average vertical stress $\bar{V}$ (in his notation) he has to relate it to the vertical stress at the wall V_w. He does this with the factor D

$$V_w = D\bar{V} \qquad 4.22$$

He states that if D is taken as unity it will give sufficiently accurate values of wall stresses. As mentioned in chapter 1, D must in fact be one or vertical equilibrium will be violated, (see Appendix E).

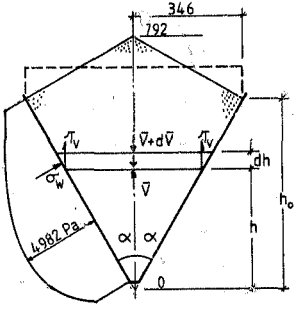

Figure 4.13 : El Walker's theory for emptying

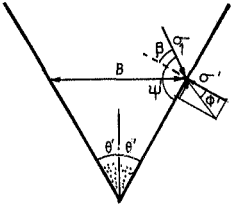

Figure 4.14 : Notation for Jenike's graphs for radial stress field

In the following calculations Walker's notation is partially used, and is defined where necessary, referring to Fig. 4.13.

Internal friction angle $\delta = 33,6°$, Wall slope $\alpha = 30°$
Wall friction angle $\phi_w = 20,1°$

$$\beta = \frac{1}{2}\left(\phi_w + \operatorname{asin}\left(\frac{\sin\phi_w}{\sin\delta}\right)\right) \qquad 4.23$$

$$\beta = 29,2°$$

The vertical shear stress at the wall τ_v is related to V_w the vertical normal stress of the wall by

$$\tau_v = B\, V_w \qquad 4.24$$

where $$B = \frac{\sin\delta\sin2(\alpha+\beta)}{1 - \sin\delta\cos2(\alpha+\beta)} = 0,3870 \qquad 4.25$$

$$C = \frac{6D}{\tan\alpha} = \frac{0,3870 \times 1}{\tan 30} = 0,6702 \qquad 4.26$$

$$\sigma_w = \frac{1 + \sin\delta\cos2\beta}{1 - \sin\delta\cos2(\alpha+\beta)} V_w = 1,022 \qquad 4.27$$

$$V_w = \overline{V} = \frac{\gamma h}{C-1}\left[1 - \left(\frac{h}{h_o}\right)^{C-1}\right] + V_o\left(\frac{h}{h_o}\right)^{C} \qquad 4.28$$

$\therefore$ from eqns 4.27 and 4.28

$$\sigma_w = 48701h\left[\left(\frac{0,601}{h}\right)^{0,3298} - 1\right] + 1526\left(\frac{h}{0,601}\right)^{0,6702} \qquad 4.29$$

The normal stress is given in table 4.6 for different heights and is plotted in Fig. 4.13.

Table 4.6 Walker's Theory

h m	0,601	0,526	0,426	0,326	0,226	0,126	0,026
σ_w Pa.	1526	2547	3705	4562	4982	4672	2487

In the following calculations Walker's notation is partially used, and is defined where necessary, referring to Fig. 4.13.

Internal friction angle $\delta = 33,8°$, Wall slope $\alpha = 30°$
Wall friction angle $\phi_w = 20,1°$

$$\beta = \frac{1}{2}\left(\phi_w + \operatorname{asin}\left(\frac{\sin\phi_w}{\sin\delta}\right)\right) \qquad 4.23$$

$$\beta = 29,2°$$

The vertical shear stress at the wall τ_v is related to V_w the vertical normal stress of the wall by

$$\tau_v = B\, V_w \qquad 4.24$$

where $$B = \frac{\sin\delta\sin2(\alpha+\beta)}{1 - \sin\delta\cos2(\alpha+\beta)} = 0,3870 \qquad 4.25$$

$$C = \frac{BD}{\tan\alpha} = \frac{0,3870 \times 1}{\tan 30} = 0,6702 \qquad 4.26$$

$$\sigma_w = \frac{1 + \sin\delta\cos2\beta}{1 - \sin\delta\cos2(\alpha+\beta)}\, V_w = 1,022 \qquad 4.27$$

$$V_w = \overline{V} = \frac{\gamma h}{C-1}\left[1 - \left(\frac{h}{h_o}\right)^{C-1}\right] + V_o\left(\frac{h}{h_o}\right)^C \qquad 4.28$$

$\therefore$ from eqns 4.27 and 4.28

$$\sigma_w = 48701h\left[\left(\frac{0,601}{h}\right)^{0,3298} - 1\right] + 1526\left(\frac{h}{0,601}\right)^{0,6702} \qquad 4.29$$

The normal stress is given in table 4.6 for different heights and is plotted in Fig. 4.13.

Table 4.6 Walker's Theory

h m	0,601	0,526	0,426	0,326	0,226	0,126	0,026
σ_w Pa.	1526	2547	3705	4562	4982	4672	2487

4.5.2. E2. Radial stress field with linear cut-off

A radial stress field has been shown to exist in the vicinity of the outlet by Jenike[16]. In a radial stress field the stresses are proportional to the radial distance from the apex where the two inclined sides intersect. Thus the normal stress on the wall will increase linearly from zero at the apex. Jenike gives values of $\sigma'/\gamma B$, Fig.4.14 ($\sigma' = \sigma_w$), in graphs for $\delta = 30°$ and $\delta = 40°$, reproduced here as Figs. 4.15 and 4.16. It is thus necessary to interpolate for the required value of $\delta = 33,8°$. The value depends on the wall friction angle ($\phi' = \phi_w$) and the bin wall slope (θ') = α. The theory for the radial stress field is given in Appendix G which also details a procedure and a program in Basic for calculating this factor.

The constants used were

$$\gamma = 15716\ N/m^3$$
$$\delta = 33,84°$$
$$\phi_w = 20,1°$$
$$\psi' - 90° = \beta = 29,2°$$

From Fig.4.15 for $\delta = 30°$ $\sigma'/\gamma B = 1,300$
From Fig.4.16 for $\delta = 40°$ $\sigma'/\gamma B = 0,982$
Interpolating for $\delta = 33,84°$ $\sigma'/\gamma B = 1,3 - (1,3-0,982) \times \frac{3,84}{10}$
$= 1,178$

From Appendix G $\sigma' \gamma \beta = \sigma_w/\gamma r = 1,3354\ \sigma'/\gamma_B$

where $\sigma' = \sigma_w$

The latter figure is probably more correct than the former because of the great care taken in its calculation, but by the stage it had been derived all calculations had already been related to the value of 1,178 so this is the value used here.

As the radial stress field would give a large value at the surface and because vertical equilibrium must be assured some

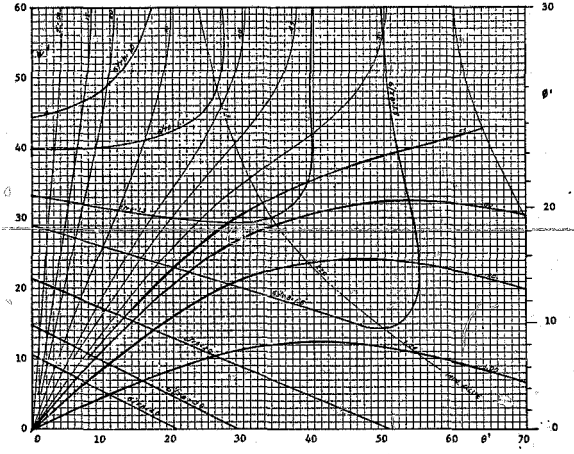

Function $\sigma'/\gamma B$, $\delta = 30°$

Plane symmetry (symmetric plane flow)

Figure 4.15: Normal stress in the radial stress field from Jenike [16] for $\delta = 30°$

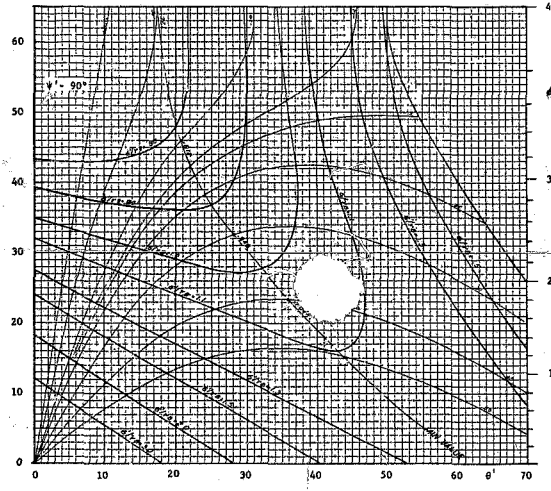

Function σ'/γ B, δ = 40°

Plane symmetry (symmetric plane flow)

Figure 4.16 : Normal stress in the radial stress field from Jenike [16] for δ = 40°

sort of reduction in wall pressure must be provided towards the surface. The simplest form is a linear cut-off, Fig. 4.17 which results in a wall stress at the surface which is zero and which ensures vertical equilibrium.

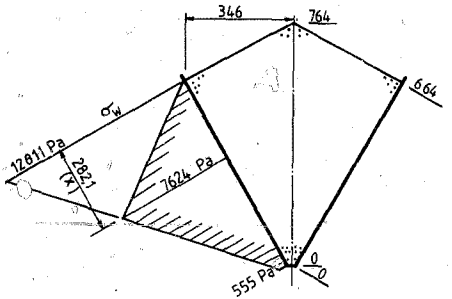

Figure 4.17 E2. Radial stress field with linear cut-off

The radial stress field values for normal stress are :

at the top B = 0,692m, σ_w = 15716 x 1,178 x 0,692 = 12811 Pa.
at the bottom B = 0,030m, σ_w = 15716 x 1,178 x 0,030 = 555 Pa.

let N = normal force on the wall
T = Ntan20,13 = shear force on wall

∴ Vertical force on both walls = 2 x (Nsin30 + Tcos30)
= 1,635 N

This must equal the total weight of 4301 N from table 4.5

∴ 1,635 N = 4301

∴ N = 2631 N

Also from Fig.4.17

$$N = (12811 + 555)\ \tfrac{1}{2}.\ 0{,}664 - \frac{12811}{2}\ .x = 2631$$

$$\therefore \quad x = 0{,}282m$$

Pressure at x = 12811 (0,664 - 0,282)/0,664 + 555 × 0,282/0,664

= 7624 Pa.

4.5.3 E3 Radial stress field with curved cut-off

As an alternative to a straight line cut-off it is possible to stipulate a curved cut-off. One such curve is shown in Fig. 4.18. The area under the curve must be equal to the excess force from the radial stress field, which is

(12811 + 555) x 0,664/2 - 2631 from section 4.5.2.

= 4438 - 2631 = 1807 N

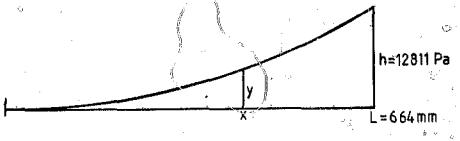

Figure 4.18 : Curve for cut-off

let the curve be given by $y = ax^n$ 4.30

Area under the curve $A = a\int_0^L y^n dx$

$$= \frac{aL^{n+1}}{n+1} \qquad 4.31$$

from eqn. 4.30 $a = \frac{h}{L^n}$ 4.32

.. $A = \frac{h.L^{n+1}}{L^n(n+1)} = \frac{hL}{n+1}$

.. $n = \frac{hL}{A} - 1$ 4.33

In this case $h = 12811$, $L = 0,664$, $A = 1807$

.. $n = \frac{12811 \times 0,664}{1807} - 1 = 3,708$

and $a = \frac{12811}{0,664^{3,708}} = 58\ 477$

.. $y = 58\ 477\ x^{3,708}$

and normal stress on wall:

$$\sigma_w = 555 + \frac{12556}{0,664} x - 58\ 477\ x^{3,708}$$

$$\sigma_w = 555 + 18\ 458\ x - 58\ 477 x^{3,708}$$

The values of σ_w are given in table 4.7 and shown plotted in Fig. 4.19:

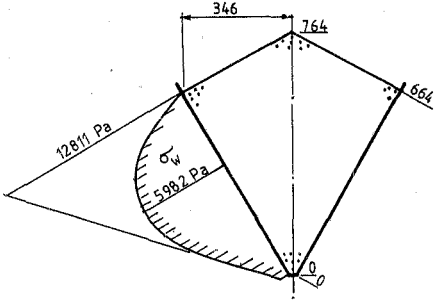

Figure 4.19 : E3. Radial stress field with curved cut-off

Table 4.7 Radial stress field with curved cut-off

x m	0	0,1	0,2	0,3	0,4	0,5	0,6	0,664
σ_w Pa	555	2389	4097	5419	5982	5309	2382	0

Note: x = slope distance from the bottom

4.5.4 E4.Framework with σ_1 horizontal

The framework is shown in Fig. 4.20. In order to avoid tensions downward sloping members at the wall were ignored and horizontal members shown by the dotted lines were used instead. This framework results in a large stress at the surface where it should be zero. The correct friction angle at the wall was allowed for. The normal stresses appear in table 4.8.

4.5.5. E5 Framework with σ_1 inclined at 30° to the horizontal

The framework is shown in Fig. 4.21. For simplicity the internal friction angle was approximated as $\delta = 30°$, then the slip slines intersect at 60°, with one set of slip lines horizontal. There is obviously a discontinuity in the direction of σ_1 at the centreline. The normal wall stress, Fig. 4.21, is zero at the surface as it should be. No additional members besides those shown were necessary. The normal stresses are given in table 4.9.

Table 4.8 E4 Framework model with σ_1 horizontal

Wall Position	Reaction N	Normal Stress σ_w Pa.
1	175	4638
2	157	4161
3	169	4479
4	174	4611
5	173	4585
6	187	4956
7	195	5168
8	201	5327
9	210	5565
10	198	5247
11	171	4532
12	157	4161
13	140	3710
14	111	2942
15	106	2809
16	72	1908
17	53	1405
18	31	822

Table 4.9. E5 *Framework model* with σ_1 inclined at 30° to the horizontal

Wall Position	Reaction N	Normal Stress σ_w Pa.
1	33	671
2	105	2134
3	169	3434
4	244	4958
5	328	6665
6	359	7295
7	323	6563
8	285	5791
9	248	5039
10	209	4247
11	172	3495
12	134	2723
13	96	1951
14	58	1179

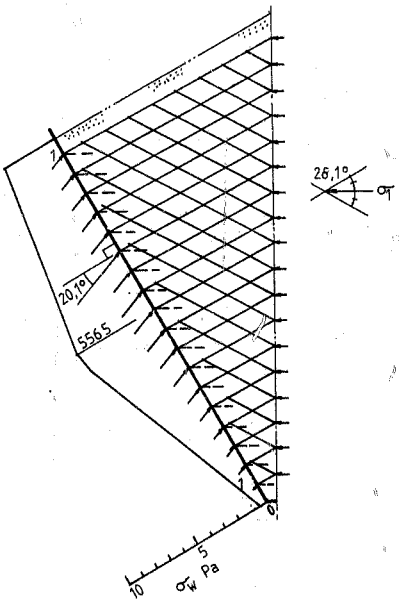

Figure 4.20 : E4 Frame with σ_1 horizontal

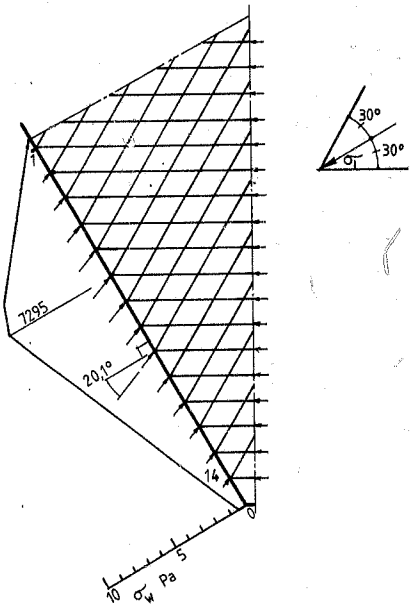

Figure 4.21 : E5 Framework: with q inclined at 30° to the horizontal

CHAPTER 5

THEORETICAL PRESSURE DISTRIBUTIONS - BIN 2

5.1 Methods for analysing pressures

The methods used follow closely those for shape 1. For example, Walker's theory is used as is Booth's adjusted Pile Theory. However, the equilibrium of forces method for filling is less simple and depends on more assumptions. More framework models are tried for the emptying case. Filling cases are designated F and emptying cases E.

5.2 Geometry for filling

Fig 5.1 shows the dimensions used for the analysis of filling and emptying conditions.

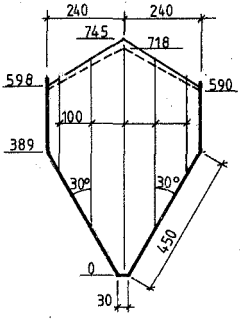

Figure 5.1 Dimensions for analysis

An average density of γ = 1602 kg/m³ = 15716 N/m³ from table 3.2 was used. The surface heights are given in table 5.1 for the five tests 27 to 31.

Table 5.1 Surface heights mm

Test	Set	Position						
		2	3	4	5	6	7	8
27	2	600	620	690	745	685	620	600
28	2	600	630	695	745	690	620	600
29	2	595	625	685	745	680	615	590
30	2	600	630	690	745	690	630	600
31	2	600	625	690	745	685	625	600
Average		599	626	690	745	686	622	598
Average both sides					745	688	624	598

5.3 Filling pressures. - Bin 2

5.3.1 F1. Active state pressure

Active pressure coefficient (see 4.3.1)

$$k = \frac{1 - \sin 33{,}8}{1 + \sin 33{,}8} = 0{,}2846$$

At B vertical pressure

$$\sigma_x = \gamma h = 15716 \times 0{,}208 = 3269 \text{ Pa.}$$

horizontal pressure

$$\sigma_y = k\sigma_x = 0{,}2846 \times 3269 = 930 \text{ Pa.}$$

normal pressure (Eqn 4.4)

$$\sigma_w = \sigma_x \sin^2 30 + \sigma_y \cos^2 30 = 3269 \times 0{,}25 + 930 \times 0{,}75 = 1515 \text{ Pa.}$$

shear stress (Eqn 4.5)

$$\tau_w = (\sigma_x - \sigma_x)\sin 30 \cos 30 = (3269 - 930) \times 0{,}5 \times 0{,}8660 = 1013 \text{ Pa.}$$

At C σ_x = 15716 x 0,745 = 11708 Pa.

σ_y = 0,2846 x 11708 = 3332 Pa.

σ_w = 11808 x 0,25 + 3332 x 0,75 = 5426 Pa.

τ_w = (11708 - 3332) x 0,5 x 0,8660 = 3627 Pa.

ϕ_w = $\text{atan}\left(\frac{\tau_w}{\sigma_w}\right)$ = $\text{atan}\left(\frac{3627}{5426}\right)$ = 33,8°

The pressures are shown plotted in Fig 5.2.

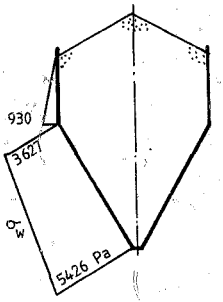

Figure 5.2 : F1 Active state pressure

5.3.2 F2 Equilibrium of forces

This case is not as simple as for bin shape 1 where there is one straight wall only. There is the force P_1 from the vertical wall as well as the force P_2 from the inclined wall, Fig. 5.4. Therefore an assumption is made to get P_1 and P_2 then follows from equilibrium.

A theory that may be used to find P_1 is the Coulomb analysis[44]. In this analysis, Fig 5.3, a wedge is maintained in a state of equilibrium. On line AB full internal friction is mobilised, while on line BC (the wall), full wall friction is mobilised. The slope of AB is varied until the maximum value of P_2 is obtained.

$$P_1 = \tfrac{1}{2}\gamma h^2 \frac{K_A}{\cos\phi_w} \quad (5.1), \quad \text{where } h = \text{length of wall}$$

where Coulomb found

$$K_A = \frac{\cos^2\delta}{\left[1 + \sqrt{\left\{\frac{\sin(\delta+\phi_w)\cdot\sin(\delta-\varepsilon)}{\cos\phi_w\cdot\cos\varepsilon}\right\}}\right]^2} \qquad 5.2$$

$$\therefore K_A = \frac{\cos^2 33,8}{\left[1 + \sqrt{\left\{\frac{\sin(33,8 + 20,1)\sin(33,8 - 31,5)}{\cos 20,1 \cdot \cos 31,5}\right\}}\right]^2} \approx 0,479$$

This corresponds to a horizontal length of X = 500mm which exceeds the distance to the centreline (240mm). Assume that the horizontal force H at the centreline of the bin is equal to the required value.

The force on the vertical wall is therefore

$$P_I = \tfrac{1}{2}\ 15716 \times \frac{0,208^2 \times 0,479}{\cos 20,1} \approx 173,4\ \text{N}$$

The force on the inclined side can now be found from vertical equilibrium, Fig 5.4. It is assumed that the horizontal force on the centreline acts at a third of the height.

W = weight of half the contents
= 15716(0,24x0,147/2 + 0,24x0,208 + 0,39x0,015 + 0,39x0,225/2)
= 1843,3 N

g = distance from centreline to W

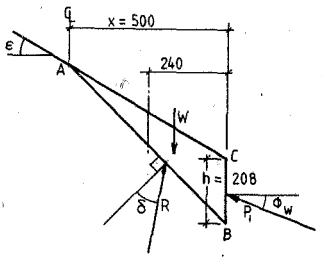

Figure 5.3: Coulomb's active earth pressure

g = 15716(0,24x0,147/2x80 + 0,24x 0,208x120+0,39x0,015x7
+ 0,39x0,225/2x90)/1843,3 = 97,1mm

ΣV : $P_2 \sin 50{,}13 = 1843{,}3 - 173{,}4 \sin 20{,}1 = 1783{,}7$ N

$P_2 = 2324$ N

ΣH : H = 2324 cos50,1 + 173,4 cos20,1 = 1654 N

ΣM about C: 2324 cos20,1 x =

1654 x 745/3 + 1843,3(97,1 -15)- 173,4(cos20,1 x 459 + sin20,1 x 225)

$\therefore$ x = 217,1mm

Normal force on BC = 2324 cos20,1 = 2182 N

Stress at C = $\frac{6 \times 2182}{0{,}450^2}$ (2/3 x 0,450 - 0,218)= 5301 Pa

Stress at B = $\frac{6 \times 2182}{0{,}450^2}$ (0,218 - 0,450/3) = 4396 Pa

Stress at B on vertical wall =
173,4 cos20,1 x2/0,208 = 1566 Pa

The normal stresses are shown plotted in Fig 5.4:

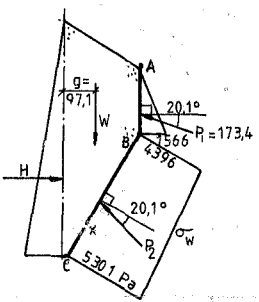

Figure 5.4 : F2 Equilibrium of forces

5.3.3 F3 Walker theory for filling

From Eqn 4.11 $\sigma_w = 0{,}6117\ \sigma_x$ on the inclined wall.

Refer to Fig 5.5

Assume the horizontal pressure on AB is active

$$\therefore\ k_A = \frac{1 - \sin 33{,}8}{1 + \sin 33{,}8} = 0{,}2846$$

Normal stress on AB at B

$= 0{,}2846 \times 15716 \times (0{,}208 + 0{,}074) = 1261$ Pa

Normal stress on BC at B

$= 0{,}6117 \times 15716 \times (0{,}208 + 0{,}074) = 2711$ Pa

at C $= 0{,}6117 \times 15716 \times (0{,}745 - 0{,}074) = 6451$ Pa

The normal stresses are shown plotted on Fig 5.5.

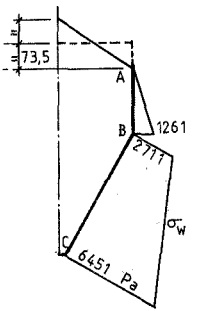

Figure 5.5 :F3 Walker's theory for filling

5.3.4 F4 Booth's adjusted pile theory

As for Bin 1 the horizontal stress is increased if necessary to prevent the wall friction angle from being exceeded.

From eqn 4.17 for the vertical wall with $\alpha = 0$

$$\sigma_w = \tau_{xy} \cot \phi_w \qquad (5.3)$$

$$\text{if } \operatorname{atan}\left(\frac{\tau_{xy}}{\sigma_y}\right) > \phi_w \qquad (5.4)$$

$$\text{otherwise } \sigma_w = \sigma_y$$

From eqn 4.18 for the sloping wall

$$\sigma_w = 0{,}612\ \sigma_x + 1{,}058\ \tau_{xy}$$

$$\text{if } \operatorname{atan}\left(\frac{\tau_{xy}}{\sigma_y}\right) > \phi_w$$

The constants and formulae used in Booth's Pile Theory are set out in 4.3.5. Table 5.2 gives the stresses at various vertical levels.

The normal stresses are shown plotted on Fig. 5.6:

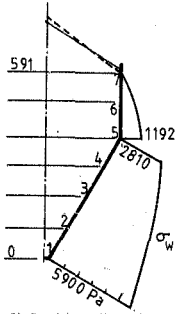

Figure 5.6: F4 Booth's adjusted pile theory

5.3.5. F5 Framework theory

Fig. 5.7 shows the substitute framework. As in section 4.3.7 *the slip lines are straight and* σ_1 *is taken as vertical.* The dotted horizontal members are provided to make the wall friction angle correct. Normal stresses are also shown on Fig. 5.7 and are given in table 5.3

5.4. Geometry for emptying

Table 5.4 gives the average surface heights. The resulting profile is shown plotted on Fig. 5.1 as a dotted line.

Table 5.2 Booth's Pile Theory

Point mm	Height mm	B mm	nB mm	n	σ_x Pa	σ_y Pa	τ_{xy} Pa	σ_w Pa	τ_w Pa	ϕ_w Deg.	Adjusted σ_w Pa
1	0	1116	15	0,013	9155	2631	175	4413	2912	33,4	5900
2	100	968	70	0,072	7911	2282	274	3927	2574	33,2	5231
3	200	820	130	0,159	6547	1933	425	3454	2210	32,6	4539
4	300	672	185	0,275	5048	1574	602	2964	1805	31,3	3790
5	389	538	240	0,446	3416	1192	643	2305	1284	29,1	2810
5								1192	643	19,2	1192
6	500	375	240	0,640	5894	1697	695	1697	695	22,3	759
7	591	240	240	1,000	0	0	0	0	0		

Table 5.3 F5 Framework for filling

Point	σ_w Pa	Point	σ_w Pa
1	823	10	3864
2	1735	11	4084
3	2575	12	4173
4 (upper)	3451	13	4322
4 (lower)	2653	14	4411
5	3279	15	4560
6	3398	16	4650
7	3607	17	4709
8	3756	18	4620
9	3845	19	4322

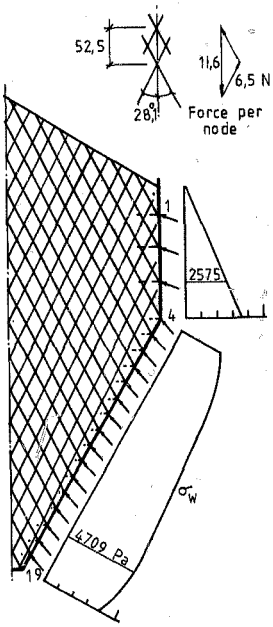

Figure 5.7 : F5 Framework for filling

Table 5.4 Surface heights (mm)

Test	Set	Position						
		2	3	4	5	6	7	8
27	5	595	610	675	730	675	615	595
28	5	590	620	680	730	675	615	590
29	6	585	615	675	720	660	605	585
30	6	590	620	675	720	675	620	590
31	6	590	615	670	720	670	615	590
Average		590	616	675	724	671	614	590
Average both sides					724	673	615	590

As for filling the density was taken as $\gamma = 15716\ N/m^3$ for calculating pressures.

5.5 *Emptying pressures - bin 2*

5.5.1 E1,Walker's theory

The calculation of pressures on the sloping part of the bin is similar to the calculations in section 4.5.1.

For the vertical part the following Janssen type calculation applies[114], see Fig. 5.8. The inclination of σ_1 to the horizontal is given by

$$\beta = \frac{1}{2}\left(\phi_w + \operatorname{asin}\left(\frac{\sin\phi_w}{\sin\delta}\right)\right) \qquad 5.5$$

$$\therefore \beta = \frac{1}{2}(20{,}1 + 38{,}1) = 29{,}2°$$

$$\text{or } \beta = \frac{1}{2}(20{,}1 + 180 - 38{,}1) = 81{,}0°$$

There are two possible inclinations for σ_1, at the wall. Lateral pressures will be worked out for both cases and later compared with experimental results.

$$B = \frac{\sin 2\beta \sin\delta}{1-\cos 2\beta \sin\delta} \qquad 5.6$$

$$B = 0{,}113 \text{ or } 0{,}639$$

$$R = \frac{2 \times \text{Area}}{\text{perimeter}} = \frac{2\ (0{,}24 \times 1)}{1} = 0{,}480$$

$\therefore$ R = width of bin

D = 1

Horizontal pressure

$$\sigma_w = \frac{R\gamma}{2\tan\phi_w}\left(1 - \exp\left(\frac{-2BDh}{R}\right)\right) + \frac{BV_o}{\tan\phi_w}\exp\left(\frac{-2BDh}{R}\right) \qquad 5.7$$

V_o = Surcharge = 15716 x 0,067 = 1053 Pa.

$$\sigma_w = \frac{0{,}480 \times 15716}{2 \times \tan 20{,}1}\left(1-\exp\left(\frac{-2 \times B.1.h}{0{,}480}\right)\right) + \frac{B.1053.\exp\left(\frac{-2\ B.1.h}{0{,}480}\right)}{\tan 20{,}1}$$

$\therefore$ $\sigma_w = 10307\ (1 - \exp(-0{,}417h)) + 825\ \exp\ (-0{,}471h)$ 5.8

or $\sigma_w = 10307\ (1 - \exp(-2{,}788h)) + 1925 \exp\ (-2{,}788h)$ 5.9

Vertical pressure $\overline{V} = \frac{\sigma_w \tan\phi_w}{B} = 3{,}238\sigma_w$ or $0{,}547\sigma_w$ 5.10

At point 3 h = 0,201 $\overline{V}$ = 3792 Pa or 3019 Pa 5.11

On the inclined part the pressure is calculated assuming that everthing above the inclined part is treated as a surcharge V_o, which is the vertical pressure at that level in the upper part, i.e. at point 3.

As in section 4.5.1

$$\beta = \tfrac{1}{2}\left(\phi_w + \operatorname{asin}\left(\frac{\sin\phi_w}{\sin\delta}\right)\right)$$

$$= \tfrac{1}{2}\left(20,1 + \operatorname{asin}\left(\frac{\sin 20,1}{\sin 33,8}\right)\right) = 29,2° < 90°$$

$$B = \frac{\sin\delta\sin 2(\alpha+\beta)}{1 - \sin\delta\cos 2(\alpha+\beta)} = 0,3870 \qquad 4.25$$

$$D = 1$$

$$C = \frac{BD}{\tan\alpha} = \frac{0,3870}{\tan 30} = 0,6702 \qquad 4.26$$

$$\bar{V} = \frac{\gamma h}{C-1}\left[1 - \left(\frac{h}{h_o}\right)^{C-1}\right] + V_o\left(\frac{h}{h_o}\right)^{C} \qquad 4.28$$

$h_o = 0,415$ m

V_o = surcharge = 3792 Pa or 3019 Pa from eqn 5.11.

from eqn 4.27 $\sigma_w = 1,022\bar{V}$

$$\therefore \quad \sigma_w = \frac{1.022.\ 15716.h}{0,6702 - 1}\left[1 - \left(\frac{h}{0,415}\right)^{-0,3298}\right] + 1.022.V_o\left(\frac{h}{0,415}\right)^{0,6702}$$

$$= 48701\ h\left[\left(\frac{0,415}{h}\right)^{0,3298} - 1\right] + 3875\left(\frac{h}{0,415}\right)^{0,6702} \qquad 5.12$$

$$\text{or} \quad \sigma_w = 48701\ h\left[\left(\frac{0,415}{h}\right)^{0,3298} - 1\right] + 3085\left(\frac{h}{0,415}\right)^{0,6702} \qquad 5.13$$

Note: h is differently defined for the upper and lower parts.

Table 5.5 gives the normal pressures at points 1 to 7 marked on Fig 5.8 for both values of β in the upper part of the bin from eqns 5.8, 5.9, 5.12 and 5.13. These values are plotted on Fig 5.8.

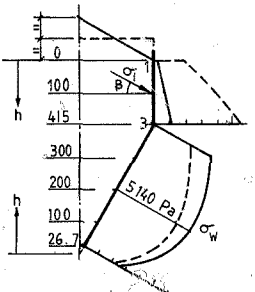

Figure 5.8 : E1 Walker's theory for emptying

Table 5.5 E1 Walker's Theory

Point	Distance h . mm	Normal wall stress Pa β = 81°	β = 29,2°
1	0	325	1925
2	100	784	3964
3	201 (upper)	1227	5521
3	415 (lower)	3875	3085
4	300	4768	4132
5	200	5027	4527
6	100	4410	4106
7	26	2496	2373

It can be seen that the higher stress in the vertical part causes a decrease in the sloping part.

5.5.2 E2 Radial stress field with curved cut-off

Fig. 5.9 shows half the bin and the resulting stress distribution. The radial stress field determines the initial straight line slope near the bottom.

from section 4.5.2

$$\sigma_w = 1{,}178\gamma B$$

or since $\frac{B}{2} = 0{,}015 + \frac{x}{2}$,

$$\sigma_w = 1{,}178\gamma(0{,}030 + x)$$

$$\therefore \quad \sigma_w = 1{,}178 \times 15716\ (0{,}03 + x) = 555 + 18513\ x \qquad 5.14$$

Once the force on the vertical wall is known the final area of the normal stress diagram on the sloping part can be found from vertical equilibrium.

This still leaves the value at the top of the slope, q, Fig.5.9 to be determined. If the value p at the same point on the vertical wall is known the two are related provided that a limiting state of slip (critical) exists along both walls in the immediate vicinity of the wall junction. Sokolovski [17] on page 115 concerned with the broken backed retaining wall derives the equation

$$q + H = (p + H)\exp(2\beta\tan\rho) \qquad 5.15$$

in his notation

where H = cohesion = 0 in this case

β = α = wall slope = $\pi/6$ radians

ρ = δ = internal friction angle = 33,8°

$$\therefore \quad q = p \exp(2\pi/6 \tan 33{,}8) = 2{,}02\ p. \qquad 5.16$$

q is an approximation that is not better than the approximation for p.

Here with value of p will be taken as full fluid pressure

$p = 15716 \times 0{,}201 = 3159$ Pa.

Hence normal force on vertical wall = $3159 \times 0{,}201/2 = 317{,}5$ N.

$\therefore$ Shear force on vertical wall = $317{,}5 \tan 20{,}1 = 116{,}1$ N.

From eqn 5.16 $q = 2{,}02 \times 3159 = 6381$ Pa.

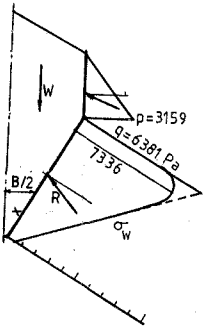

Figure 5.9:E2 Radial stress field

Weight of sand in half bin W

$$= 15716 \times \frac{(240 \times (744 + 201)/2 - 26 \times 15/2)}{10^6}$$

$$= 1779 \text{ N/m width}$$

For vertical equilibrium

$$R \sin 50{,}1 = 1779 - 116{,}1$$

$$\therefore \quad R = 2168 \text{ N}$$

Normal component $N = 2168 \cos 20{,}1 = 2036 \text{N}$

Normal component from radial stress field

$$= \frac{555 + 88}{2} \times 0{,}45 = \underset{\text{Excess}}{\frac{2124 \text{ N}}{88}}$$

Curved cutoff from 4.5.3 $h = 8886 - 6381 = 2505$

$$\therefore n = \frac{hL}{A} - 1 = \frac{2505 \times 0{,}450}{88} - 1 = 11{,}8$$

$$a = h/L^n = 2505/0{,}45^{11{,}8} = 3{,}097 \text{ E7}$$

$$\therefore \quad \sigma_w = 555 + 18513 \times - 3{,}097\ E7\ x^{11{,}8} \qquad 5.17$$

Values of normal stress calculated by this formulae are given in table 5.6 and are plotted on Fig 5.9.

Table 5.6 Radial Stress Field with Curved Cutoff

x mm	σ_w Pa
0	555
100	2407
200	4258
300	6088
400	7336
450	6381

x: = Slope Distance

5.5.3 E3, Framework with σ_1 horizontal

Fig 5.10 shows the framework. As with case E4 for bin 1, downward sloping members are omitted at the walls and horizontal members are put in shown by the dotted lines. The correct friction angle is maintained on the vertical and sloping walls. The normal stresses are also shown on Fig 5.10. Note that the normal stress on the vertical wall at the junction exceeds that on the inclined wall. The normal stresses are given in table 5.7.

5.5.4 E4 Framework with σ_1 inclined at 30° to the horizontal

Fig 5.11 shows the framework and normal wall stresses. This case is similar to 4.5.5. The values of the stresses are given in table 5.8.

Table 5.7 E3 Framework with σ_1 Horizontal

Point	Normal Stress σ_w Pa	Point	Normal Stress σ_w Pa
1	5266	11	4650
2	5661	12	4498
3	6305	13	4315
4	6976	14	4133
5	7647	15	3586
6	8344	16	3039
7	4771	17	2583
8	4934	18	2006
9	5014	19	1732
10	4832	20	1155
		21	608

Table 5.8 Framework Models for Emptying

Point	Normal Stress σ_w Pa			
	E4	E5	E6	E7
1	2622	1680	1680	1680
2	4947	2428	2428	2428
3(lower)	5734	2970	4541	8133
4	6965	5754	9000	6965
5	6743	5745	9563	6743
6	6276	6653	6474	6276
7	5587	7193	5587	5587
8	4947	7929	4947	4947
9	4356	8616	4356	4356
10	3642	3642	3642	3642
11	2978	2978	2978	2978
12	2387	2387	2387	2387
13	1674	1674	1674	1674
14	1034	1034	1034	1034

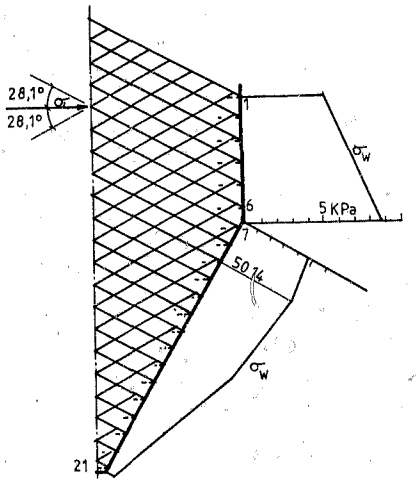

Figure 5.10 : E3 Framework with σ_1 horizontal

5.5.5 E5 Combined framework no. 1

An attempt was made to recognise that the same stress state cannot prevail throughout. Above the junction σ_1 is vertical, while below it is inclined at 30° to the horizontal. From Fig. 5.12 it can be seen that this results in a sudden transition in pressures half way down the slope. The pressures on the vertical wall at the junction are now much less than on the sloping wall. The values of the stresses are given in table 5.8.

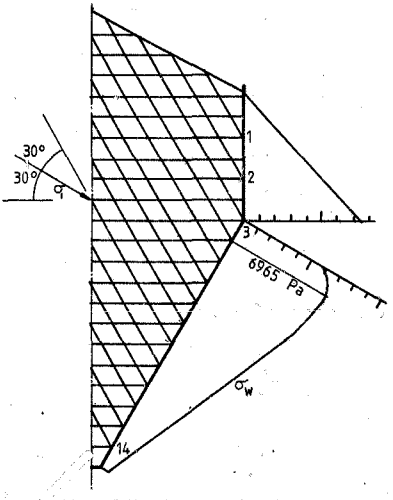

Figure 5.11 : E4 Framework with q_1 at 30° to the horizontal

5.5.6 E6 Combined framework no.2

In this case the demarcation between the upper and lower stress states is moved upwards. As with E5 a step results in normal pressure, Fig 5.13. The values of the stresses are given in table 5.8.

5.5.7 E7 Combined Framework no.3

The boundary between upper and lower stress states was moved further up. As can be seen from Fig. 5.14 the step in pressure

on the sloping wall is confined to the top point. The values of the stresses are given in table 5.8.

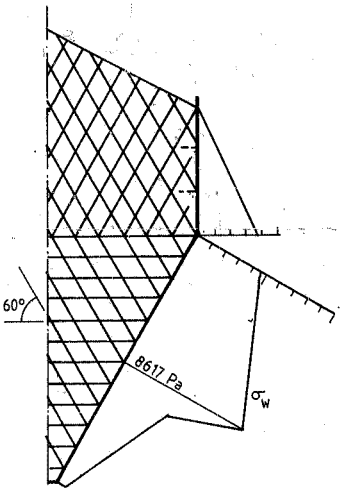

Figure 5.12 : E5 Combined framework no.1

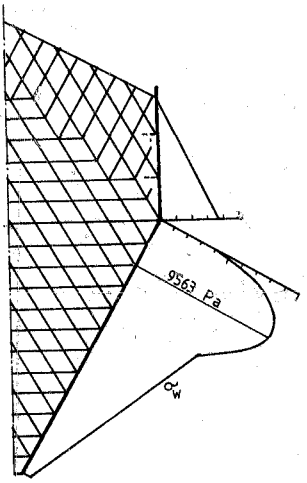

Figure 5.13 : E6 Combined framework no.2

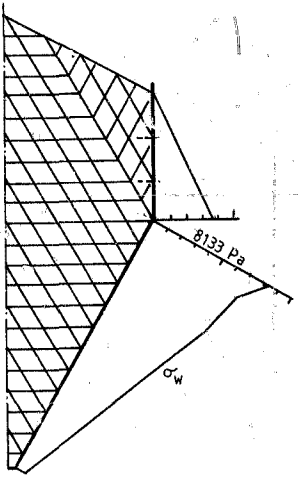

Figure 5.14:E7 Combined framework no.3

5.5.8 EG. Pseudo radial stress field

A principal of the radial stress field is used, Fig. 5.15 in that the normal wall stress on the inclined section BC is assumed to increase linearly from zero at the apex. It's slope is determined so that equilibrium is preserved. The vertical force on the sloping part depends on the shear force on the vertical part AB.

As in 5.5.2 full fluid pressure will be assumed on the vertical wall AB.

σ_w = 15715 x 0,201 = 3150 Pa. at B

Normal force = 3159 x 0,201/2 = 317,5 N/m
Shear force = 317,5 x tan20,1 = 116,1 N/m
Weight in half bin W = 1779,0 N/m

Let normal stress on BC be $\sigma_w = C(x + 0,03)$

where C is a constant, Fig. 5.15.

Then the normal force = N, and shear force = T = Ntan20,1.

For vertical equilibrium 0,8169 N + 116,1 = 1779

$\therefore$ N = 2036 N

Also $N = \frac{1}{2}\ 0,45 \times C(0,03 + 0,03 + 0,45) = 0,11475\ C$

$\therefore$ 0,11475 C = 2036

C = 17743

$\therefore$ $\sigma_w = 17743\ (x + 0,03)$ 5.17

Compare the radial stress field solution

$\sigma_w = 18513\ (x + 0,03)$ (Eqn.5.14)

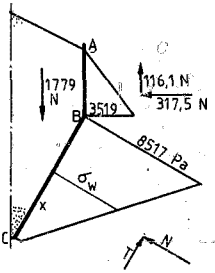

Figure 5.15 : E8 Pseudo radial stress field

CHAPTER 6

COMPARISON OF THEORIES WITH EXPERIMENTS

6.1 Graphs

In chapter 3 all the experimental results are given. The pressures are shown on a cross-section of the bin. This enables the surface to be shown at the same time to get a full picture. In this chapter larger graphs are used to show the normal pressure only. The results for measuring points on opposite sides are combined, so that with five tests there are ten results plotted at each of the fifteen measuring points.

6.2. Bin shape 1

6.2.1 Tables

Table 6.1 gives the experimental normal pressures (σ_w) for each of the tests for filling. Table 6.2 gives the pressures at the measuring points by the various theories, and the standard deviations from the measured values. For this purpose the 10 values at each of the 15 points were averaged.

then standard deviation $= \sqrt{\{\Sigma(Y_m - Y_c)^2/14\}}$ 6.1

where Ym = average measured value

Y_c = calculated value

Table 6.3 and 6.4 are the corresponding tables for the emptying cases.

6.2.2 Filling cases - bin 1

6.2.2.1 F1 Active state pressure, Fig 6.1

The straight line graph undercuts most of the results. This must be due to exceeding the wall friction angle. The standard deviation is 1773 Pa.

6.2.2.2 F2 Equilibrium of forces. Linear distribution, Fig.6.2.

This straight line fits the results much better than F1. The wall friction angle has been allowed for. The standard deviation of 960 pa is better than 1773 for F1.

6.2.2.3 F3 Equilibrium of forces. Parabolic distribution, Fig.6.3.

A parabola fits the results the best so far. Standard deviation is 550 Pa.

6.2.2.4 Walker theory for filling, Fig. 6.4.

This straight line is an improvement on F1, active state in that it uses a similar vertical pressure but adjusts the horizontal pressure to get the correct wall friction angle. The standard deviation is 1100, not quite as good as linear equilibrium, F2.

6.2.2.5 F5 Booth's pile theory, Fig. 6.5

This is the second curved graph. No allowance is made for wall friction angle and the line falls well below the experiments as for F1. This denies Booth's claim that the wall friction is of minor importance. The standard deviation at 1552 Pa is in the same league as F1 although a bit less.

6.2.2.6 F6 Booth's adjusted pile theory, Fig. 6.6.

The fit is much better than F5 as shown by the standard deviation of 841, which is the third lowest so far after F7. This must be due to the adjustment which increases the horizontal pressure to generate the correct wall friction angle.

6.2.2.7 F7 Framework theory , Fig. 6.7

With the second lowest standard deviation of 742 Pa the fit is surprisingly good in view of the simple framework chosen with slip line directions those of the classic active case, although horizontal members were added to obtain the correct wall friction angle. The advantage of this over F4, the Walker theory, is that the framework can effectively transfer vertical shears.

6.2.2.8 F8 Fitted curve, Fig. 6.8

A fourth order polynomial of the form

$$Y = A + Bx + Cx^2 + Dx^3 + Ex^4 \qquad 6.2$$

was fitted so as to minimise the sum of the squares of the errors(least squares). For this case it was found that:

A = 3529,03
B = 39988,4
C = 213715
D = 420108
E = -306336

The program used is given in Appendix H. The result is rather surprising when compared with the theories F1 to F7 as it shows a marked decrease in pressure towards the bottom. The lowest standard deviation results at 409, as would be expected.

6.2.3 Emptying case - bin 1

6.2.3.1 E1 Walker's theory - bin1, Fig. 6.9

As can be seen the fit is ot very good with a standard deviation of 1581 Pa.

6.2.3.2 E2 Radial stress field with linear cut-off, Fig. 6.10.

This simple graph of two straight lines provides the best fit of the 5 theories with a standard deviation of 836 Pa.

6.2.2.3 E2 Radial stress field with curved cut-off, Fig.6.11

The curve was added to bend towards the X axis. This takes the graph away from the results on the other side of the initial straight line, Fig. 6.10 and the result is a worse fit than E2 with a standard deviation of [illegible]7 Pa.

6.2.3.4 E4 Framework with σ_1 horizontal, Fig. 6.12.

Pressures increase from the bottom as they should but are too small lower down and too high at the top. The standard deviation is the most of all the theories at 1740 Pa.

6.2.3.5 E5 Framework with σ_1 inclined at 30° to the horizontal, Fig. 6.13.

The result is similar to E2, only not quite such a good fit. Standard deviation = 1103 Pa.

6.2.3.6. E6 Fitted curve, Fig. 6.14.

A fourth order polynomial was fitted with eqn. 6.2 and constants:

A = 180,531
B = 33404,1
C = -5334,31
D = 144 244
E = 112 107

The curve is almost a parabola and has a standard deviation of 251 Pa.

A comparison of the filling and emptying fitted curves is given in Fig. 6.15. There is a marked difference between the two.

6.3 Bin shape 2

6.3.1 Table 6.5 and 6.7 gives the experimental normal pressures for filling and emptying at each of the measuring points. 6.6 and 6.8 give the pressures at the measuring p... filling and emptying respectively by various theories, ...he standard deviations, eqn. 6.1 against the average test results at each measuring point. Fitted curves are also given.

6.3.2 Filling cases - bin 2

6.3.2.1. F1 Active state (Fig. 6.16)

Predicted pressures are on the low side due to the proper wall friction angle being exceeded. Standard deviation is highest at 1203 Pa.

6.3.2.2 F2 Equilibrium of forces (Fig.6.17)

The Coulomb theory gives a good approximation for the vertical part. On the sloping part the straight line fit is good. The standard deviation at 370 is the lowest of the theories.

6.3.2.3 F3 Walker theory (Fig. 6.18)

Another fairly good straight line. The standard deviation is 586 Pa.

6.3.2.4 F4 Booth's adjusted pile theory (Fig. 6.19)

The first curved theory. The fit is good with the second lowest standard deviation at 419.

6.3.2.5 F5 Framework theory (Fig. 6.20)

The shape of the pressure curve is the best along BC, but it undercuts the results and the values along AB are much too high. A standard deviation of 709 Pa is obtained.

6.3.2.6 F6 Fitted curves (Fig. 6.21)

Separate fourth order polynominals were applied to AB and BC, eqn. 6.2. For AB x = distance from B + 500.

Coefficients are as follows :

	CB	BA
A	4578,77	1519,63
B	10430,00	1576,46
C	-42922,4	2959,65
D	42,7060	-9453,59
E	74959,1	-3555,04

The standard deviation is lowest at 161 Pa.

6.3.3. Emptying cases - bin 2

6.3.3.1 E1 Walker's theory (Fig. 6.22)

Curve (a) grossly underestimates the pressures in BA and curve (b) grossly overestimates them. Curve (a) produces the closest overall fit with a standard deviation of 1320 against 1995 for curve (b). Neither curve produces a good fit in the sloping part CB.

6.3.3.2 E2 Radial stress field with curved cut-off (Fig.6.23)

The pressures in BA were taken with hindsight as hydrostatic which provides a very good fit. In CB the curved cutoff does not assist much in improving the fit. The standard deviation is lowest at 859 Pa.

6.3.3.3 E3 Framework with σ_1 horizontal (Fig. 6.24)

The pressures in the top BA turn out ridiculously high and the pressures in CB undercut the results, although the shape is good. The standard deviation is 3443 which improves to 945 if the values in E2 are used for BA.

6.3.3.4 E4 Framework with σ_1 at 30° to the horizontal (Fig. 6.25)

Again much too high pressures in BA, but the pressures in CB are very similar to E2. The standard deviation is 1685 and would be lowest at 836 if the values in E2 are used for BA.

6.3.3.5 E5 Combined framework no.1 (Fig.6.26)

Pressures in BA are improved. A sudden jump in pressure exceeds the measured values in CB. A better fit is obtained towards the top of the sloping part. Standard deviation is 1129.

6.3.3.6 E6 Combined framework no.2 (Fig. 6.27)

Another bulge produced in the wrong place. Standard deviation is 1648 Pa.

6.3.3.7 E7 Combined framework no. 1 (Fig. 6.28)

The best of the combined frameworks with a standard deviation of 1040 Pa.

6.3.3.8 E8 Pseudo radial stress field (Fig. 6.29)

A very simple result with two straight lines gives the second best fit. Standard deviation is 1019 Pa.

6.3.3.9 E9 Fitted curves. (Figs. 6.30 and 6.31)

The coefficients for the eqn. 6.2 are as follows :

	CB	BA
A	710,081	3706,91
B	19271,8	805,20
C	13979,0	3997,87
D	-53,2614	-19571,17
E	-20,1029	1154,01

The lowest standard deviation at 227 is obtained. Emptying and filling fitted curves are compared in Fig. 6.31. There is a marked difference between the two.

6.4. Summary

Table 6.9 summarises the theories in order of goodness of fit for both bin shapes for filling and emptying.

In both bins equilibrium of forces followed by Booth's adjusted pile theory (leaving out the one framework) are better than Walker for filling, and the radial stress field with a cut-off is best for emptying.

The question arises as to which of the theories is the most satisfactory to apply in all situations. The answer can only be given for the two shapes of bin and the material tested here, although reasonable extrapolation to other shapes and materials should be possible. A practical bin is seldom two dimensional. Usually there are dividing walls and there is a slope in both directions at the outlet. A typical configuration is shown in Fig. 6.32. Such a bin would be designed for two dimensional pressures acting in a plane normal to each wall. This would presumably err on the safe side. A square deep bunker is different and solutions for a circular cross section may be applied.

The theories for pressures in two dimensional bins may be divided into two types : filling pressures and emptying pressures.

For filling, equilibrium of forces is easy to apply and produces good results when a straight line or curved distribution of wall pressure is assumed. This shows that the assumption that horizontal stress on the centreline increases linearly with depth is a reasonable one for a shallow bin. The line of action and weight of the material is fully determined. Some difficulty arises with bin 2 in getting the force on the vertical wall. The pressure is more than the active pressure. Coulomb's analysis which takes wall friction into account gave reasonable results here.

Provided it is adjusted to give the correct wall friction angle, Booth's pile theory gives good results, but needs a lot of calculation. Stresses are always in equilibrium for any shape of bin. The free surface is adjusted to slope at the angle of friction δ .

Walker's theory for filling, which neglects vertical friction and accounts for the correct wall friction angle, is easy to apply and gives reasonable results, although the sloping free surface must be levelled off and treated as a surcharge.

The frameworks applied here had straight members with σ_1 vertical which is correct at the centreline but wrong at the wall. Consequently extra horizontal members were required at the wall. Nevertheless very good results were found for bin 1 and for the sloping part of bin 2. Pressures in the vertical part of bin 2 were too high. A compromise framework with straight lines inclined at 18° and 38° to the vertical should give better results for bin 1 (these angles will vary with δ and ϕ_w).

For calculating emptying pressures the radial stress field with linear cut off is simple and effective. In the case of bin 2 the pressure on the vertical wall, and the ratio between normal wall pressure below and above the transition must first be calculated. The use of full fluid pressure for the normal stress with full wall friction angle was a good approximation for the vertical part. The ratio of pressures below to above was too hight at 2. a value of 1 would be better. The pseudo radial stress field for bin 2 was simple and fairly good.

The framework with straight members and σ_1 at 30° to the horizontal provides an average value of the slope of σ_1 between that one the centreline (0°) and that on the sloping wall (60°). Good results were obtained for bin 1 and the sloping part of bin 2, but the values for the vertical part of bin 2 were too high. This may be improved by changing the slope of σ_1 to 15° in the vertical part.

Walker's method for the hopper treats the load above that as surcharge. The fit is not very good. This may be due to *the assumption that the vertical stress on a horizontal section* remains constant.

It is important that the density γ, effective internal friction angle δ and wall friction angle ϕ_w be determined accurately whatever theory is employed.

In comparing theories with experiment the high pressure peaks measured at the plate overlap in bin 1 should be noted. There a relatively minor feature has caused a pressure peak which indicates that some irregularity could cause a local high pressure in a full size bin.

TABLE 6.1 Bin 1 Filling Measured Normal Pressures (Pa.)

	X (1)	1 20 - 4 (2)		2 21 - 4		3 22 - 4		4 23 - 4		5 24 - 4		Average
	mm	L	R	L	R	L	R	L	R	L	R	
1	32,5	4747	4928	5614	4987	4704	4021	5155	4452	4430	5097	4813
2	72,5	5760	6198	5603	4945	5535	5461	5485	5425	5611	5804	5583
3	112,5	6033	5597	5338	4459	5182	4973	5510	4323	5476	4992	5188
4	152,5	5590	6453	5705	5582	5315	5799	6241	6011	5574	6254	5852
5	192,5	5975	5634	4637	5314	8273	7292	6857	7118	9330	8881	6928
6	257,5	5132	5673	4939	5030	4935	5086	4967	5031	5128	5200	5116
7	297,5	5017	4894	4716	4578	4656	4281	4456	4460	4889	4743	4669
8	337,5	4740	5267	4638	5219	4346	4568	4632	4800	4869	4962	4804
9	377,5	4520	5201	4604	4798	3911	4791	4661	4458	4647	4966	4656
10	417,5	4580	3935	4227	3827	3894	7929	4004	3454	4309	4044	4620
11	482,5	3896	3567	3382	3397	3373	3264	3492	3623	3776	3337	3511
12	522,5	3619	3357	3028	3112	3392	3028	3644	3259	3930	3223	3359
13	562,5	2255	2677	2002	2403	2072	2429	2227	2712	2440	2394	2361
14	602,5	1323	1349	!!!!	!!!?	1116	1119	1466	1339	1632	1308	1288
15	642,5	628	421	32	145	153	253	526	420	705	504	379

Notes (1) Slope distance from bottom

(2) 20 - 4 Test 20, set 4.

TABLE 6.1 Bin 1 Filling Measured Normal Pressures (Pa.)

	X (1)	1 20 - 4 (2)		2 21 - 4		3 22 - 4		4 23 - 4		5 24 - 4		Average
	mm	L	R	L	R	L	R	L	R	L	R	
1	32,5	4747	4928	5614	4987	4704	4021	5155	4452	4430	5097	4813
2	72,5	5760	6198	5603	4945	5535	5461	5485	5425	5611	5804	5583
3	112,5	6033	5597	5338	4459	5182	4973	5510	4323	5474	4992	5188
4	152,5	5590	6453	5705	5582	5315	5799	6241	6011	5574	6254	5852
5	192,5	5975	5634	4637	5314	8273	7292	6857	7118	9330	8881	6928
6	257,5	5132	5673	4939	5030	4935	5080	4987	5031	5128	5200	5114
7	297,5	5017	4894	4716	4578	4656	4281	4456	4460	4889	4743	4669
8	337,5	4740	5267	4033	5219	4346	4568	4632	4800	4869	4962	4804
9	377,5	4520	5201	4604	4798	3911	4791	4661	4458	4647	4966	4656
10	417,5	4580	3935	4227	3827	3894	7929	4004	3454	4309	4044	4620
11	482,5	3896	3567	3382	3397	3373	3264	3492	3623	3776	3337	3511
12	522,5	3619	3357	3028	3112	3392	3028	3644	3259	3930	3223	3359
13	562,5	2255	2677	2002	2403	2072	2429	2227	2712	2440	2394	2361
14	602,5	1323	1349	1111	1117	1116	1119	1466	1339	1632	1308	1288
15	642,5	628	421	32	145	153	253	526	420	705	504	379

Notes (1) Slope distance from bottom

(2) 20 - 4 Test 20, set 4.

TABLE 6.2 BIN 1 Filling Pressures According to Seven Theories, & Fitted Curve (Pa.)

	X mm	Y meas.	F1	F2	F3	F4	F5	F6	F7	F8
1	32,5	4813	5407	6398	5299	6211	4409	5828	6343	4616
2	72,5	5583	5061	6085	5451	5878	4271	5534	5686	5456
3	112,5	5188	4715	5771	5535	5545	4129	5433	5332	5871
4	152,5	5852	4370	5458	5553	5212	3984	5225	5175	5980
5	192,5	6928	4024	5144	5503	4879	3834	5008	5014	5881
6	257,5	5114	3462	4365	5280	4338	3577	4630	4828	5478
7	297,5	4669	3116	4321	5054	4005	3407	4377	4664	5168
8	337,5	4804	2770	4008	4762	3672	3224	4103	4490	4852
9	377,5	4656	2425	3695	4403	3339	3024	3804	4300	4542
10	417,5	4620	2079	3381	3976	3005	2799	3471	4203	4230
11	482,5	3511	1517	2872	3140	2464	2355	2830	3574	3647
12	522,5	3359	1171	2558	2538	2131	2005	2348	3107	161
13	562,5	2361	825	2245	1869	1798	1561	1773	2494	2490
14	602,5	1288	479	1931	1133	1465	980	1072	1853	1542
15	642,5	379	134	1618	329	1132	204	213	942	203
Standard Deviation			1773	960	550	1100	1522	841	742	409

TABLE 6.3 Bin 1 Emptying Measured Normal Pressures, (Pa)

	X mm	1 20 - 5		2 21 - 6		3 22 - 6		4 23 - 6		5 24 - 8		Average
		L	R	L	R	L	R	L	R	L	R	
1	32,5	1482	1438	1508	1230	1367	1203	1678	1343	1535	1325	1411
2	72,5	2305	2306	2872	2508	2482	2306	2375	2611	2614	2468	2487
3	112,5	3310	2529	3303	3147	2844	2916	3843	3038	3099	3181	3121
4	152,5	4466	6422	6176	6196	4699	5449	4336	4491	4301	3908	5044
5	192,5	5416	4518	7385	7348	7479	6609	4835	4297	5789	3742	5742
6	257,5	6641	7103	6443	6933	6051	6444	6562	7395	6037	6503	6611
7	297,5	6320	6619	6162	6387	6144	6106	7063	6654	6479	6469	6440
8	337,5	6544	7069	6399	7230	6089	6199	7329	7074	7406	6676	6802
9	377,5	6269	7077	6086	6440	5726	6064	6615	6252	7154	7151	6483
10	417,5	6085	5466	5036	4945	6393	10120	5779	4883	6595	5921	6122
11	482,5	5156	4684	4451	4102	4390	4228	4683	4746	5695	4963	4710
12	522,5	4685	4251	3894	3640	4254	3716	4372	4116	5466	4609	4300
13	562,5	2944	3272	2478	2780	2532	2826	2827	3155	3464	3204	2948
14	602,5	1703	1626	1322	1262	1262	1339	1660	1584	2039	1740	1298
15	642,5	435	376	278	232	278	277	585	464	781	407	378

TABLE 6.4 Bin 1 Emptying Pressures According to Five Theories and Fitted Curves (Pa.)

	X mm	Y meas.	E1	E2	E3	E4	E5	E6 (fitted)
1	32,5	1411	3498	1156	1156	786	959	1235
2	72,5	2487	4223	1897	1894	1451	1640	2522
3	112,5	3121	4648	2637	2622	2131	2320	3682
4	152,5	5044	4883	3378	3329	2862	3002	4699
5	192,5	5742	4983	4118	4001	3369	3677	5538
6	257,5	6611	4934	5322	4965	4322	4781	6458
7	297,5	6440	4804	6062	5444	4953	5456	6726
8	337,5	6802	4612	6803	5803	5493	6127	6756
9	377,5	6483	4367	7544	6011	5350	6796	6547
10	417,5	6122	4075	6726	6034	5156	7168	6106
11	482,5	4710	3518	4908	5583	4609	5585	4929
12	522,5	4300	3129	3790	4938	4599	4175	3957
13	562,5	2948	2710	2671	3962	4401	2918	2833
14	602,5	1298	2262	1552	2605	3953	1727	1595
15	642,5	378	1789	433	819	3360	55	287
Standard Deviation			1581	836	1057	1740	1103	251

Table 6.5 Bin 2 Filling.measured normal pressures, (Pa.)

	x(1) mm	1 27-2(2) L	1 27-2(2) R	2 28 - 2 L	2 28 - 2 R	3 29 - 2 L	3 29 - 2 R	4 30 - 2 L	4 30 - 2 R	5 31 - 2 L	5 31 - 2 R	Average
1	32,5	5031	4039	5232	4359	5011	4058	5378	4111	5390	4066	4668
2	72,5	3885	4949	5863	4987	5789	5146	5622	4835	5653	5032	5376
3	112,5	5816	4714	5446	4719	5638	4953	5547	4770	5993	4861	5228
4	152,5	5310	5377	5447	5351	5324	5390	5782	5210	5418	5259	5328
5	192,5	4931	5130	5025	5027	4575	5369	4840	5001	4881	4780	4956
6	257,5	4818	4822	5001	4201	4794	4807	5009	4422	4841	4383	4710
7	297,5	4117	4252	4496	4048	4351	4143	4382	4086	4445	4212	4253
8	337,5	4277	4367	4417	4700	3904	4118	3996	4206	3942	4573	4250
9	377,5	4224	4414	4374	4199	4059	4372	4092	4419	4127	4414	4269
10	417,5	3699	3336	3894	3188	3760	3325	4025	3280	3922	2946	3538
11	34	1596	1323	1548	1372	1458	1427	1625	1419	1423	1325	1452
12	74	1277	1227	1279	1258	1346	1254	1160	1188	951	1295	1224
13	114	835	1263	815	1095	732	1066	744	1143	719	1104	952
14	154	488	520	689	576	671	480	496	530	367	377	519
15	194	189	95	158	95	0	0	193	72	-372	-46	38

(1) 1 - 10 Slope distance from C (bottom)
11 - 15 Vertical distance from B (junction)

(2) 17 - 2 Test 27, Set 2.

Table 6.6 Bin 2 . Filling Pressures according to Five Theories and Fitted Curves (Pa.)

	x mm	y meas. (av_1)	F1	F2	F3	F4	F5	F6 (fitted)
1	32,5	4668	5143	5235	6180	5523	4368	4872
2	72,5	5376	4796	5155	5848	5328	4671	5111
3	112,5	5228	4448	5074	5516	5126	4650	5220
4	152,5	5328	4101	4994	5183	4916	4496	5211
5	192,5	4956	3752	4913	4851	4696	4336	5099
6	257,5	4710	3188	4783	4310	4310	4049	4748
7	297,5	4253	2840	4704	3918	4050	3853	4471
8	337,5	4250	2492	4622	3646	3765	3756	4183
9	377,5	4269	2145	4541	3313	3450	3518	3923
10	417,5	3538	1793	4461	2981	3094	3297	3732
11	34	1452	778	1310	1110	1609	2880	1476
12	74	1224	600	1011	932	1424	2228	1225
13	114	952	422	711	754	1157	1569	909
14	154	519	244	411	576	761	871	520
15	194	38	66	111	398	156	237	53
Standard Deviation			1203	370	586	419	709	161

Table 6.7 Bin 2 Emptying, Measured Normal Pressures, Pa.

	x mm	1 27 - 5 L	R	2 28 - 5 L	R	3 29 - 6 L	R	4 30 - 6 L	R	5 31 - 6 L	R	Average
1	32,5	1340	1235	1282	1293	1137	1134	1205	1265	1116	1228	1223
2	72,5	2238	2438	2504	2237	2612	1980	2403	2363	2115	2088	2298
3	112,5	3326	2668	3526	2661	3070	3064	3191	2489	2475	2295	2886
4	152,5	3758	4090	4433	4964	4671	4505	4420	4447	4182	4461	4393
5	192,5	3844	4888	3545	5273	4330	4725	3226	4679	3831	3792	4213
6	257,5	6131	5729	6189	5067	6575	6130	6202	5424	6074	5695	5922
7	297,5	5599	5878	5924	5775	6146	5542	5965	5662	6163	5638	5830
8	337,5	6094	6388	6183	6416	5917	6086	6077	6353	6160	6466	6209
9	377,5	6158	6428	6056	6088	5843	5936	5664	6397	6076	6407	6105
10	417,5	5306	4601	5696	4774	5038	4663	5785	4749	4996	4237	4985
11	34	2514	2220	2605	2168	2241	2258	2599	2273	2439	2287	2360
12	74	1994	2079	2157	1928	1862	1925	1938	1889	1826	2060	1966
13	114	1349	1620	1304	1561	1284	1460	1318	1659	1292	1624	1447
14	154	646	590	728	668	651	492	719	549	458	492	599
15	194	31	0	0	23	-30	0	63	24	-220	-24	-13

Table 6.8 Bin 2 Emptying Pressures according to *Eight Theories* and Fitted Curve

	x mm	y meas. (av.)	E1 (a)	E1 (b)	E2	E3	E4	E5	E6	E7	E8	E9 *(fitted)*
1	32,5	1223	3514	3312	1156	1032	942	948	948	948	1108	1350
2	72,5	2298	4245	3964	1897	1758	1631	1631	1631	1631	1818	2175
3	112,5	2886	4675	4324	2637	2246	2387	2387	2387	2387	2528	3022
4	152,5	4393	4915	4501	3378	2920	3022	3022	3022	3022	3238	3865
5	192,5	4213	5019	4547	4118	3618	3737	4305	3737	3737	3947	4661
6	257,5	5922	4918	4416	5318	4352	4868	8019	4868	4868	5105	5714
7	297,5	5830	4850	4238	6043	4577	5544	7241	5544	5544	5810	6104
8	337,5	6209	4661	4000	6719	03	6276	6653	6474	6276	6520	6196
9	377,5	6105	4420	3711	722	000	6757	5712	9525	6757	7230	5891
10	417,5	4985	4132	3378	7	4854	6800	5188	9000	7120	7939	5080
11	34	2360	1080	5045	2624	7938	6021	2796	2796	2796	2624	2405
12	74	1966	905	4424	1996	7217	4625	2324	2324	2324	1996	1929
13	114	1447	726	3730	1367	6507	3194	1864	1864	1864	1367	1365
14	154	599	544	2954	738	5817	1653	1694	1694	1694	738	707
15	194	-13	358	2087	110	5122	40	943	943	943	110	-49
Standard Deviation			1320	1995	859	3443	1685	1129	1648	1040	1019	227
						945	836	(1)				

(1) These values of standard deviation were obtained when the 11 to 15 (vertical wall) values of E2 were used instead of those shown for E3 and E4 respectively.

Table 6.9 Order of fit for theories

Note: Standard deviation in brackets.

Filling - Bin 1

F3 Equilibrium of forces. Parabolic Distribution (550)
F7 Framework theory (742)
F6 Booths Adjusted Pile Theory (841)
F2 Equilibrium of Forces. Linear distribution (960)
F4 Walker Theory (1100)
F5 Booth's Pile Theory (1522)
F1 Active state (1773).

Filling - Bin 2

F2 Equilibrium of forces (370)
F4 Booth's Adjusted Pile Theory (419)
F3 Walker Theory (586)
F5 Framework Theory (709)
F1 Active state (1203).

Emptying - Bin 1

E2 Radial Stress Field with Linear Cutoff (836)
E3 Radial Stress Field with Curved Cutoff (1057)
E5 Framework with σ_1 inclined at 30° to horizontal (1103)
E1 Walker's theory (1581)
E4 Framework with σ_1 Horizontal (1740)

Emptying - Bin 2

E2 Radial Stress field with curved cutoff (859)
E6 Pseudo Radial Stress Field (1019)
E7 Combined Framework No.3 (1040)
E5 Combined Framework No.1 (1129)
E1(a) Walker's Theory (1320)
E4 Framework with σ_1 at 30° to horizontal (1685)
E1(b) Walker's Theory (1995)
E3 Framework with σ_1 horizontal (3443).

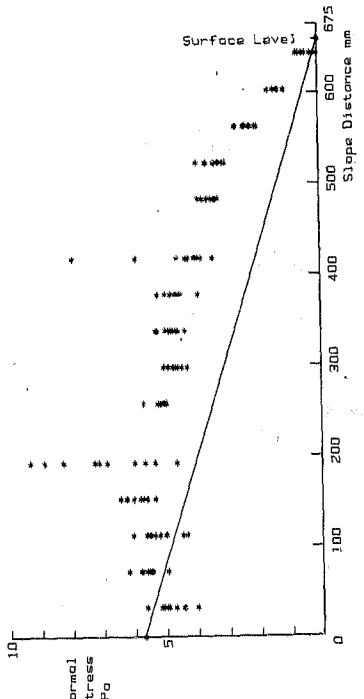

Figure 6.1: Bin 1 filling F1. Active state pressure

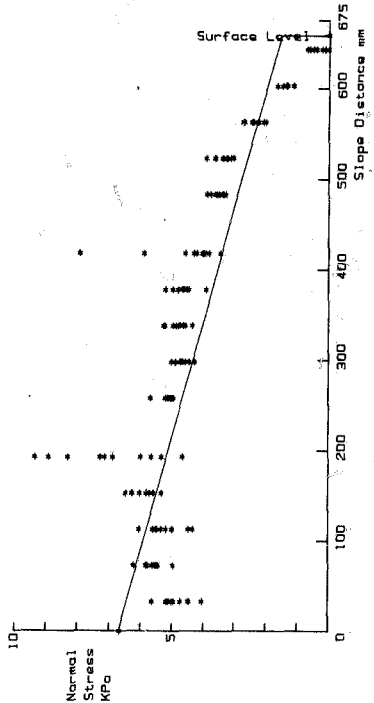

Figure 6.2: Bin 1 filling F2. Equilibrium of forces - linear distribution

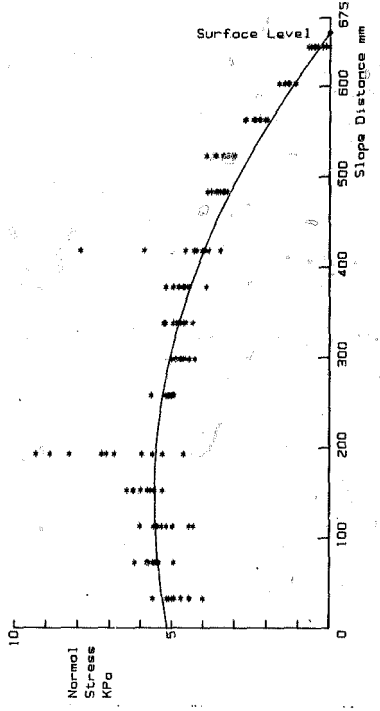

Figure 6.3: Bin 1 filling F3. Equilibrium of forces - parabolic distribution

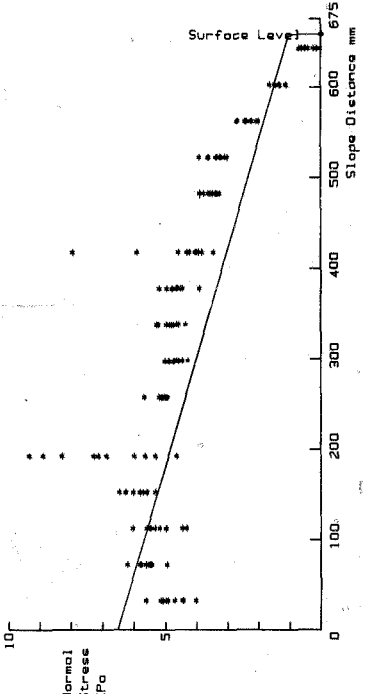

Figure 6.4 : Bin 1 filling F4. Walker theory for filling

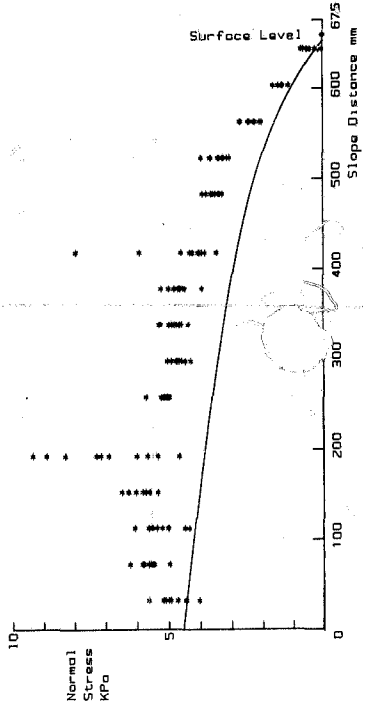

Figure 6.5 : Bin 1 filling FS. Booth's pile theory

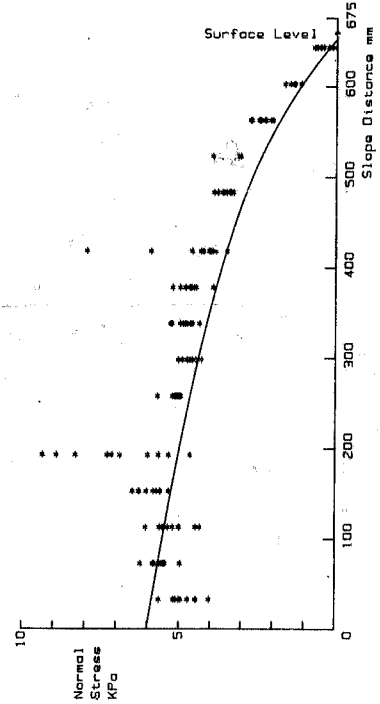

Figure 6.6 : Bin 1 filling F6. Booth's adjusted pile theory

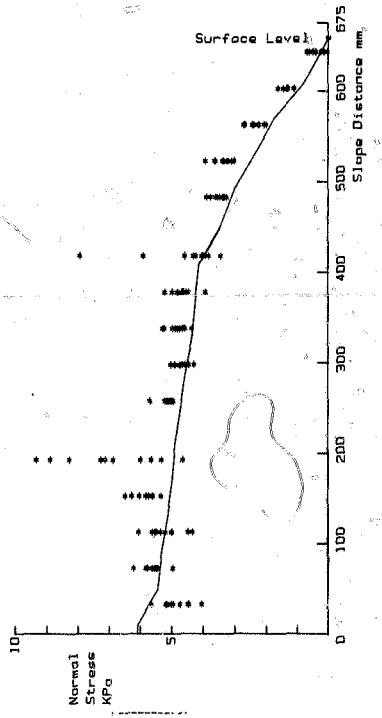

Figure 6.7 : Bin 1 filling F7 . Framework theory

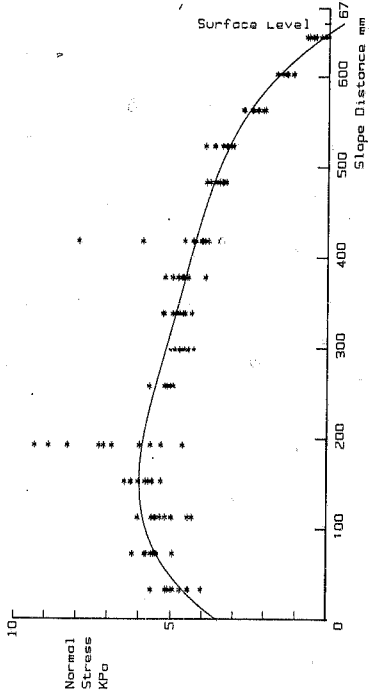

Figure 6.8 : Bin 1 filling F8. Fitted curved (fourth order polynomial)

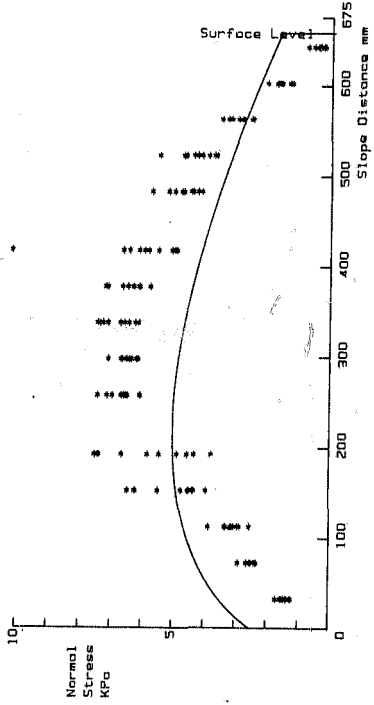

Figure 6.9 : Bin 1 emptying . El Walker's theory

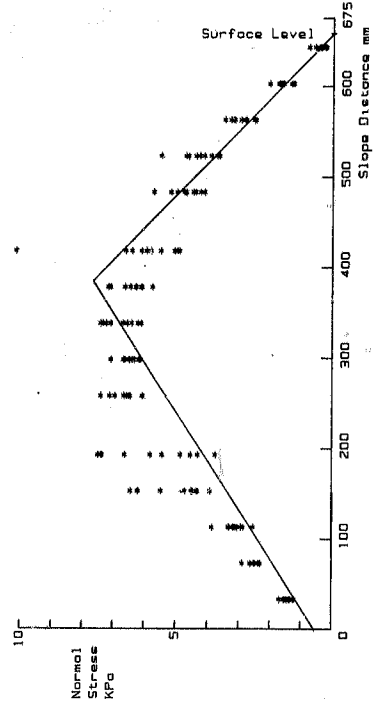

Figure 6.10: Bin 1 emptying. E2 Radial stress field with linear cut-off

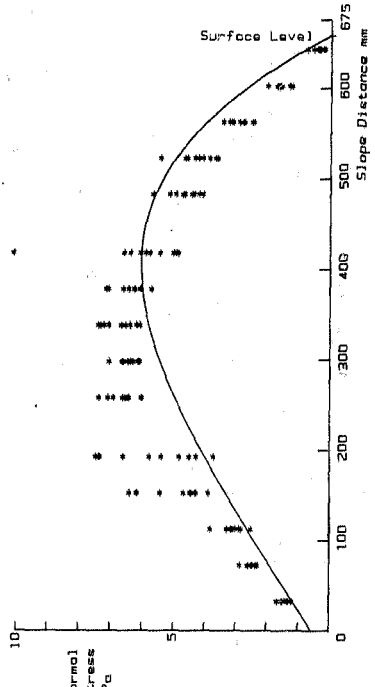

Figure 6.11: Bin 1 emptying. E3 Radial stress field with curved cut-off

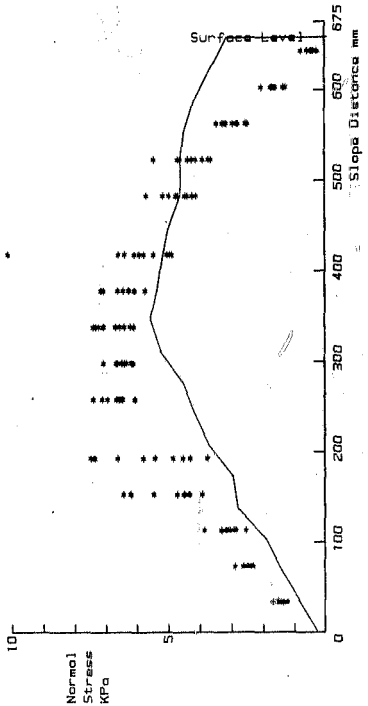

Figure 6.12 : Bin 1 emptying. EA Framework with θ_1 horizontal

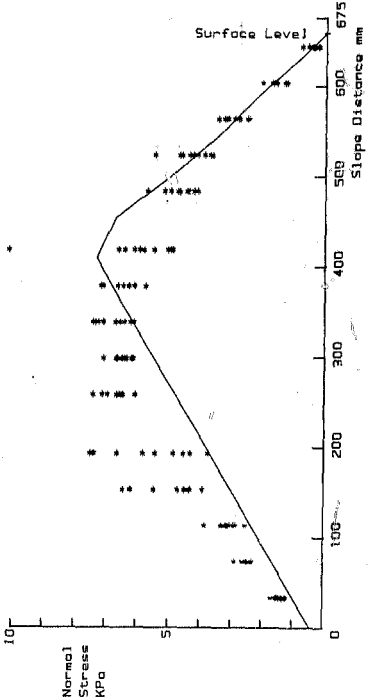

Figure 6.13 : Bin 1 emptying. E5 Framework with σ_1 inclined at 30° to the horizontal

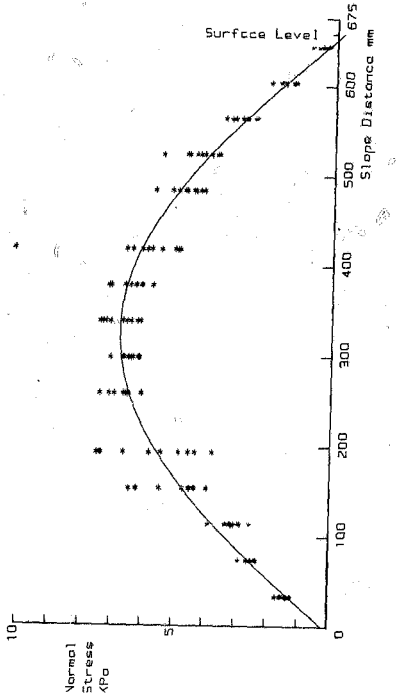

Figure 6.14 : Bin 1 emptying. E6 Fitted curve (fourth order polynomial)

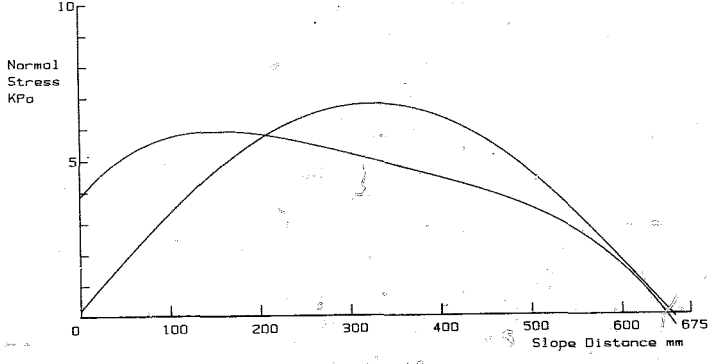

Figure 6.15 : Bin 1. Comparison of filling and emptying fitted curves

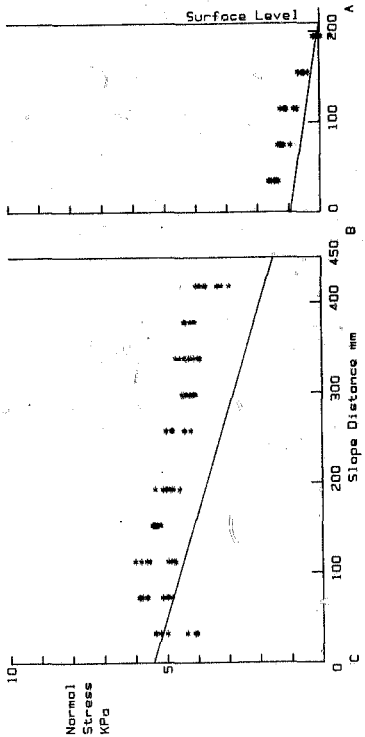

Figure 6.16: Bin 2 filling F1. Active state pressure

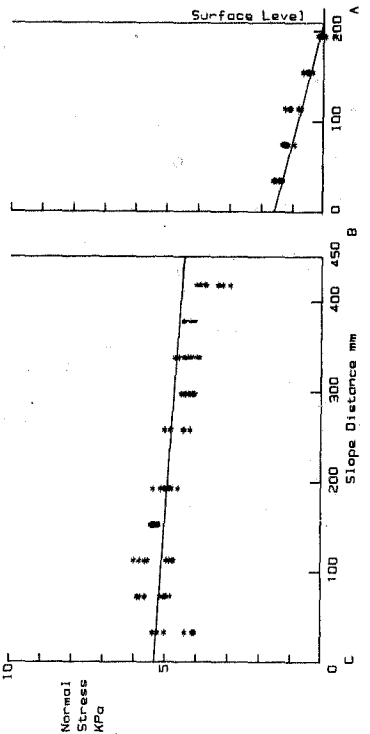

Figure 6.17: Bin 2 filling F2. Equilibrium of forces

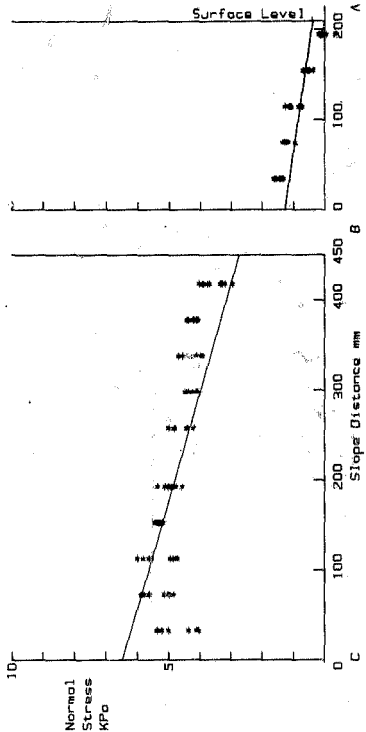

Figure 6.18: Bin 2 filling F3. Walker's theory

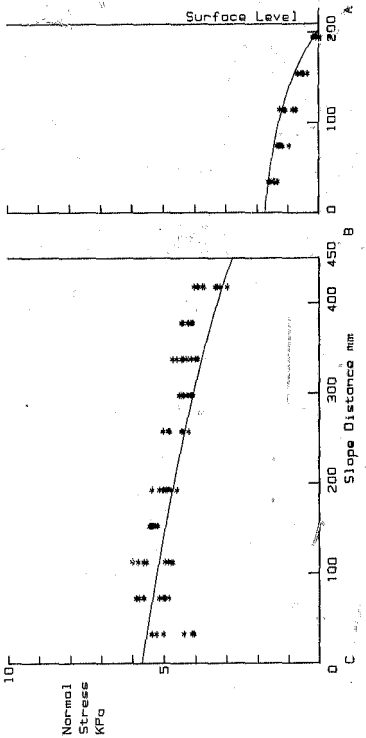

Figure 6.19: Bin 2 filling F4. Booth's *adjusted pile theory*

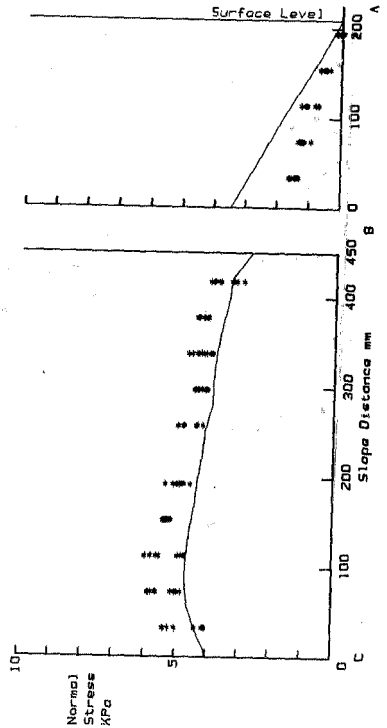

Figure 6.20: Bin 2 filling F5. Framework theory

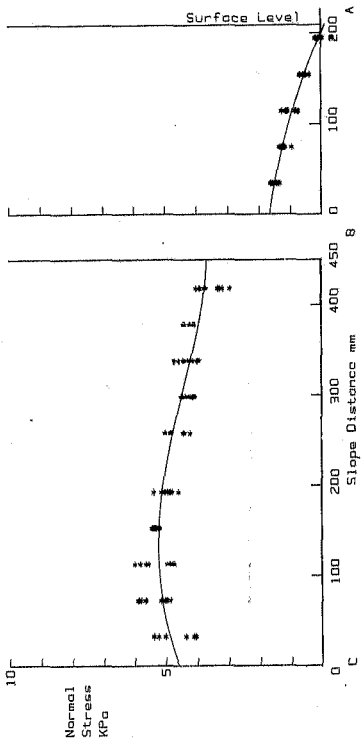

Figure 6.21 : Bin 2 filling F6. Fitted curves (fourth order polynomials)

Figure 6.22 : Bin 2 emptying E1. Walker's theory

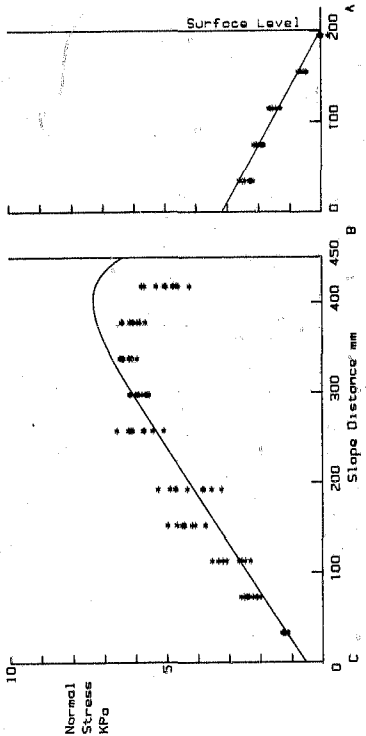

Figure 6.23 : Bin 2 emptying E2. Radial stress field with curved cut-off

Figure 6.24 : Bin 2 *emptying* E3. Framework with σ_1 horizontal

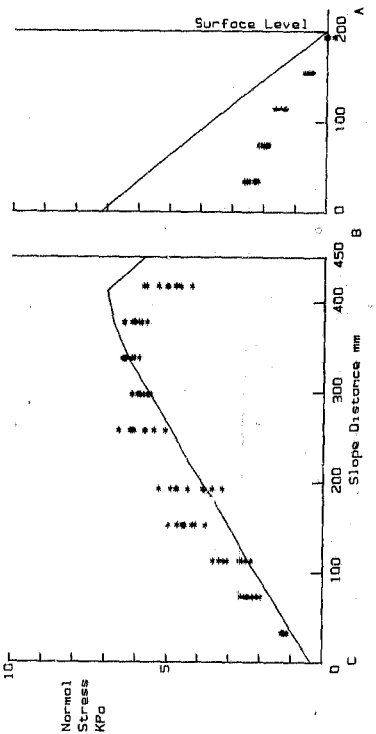

Figure 6.25: Bin 2 emptying E4. Framework with σ_1 inclined at 30° to the horizontal

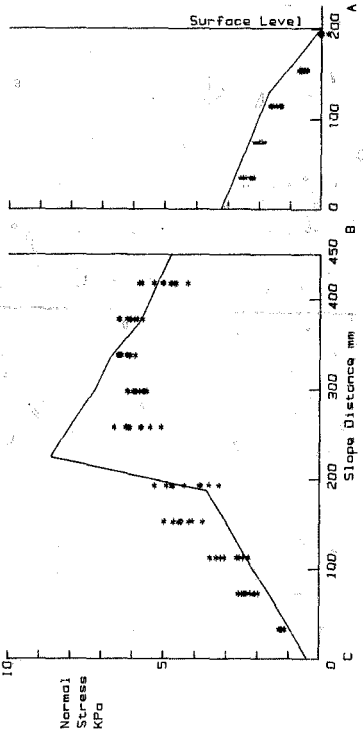

Figure 6.26 : Bin 2 emptying E5. Combined framework no.1

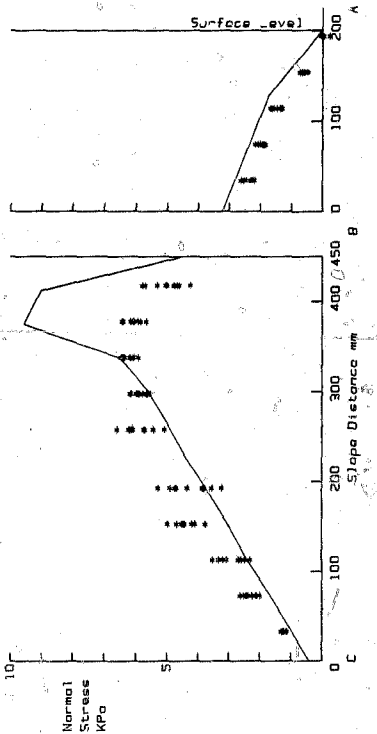

Figure 6.27 : Bin 2 emptying E6, Combined framework no.2

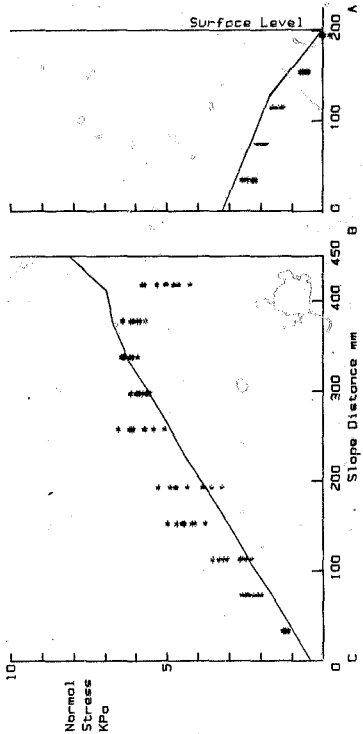

Figure 6.28 : Bin 2 emptying E7. Combined framework no.3

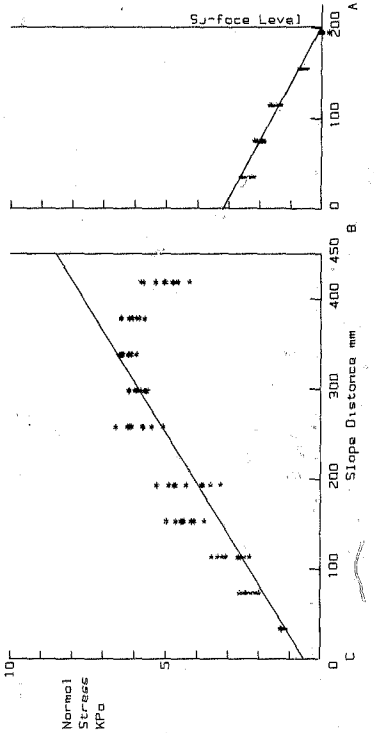

Figure 6.29 : Bin 2 emptying E8. Pseudo radial stress field

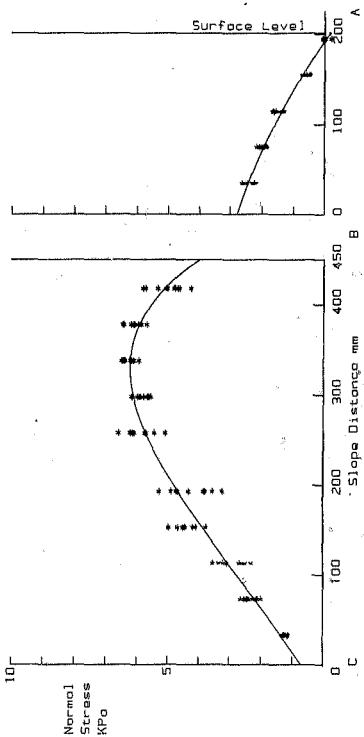

Figure 6.30 : Bin 2 emptying E9. Fitted curves (fourth order polynomials)

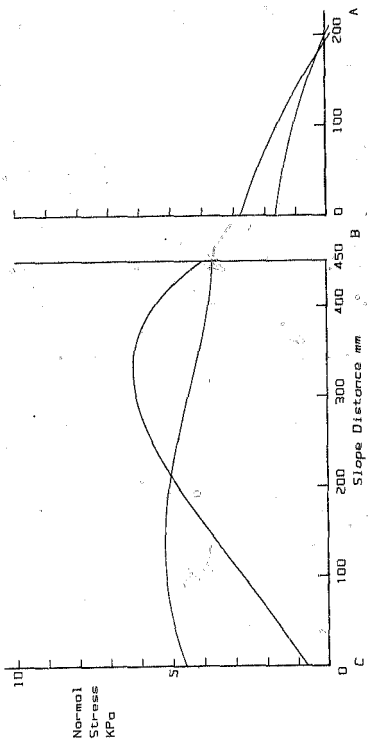

Figure 6.31 : Bin 2. Comparison of fitted filling and emptying curves

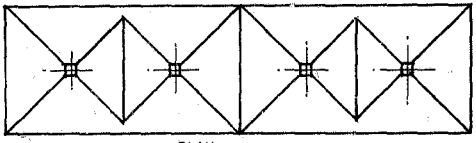

PLAN

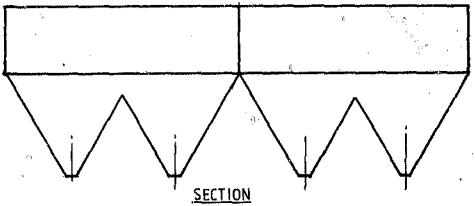

SECTION

FIGURE 6.32: *Practical Bin*

CHAPTER 7

DISCUSSION AND CONCLUSIONS

7.1 Measurement of normal and shear stresses

The method of measuring normal pressures was to instrument each of 5 plate spans on each of six plate elements. Shear stress was measured as an average for each plate. The advantages were simplicity, avoiding sealing around separate load cells, less worry about the stiffness of a separate load cell, in which the pressure might reduce as it deflects, and a large number of normal pressure measurements per side. The shear stress measurement had the disadvantage of only one measurement per plate. The overlap of plates necessary to seal the bin created pressure peaks in some tests of bin 1 (for example, Fig 3.6). In calibrating for normal pressure one span at a time it was found that adjacent spans were affected. This was ignored and taken partially into account by calibrating in situ with water at different depths (chapter 2). This is a disadvantage compared to using separate load cells. There is some slight assymmetry evident, Figs 3.38 and 3.39 in bin 2 and nothing detectable in bin 1.

The flexibility of the bin may also have changed the pressure readings. For example the drop in pressure at the bottom for filling, Figs 3.17 and 3.38.

7.2 Scale effect

Apart from the possible defects in the measuring system, there is the question of scale effects. The usual problem is how to predict stress and strain and other quantities on the prototype from model measurements [42]. The problem here is: would the distribution of stress on the walls be geometrically similar, and would a theory used to predict the stresses give the same accuracy for model and prototype? The best way to

investigate this would be to test, using the same sand, a geometrically similar model made as large as possible . The quantities affecting the results are density, and internal and wall friction angle which would be known for model and prototype. Varying flexibility of the bin walls and the ratio of particle size to bin size could produce a scale effect. On the other hand because the movement is large flexibility of the bin should not matter, especially at discharge. The particle size is small compared to the model size and so it should have no effect.

7.3 Effect of end walls

The glass end walls were 400mm apart and had an observed friction effect, although the angle of friction of sand on glass is lower than that of sand on steel. As noted in chapter 3 the surface was higher at the glass than in between on emptying and the summed weight was always less than that from the load cells. Therefore the measured normal and shear stresses were scaled up by the appropriate ratio for each test. The average ratio was 1,24 for bin 1, table 3.1 and 1,18 for bin 2, table 3.4. This correction enabled the comparison of theory with experiment to be made. The end wall friction therefore makes the flow to some extent three-dimensional and this may result in a change in condition compared to the two-dimensional case. It is assumed that the three-dimensional effect once the above correction had been made was negligible.

7.4 Switch pressure

An attempt was made to observe switch pressures, section 3.3. A switch pressure is postulated as a point load at the interface of the filling and emptying regimes, assuming that below it the emptying regime is fully established and above it the filling regime is still undisturbed. This was shown to be false for the bins tested. An important discovery was that (a) there was a rapid transition over the full wall from filling to

emptying pressures and that (b) intermediate pressure distributions lay between the two extremes and thus no point load occurred. There could be a switch pressure that occurs in hoppers with very much steeper sides. In reference [40] the pressure peak at the junction of inclined and vertical wall is erroneously referred to as a switch pressure. There were 15 points down a side for measurement of normal pressure, so if there was a switch pressure it should have been picked up. High concentrations were picked up in bin 1 in some tests due to arching at the plate overlaps (Fig 3.2).

7.5 Mass flow and piping

In bin 1 initial flow was observed to occur down the centre with the result that the surface dropped faster in the middle. Towards the end the surface levelled out again, Fig 3.3, indicating flow of all the material. A fairly broad active zone could be observed with feeder zones on the side and on the surface. The friction angles measured on the walls indicated that there was downward movement there all the time although not seen by the naked eye.

In bin 2 a distinct broad column was observed to be moving, Fig 3.24, the apex formed into a trough and then the surface flattened out again after the surface dropped below the vertical part.

7.6 Dynamic effects

It was assumed that acceleration or velocity effects were negligible so that no flow pressures would be the same as flow pressures at the instant when flow stopped. This still allows changes with time to be measured as can be seen in the plots of normal pressure, for example, test 24, Figs. 3.10 and 3.11.

7.7 Measured pressures and theories

The tests showed definite differences between filling and emptying pressures in both bin shapes and good agreement between successive tests. If it is assumed that the measured pressures and shear stresses are an accurate reflection of what would occur in a full size bin notwithstanding the possible variations introduced by the factors already mentioned, i.e. measuring system, bin flexibility, scale effect, then the various theories can be rated in order of their goodness of fit, table 6.9.

For filling the active state theory is a poor fit because the wall friction required is excessive. The results with frameworks are variable, and depend very much on the attention given to choosing suitable ones. This method gives a clear insight into the generation of forces for both filling and emptying. Walker's theory for filling, which allows no shear on vertical planes and determines the horizontal stress to get the correct wall friction angle, gives good results. The fit of the Walker emptying theory is disappointing in the bin shapes tested here. It will probably improve if the walls are steeper. Booth's unadjusted pile theory does not satisfy the wall friction condition and gives poor results. Adjusted so that the horizontal stresses are increased the results are good. It is a versatile theory that can be applied to any shape bin for filling conditions. Equilibrium of forces for filling depends on the assumption of linearly increasing pressure on the centreline and on the choice of a suitable pressure distribution on the vertical walls. It is simple and gives very good results. The radial stress field with linear or curved cutoff gives the best results for discharge. Even simpler the pseudo radial stress field works very well for bin 2.

In conclusion there are several simple theories which produce acceptable results for predicting filling and discharge pressures in the shapes tested.

7.8 Axisymmetric and square bins

Walker's theory and the radial stress field can be equally easily applied to axisymmetric bins. The framework method would require a three-dimensional slice, which may prove difficult, Booth's pile theory was only developed in two-dimensions. It should not prove too difficult to extend it to the axi-symmetric case.

7.9 Further experiments

7.9.1 Displacement fields

The displacements and hence strain distribution could be determined using a stereo-photogrammetric method [43]. This will improve the framework modelling and will show how the change propogates at the start of discharge. Photographs have already been taken through the glass end wall. Movement was seen but not analysed or incorporated in this report. The method depends on the movements at the glass being a true reflection of what happens internally.

7.9.2. Different shapes

The present apparatus an accommodate bin half angles of 45° and 60° with the vertical as well as 30° or an assymmetrical bin with the left side at 45° and the right side at 30°.

7.9.3 Internal pressure cell

An internal pressure cell, Fig 7.1 capable of measuring three virtually perpendicular pressures could be introduced from above. In this way stresses could be monitored on the centre line. Taking measurements across the bin would show the effect of the end wall.

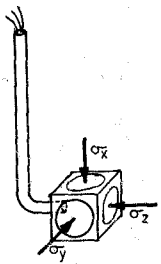

Figure 7.1 : Internal pressure cell

7.9.4 *Different materials*

Materials with different densities, friction angles, particle sizes and other properties could be tested. Slight cohesion could be introduced by wetting the sand. Although this would be negligible in soil mechanics terms it could result in appreciable differences in bin pressures.

7.9.5 *Bigger bin*

A very much larger bin of the same geometry in cross section could be tested. Apart from greater accuracy the effect of scale would be seen. The bin should be twice as wide proportionately to reduce the effect of end walls. A mechanical handling system would be a necessity for taking the material from the bin and lifting it up to the feed hopper. It may help to slope the end walls out from top to bottom slightly to reduce end effect. Inserts could be placed in the bin to

produce a three-dimensional situation, for example a square cross-section or a multi-outlet bottom.

7.9.6. Improved wall stress measurement

Individual pressure cells, each one measuring normal and shear stresses would be an improvement although more expensive. There will then be careful sealing required so that the shear movement in particular is not inhibited. Stiffness is also important to prevent false readings from a cell that deflects too much. Load cells should be placed down the centreline of the bin to reduce the end effect. Individual load cells would not have the cross-talk effect of the present measuring system where the pressure on a given panel affects those adjacent to it.

7.9.7 Dynamic effects

Some tests could be run with continuous recording. If this was arranged on all channels it would give a precise picture of changes occurring at the start of discharge and show if any switch pressures developed and whether there were significant differences between flow and no flow pressures.

7.10 Further methods of analysis

7.10.1. Use of the computer

As can be seen the methods used in this report have been kept simple with no computer involvement really necessary. By employing the computer it is possible to explore other more sophisticated methods which may or may not yield better results. The advantage would be a more fundamental approach that removes empiricism.

7.10.2. Frameworks with curved slip lines

If the framework members follow the curved slip lines actually present very much better results should be obtained. Although

th principles are as simple as for frameworks with straight lines, analysis by hand is too time consuming and prone to

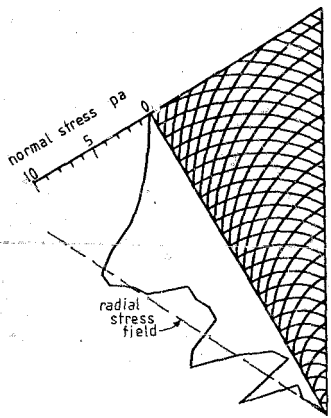

Figure 7.2: Framework – curved slip lines

errors. Loads have to be determined, different for each joint. Equilibrium at a joint depends on a unique set of angles between the members. An analysis by computer with curved slip lines [10] produced dissappointing results, Fig 7.2. Large oscillations were produced, showing no damping as would be anticipated. using the scheme shown in Fig 7.3 there might be an improvement. The difference between the framework in Fig 7.2 and that in Fig 7.3 is that in the former spacing down the wall was kept constant while in the latter, one slip line produces another reflecting from wall and centreline down the bin reducing the spacing towards the outlet.

The stero-photogrammetric method could be used first to determine the direction of the principal strains and hence slip lines.

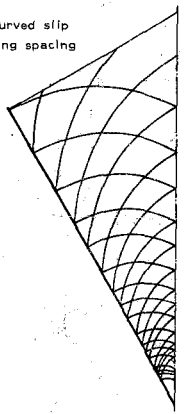

Figure 7.3: Curved slip lines - reducing spacing down wall

7.10.3 Limit plasticity approach

The method of Mroz and Drescher [24] mentioned in chapter 1 is promising, Fig 7.4. As can be seen the material is divided into rigid blocks from which an approximate kinematically admissible velocity field is constructed. Using the Coulomb law for friction between blocks an energy equation is applied either to the whole, or to a part to determine intermediate pressures. The method is equivalent to the kinematic method for analysing plastic collapse of frameworks.

7.10.4 Method of characteristics

The basis of the method is derived in Appendix I. The equations of equilibrium and the Mohr Coulomb law provide sufficient equations for the three stresses σ_x, σ_y, τ_{xy}, without reference to the strains. The only requirement of the strain is that they must be large enough for slip to develop.

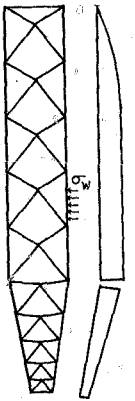

Figure 7.4 : Limit plasticity approach from reference (24)

The solution, however, is not as simple as it seems at this stage and the equations are rearranged for solution along the slip lines which coincide with the mathematically defined characteristics. Figs 7.5 and 7.6 show results obtained by Horne and Nedderman [38] for bins of half angles 10° and 40° for discharge with a free surface that is horizontal. As

can be seen there are regional stress fields separated by discontinuities. The resulting pressure on the wall oscillates about the radial stress field presssure. The solution proceeds from the surface and the discontinuities start at the junction of wall and free surface. Conversely as the radial stress field

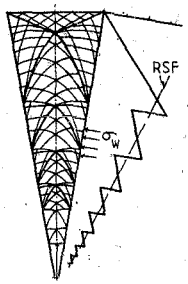

Figure 7.5 : Pattern of characteristics and discontinuities in an emptying hopper with wall stresses plotted alongside for :

$\theta_w = 10°$
$\delta = 30°$
$\phi_w = 25°$

from reference (39)

has only one stress field it has no oscillation caused by discontinuities. The method of characteristics produces good results but is difficult to apply because of the discontinuities.

7.10.5 Finite element method

The finite element method can accommodate different boundary conditions and can easily be applied to three-dimensional cases. A time stepping approach is necessary to go from

filling to emptying conditions. This requires a sophisticated visco-plastic constitutive law and therefore it is very difficult to produce a program. Häussler and Eibl [40] have had remarkable success developing such a program and give results for a tall silo that look good. The method may require a large amount of computer time, especially for three-dimensions.

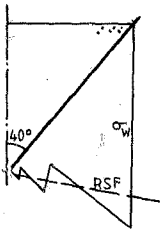

Figure **7.6** : Pattern of wall stresses for : $\theta_w = 40°$ $\delta = 30°$ $\phi_w = 20°$ from reference (39)

7.11 Conclusions and summary

It is not easy to measure wall pressures in a bin really well. The method used here was simple and inexpensive and yielded reasonably consistent and believable results.

The theories chosen to calculate wall pressures were divided into those for filling pressures and those for emptying. They were all simple formulas that did not require a computer, although a computer was used in some cases.

Agreement between theories and experiment was fairly good for the best theories, for both shapes of bin.

The switch pressure could not be detected, and instead a rapid change over the whole wall from filling to emptying

pressures occurred.

More sophisticated methods of calculating pressures are complicated and need computers. They are still at an early development stage but show great promise for the future.

APPENDIX A

TEST ON SAND

The summarised values are given in table 2.1 and table A1.

TABLE A1 Properties of Sand

Density loose		1,593 g/cc
dense		1,757 g/cc
Internal friction angle	δ =	33,8°
Wall friction angle (steel)		
from triaxial	ϕ_w =	20,1°
from shearbox	ϕ_w =	18,8°
Wall friction angle (glass)		
from shearbox	ϕ_w =	9,1°
Angle of repose	ε =	31,0°

A.1 Internal friction angle δ

The readings are given in table A2 where σ_3 values are calculated. Fig A1 shows the Möhr's circles which yield a value of effective friction angle δ = 34°. δ is calculated, Fig A2, according to the formula:

$$\delta = \text{asin}\left(\frac{\sigma_1 - \sigma_3}{\sigma_1 + \sigma_3}\right) \qquad \text{A.1}$$

for each test, and an average weighted proportionately to σ_3 is produced in table A3. The calculated value of δ = 33,8 was preferred as more accurate than the value of 34,2 from the graph.

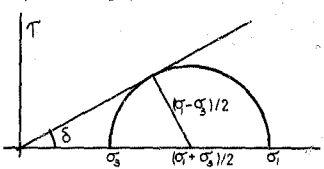

Figure A2
Calculation of δ

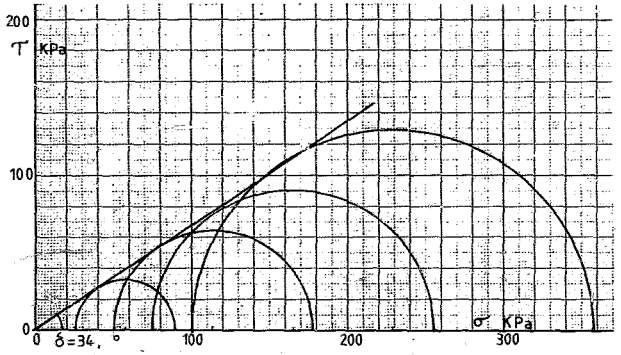

Figure A1 : Internal friction angle δ

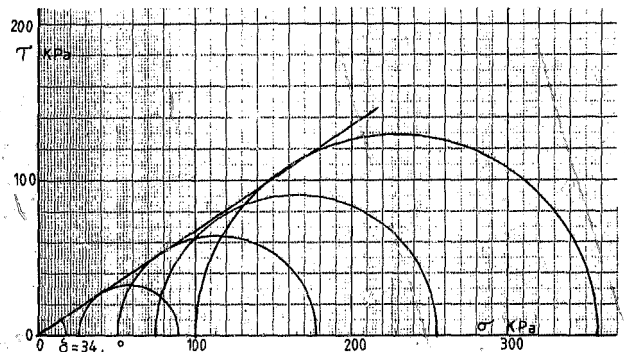

Figure A1 : Internal friction angle δ

TABLE A2 Readings and values of σ_1 - internal friction angle
Proving ring calibration = 1,302 kPa/div

σ_3 kPa	25	50	75	100
Weight gm	123,7	123,8	126,4	126,0
Size mm x mm ϕ	62 x 38	62 x 38	64 x 38	64 x 38
Density g/cc	1,760	1,7615	1,7425	1,737
Deflection 0,01 mm	500	500	500	500
$1/(1-\varepsilon_1)$	1,0081	1,0081	1,0079	1,0079
$\sigma_1 - \sigma_3$ kPa	64,3	127,3	179,8	257,2
σ_1 kPa	89,3	177,3	254,8	357,2

TABLE A3 Calculation of Internal Friction Angle
$\delta = \sin [(\sigma_1 - \sigma_3)/(\sigma_1 + \sigma_3)]$

σ_1 kPa	σ_3 kPa	$\sigma_1 - \sigma_3$ kPa	$\sigma_1 + \sigma_3$ kPa	sinδ	δ°
89,3	25	64,3	114,3	0,5626	34,23
177,3	50	127,3	227,3	0,5601	34,06
254,8	75	179,8	329,8	0,5452	33,04
357,2	100	257,2	457,2	0,5626	34,23

Weighted Average $\delta = \dfrac{34,23x25 + 34,06x50 + 33,04x75 + 34,23x100}{25 + 50 + 75 + 100}$

$= 33,84°$

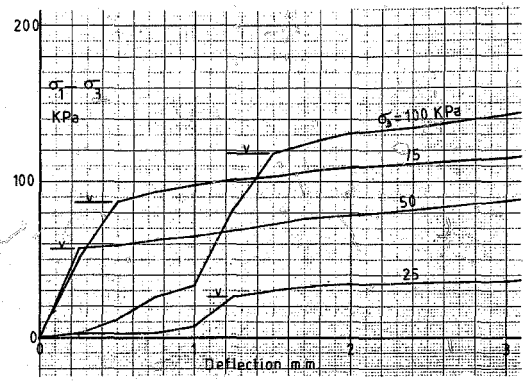

Figure A3 : Wall friction

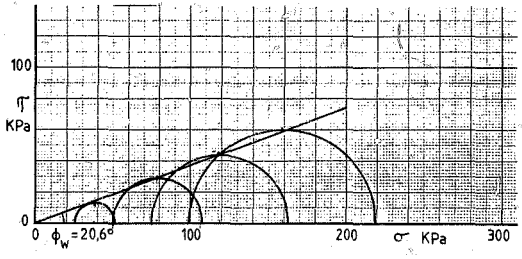

Figure A4 : Wall friction angle ϕ_w

A.2 Wall friction angle ϕ_w sand on steel

Triaxial test

A steel plate was placed in the specimen at 45°. Slip was observed to take place along the plate. In Fig A3 $\sigma_1 - \sigma_3$ is plotted against deflection . The points of sharp direction change are indicated, and give the values for $\sigma_1 - \sigma_3$ used. The readings and values of σ_1 are given in table A4. Möhr's circles are plotted in Fig A4. Note that the inclined line must pass through the highest point of each circle. The measured value from the graph is $\phi_w = 20,6°$.

The wall friction angle is also calculated in table A4, Fig. A5. The value found for ϕ_w is 20,1° which was the preferred value.

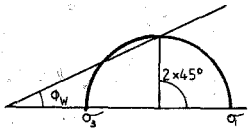

The formula used was

$$\phi_w = \text{atan}\left(\frac{\sigma_1 - \sigma_3}{\sigma_1 + \sigma_3}\right) \quad \text{A.2}$$

Figure A5 : Möhr's circle for wall friction

TABLE A4 Readings and values of σ_1 - wall friction angle. ; Proving ring calibration = 1,302kPa/div

σ_3 kPa	25	50	75	100
$\sigma_1 - \sigma_3$ kPa	26,1	57,3	87,3	118,8
σ_1 kPa	51,1	107,3	162,3	218,8
$\sigma_1 + \sigma_3$ kPa	76,1	157,3	237,3	318,8
tan ϕ_w	0,3430	0,3643	0,3679	0,3726
ϕ_w°	18,93	20,02	20,20	20,44

Weighted average

$$\phi_w = \frac{25 \times 18,93 + 150 \times 20,02 + 75 \times 10,20 + 100 \times 20,44}{25 + 50 + 75 + 100}$$

$$= \underline{\underline{20,13°}}$$

A.3 Wall friction angle ϕ_w sand on steel

Shearbox test

A 100mm x 100mm shear box was used. packs were used to make the 100mm x 100mm x 3mm steel plate flush with the top of the lower half, Fig. A . The top half was positioned with the lifting screws holding it up by approximately

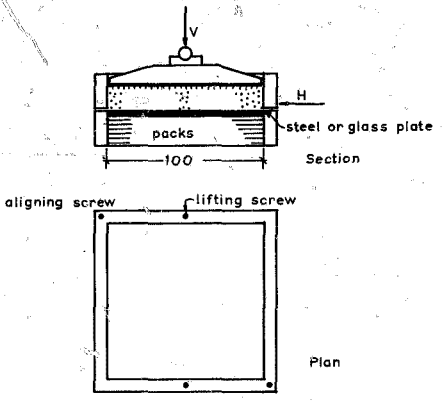

FIGURE A6: Shearbox test for sand-steel and sand-glass friction

2mm. Sand was poured in, levelled off and tamped after which the ribbed plate, loading plate, ball bearing and vertical load were position. The lifting screws were screwed up and the aligning screws were removed before commencing the test. The test was carried out at a speed of 40mm/hour and readings were taken of horizontal load every 0,25mm up to a maximum of 3mm.

In the first test a medium emery paper was used on the steel plate in the direction of shearing. The results are shown in table A5. The slope ($\tan \phi_w$) of the graph was found by least squares. In the second test, table A6, the steel plate was sanded with a coarser emery paper perpendicular to the direction of shearing. The results are plotted in Fig. A7.

A.4 Wall friction angle Sand on glass

Shearbox test

A 100mm x 100mm x 3mm piece of clear window glass was used. The same test procedure as in section A.3 was followed. The results are shown in table A7. The results are plotted in Fig. A7.

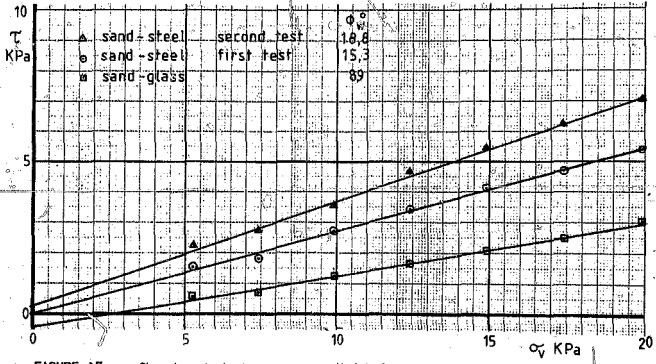

FIGURE A7 : Shearbox tests to measure wall friction angles.

TABLE A5: Shearbox test results for sand-steel friction angle. Plate sanded parallel to direction of shearing.

Δ_H 0,01 mm	Horizontal load, divisions (1 div = 1,397 N) for vertical stress (σ_v kPa) of:						
	5,27	7,40	9,90	12,40	14,90	17,40	19,90
0	0	0	0	0	0	0	0
25	7,9	8,0	11,0	12,0	15,5	16,0	8,0
50	9,0	9,0	17,0	19,0	24,0	24,8	32,8
75	9,0	10,0	18,6	22,0	27,5	28,9	37,0
100	10,1	13,2	18,2	23,0	27,5	31,4	38,0
125	10,0	13,1	19,6	20,9	27,6	32,8	38,0
150	9,9	12,8	19,6	22,0	27,2	32,4	38,3
175	10,0	12,9	19,2	21,9	27,5	32,4	38,3
200	10,0	11,2	19,6	21,2	27,2	33,0	38,9
225	9,7	11,1	19,6	24,0	28,7	33,2	39,0
250	9,9	12,9	19,2	25,0	30,0	33,4	39,0
275	10,0	12,0	18,4	22,2	30,0	33,6	39,0
300	10,9	11,2	19,1	22,5	29,0	33,9	38,9
325					28,2		
350					28,2		
τ-kPa	1,511	1,831	2,718	3,467	4,161	4,702	5,409

Least squares $\tau = -0,01 + 0,2742\ \sigma_v$

$\sigma_w = \text{atan}(0,2742) = \underline{15,33}°$

Correlation coefficient 0,9977

Note : Underlined values were used

TABLE A6 : Shearbox test results for sand-steel friction angle. Plate sanded normal to direction of shearing.

Δ_H	Horizontal load, divisions (1 div = 1,397 N) for vertical stress (σ_v kPa) for :						
0,01 mm	5,27	7,40	9,90	12,40	14,90	17,40	19,90
25	14,0	8,5	13,5	9,0	16,0	15,0	16,0
50	14,5	13,0	10,7	26,9	30,0	31,0	38,0
75	14,6	15,2	24,8	30,6	31,4	35,2	45,5
100	14,8	17,2	25,0	32,1	32,0	41,1	49,6
125	14,8	17,8	24,8	32,0	33,5	42,0	49,6
150	14,9	18,9	24,2	32,0	34,1	42,9	49,8
175	15,2	19,4	23,9	32,1	33,9	43,8	49,9
200	16,0	19,2	23,8	32,1	33,9	44,1	48,9
225	15,8	19,2	24,2	32,9	34,0	44,4	49,6
250	15,5	18,8	24,8	33,2	35,2	45,0	49,5
275	15,7	18,8	24,8	33,2	38,0	45,0	50,2
300	15,7	18,9	25,2	33,2	38,6	45,0	50,2
325					39,2		
350							
τ kPa	2,23	2,71	3,52	4,64	5,48	6,29	7,01

Least squares $\tau = 0{,}310 + 0{,}3408\ \sigma_v$

$\sigma_w = \text{atan}(0{,}3408) = 18{,}82°$

Correlation coefficient = 0,9977

Note: Underlined values were used

TABLE A7: Shearbox test results for sand-glass friction angle.

Δ_H 0,01 mm	Horizontal load, divisions (1 div = 1,397 N) for vertical stress (σ_v kPa) of :						
	5,27	7,40	9,90	12,40	14,90	17,40	19,90
0	0	0	0	0	0	0	0
25	1,8	7,0	6,9	9,0	11,0	16,0	9,?
50	2,9	7,8	8,8	10,5	11,8	23,0	18,8
75	2,9	7,8	9,4	11,2	14,0	23,8	19,2
100	3,2	7,6	9,5	11,6	14,0	24,0	20,0
125	3,8	6,8	9,1	11,9	13,2	20,2	20,9
150	3,8	6,8	9,2	11,8	13,9	20,1	21,0
175	3,7	5,2	8,6	11,4	14,0	20,1	21,5
200	3,6	5,0	9,2	12,0	13,9	19,9	21,9
225	3,8	4,9	9,4	11,0	14,9	18,0	21,9
250	3,5	4,7	10,5	11,6	15,0	17,9	21,9
275	3,8	4,8	10,4	11,6	15,0	17,9	21,5
300	3,8	4,9	10,6	11,9	15,1	17,9	22,0
325							
350							
τ kPa	,53	1,09	1,48	1,68	2,11	2,50	3,07

Least squares $\tau = 0,22 + 0,1605\ \sigma_v$

$\sigma_w = \text{atan}(0,1605) = 9,12°$

Correlation coefficient = 0,9929

Note : Underlined values were used